PSERC

Electric Transmission Line Flashover Prediction System

Ph.D. Thesis and
Final Project Report

Power Systems Engineering Research Center

A National Science Foundation
Industry/University Cooperative Research Center
since 1996

Power Systems Engineering Research Center

Electric Transmission Line Flashover Prediction System

Ph.D. Thesis and Final Report

Felix Amarh
Arizona State University

PSERC Publication 01-16

May 2001

Information about this Report

For information about this project contact:

George G. Karady
Salt River Chair Professor
Arizona State University
Department of Electrical Engineering
P.O. Box 875706
Tempe, AZ 85287-5706
Phone: 480 965 6569
Fax: 480 965 0745
Email: karady@asu.edu

Power Systems Engineering Research Center

This is a project report from the Power Systems Engineering Research Center (PSERC). PSERC is a multi-university Center conducting research on challenges facing a restructuring electric power industry and educating the next generation of power engineers. More information about PSERC can be found at the Center's website: http://www.pserc.wisc.edu.

For additional information, contact:

Power Systems Engineering Research Center
Cornell University
428 Phillips Hall
Ithaca, New York 14853
Phone: 607-255-5601
Fax: 607-255-8871

Notice Concerning Copyright Material

Acknowledgements

The work described in this thesis and project report was sponsored by the Power Systems Engineering Research Center (PSERC). George Karady was the project leader and major advisor in the preparation of the thesis. We express our appreciation for the support provided by PSERC's industrial members and by the National Science Foundation under grant NSF EEC 0001880 received under the Industry/University Cooperative Research Center program. Thanks are also given to EPRI and the Salt River Project for their support.

Executive Summary

Near industrial, agricultural, or coastal areas, contamination is a frequent cause of insulator flashover, most cases of which result in lengthy service interruptions. Utilities spend significant amounts of money on insulator washing and cleaning before the restoration of the service. Laboratory studies and industrial experience have shown that both contamination and wetting of insulator surfaces, which initiate the flow of leakage current, are required for insulator flashover. The leakage current leading to flashover has distinctive stages of development. Flashover is preceded by dry-band arcing and extension of the arc to bridge the insulator. This combination significantly modifies both the magnitude and shape of the leakage current.

A condition-based monitoring (CBM) system that monitors the easily measurable insulator leakage current as a means of assessing pollution severity and would possibly predict an approaching flashover could prove beneficial to utilities. The overall aim of this project is the development of a system that monitors pollution build-up through the signature changes in the leakage current and alerts an operator when there is a danger of flashover. The operator can, in turn, order maintenance personnel to wash the insulators. This will safeguard against unforeseen flashovers, since the system is constantly being monitored and diagnosed. Additionally, the washing cycles of insulators will be optimized, saving money and eventually rendering the power transmission system more reliable.

TABLE OF CONTENTS

Page

LIST OF TABLES

LIST OF FIGURES

LIST OF SYMBOLS

ACS	autocorrelation sequence
ARMA	autoregressive-moving average
CBM	condition-based monitoring
ECS	empirical crossing spectrum
ESDD	equivalent salt deposit density
EVA	extreme value analysis
EVRF	extreme value risk function
$E(z)$	expectation of z
FFT	Fast Fourier Transform
$f(x)$	true probabilty density function
$\hat{f}(x)$	estimated probabilty density function
$G(z)$	Gumbel probability distribution function
$g(z)$	Gumbel probability density function
$H(t)$	Hilbert transform
$h(n)$	window width of the Epanechnikov kernel
I/O	input/output
$i(t)$	time variation of leakage current
$i_a(t)$	analytic signal for leakage current
$i_{env}(t)$	leakage current signal envelope
$\tilde{i}(t)$	Hilbert transform of the leakage current

$K(z)$	general kernel function
$K_e(z)$	Epanechnikov kernel
LCA	level crossing analysis
MLE	maximum likelihood estimation
N_a	number of crossings at level a
PC	personal computer
PDF	probability distribution function
PSD	power spectral density
p	partitioning probability
pdf	probability density function
$\hat{P}_{AR}(f)$	autoregressive PSD estimate
$\hat{P}_{BT}(f)$	Blackman-Tukey correlogram PSD estimate
$\hat{P}_W(f)$	Welch periodogram PSD estimate
$R(\chi_p)$	extreme value risk function of χ_p
S_a	salinity of the salt-water solution
TDA	time domain averaging
$T(\chi_p)$	return period of the percentile χ_p
u	location parameter of the Gumbel pdf
VI	virtual Instrument
$z(t)$	digitized samples of the current envelope

α scale parameter of the Gumbel pdf

α_L level of significance

σ_s layer (surface) conductivity

σ_v volume conductivity

ν parameter of the non-central Rayleigh distribution

λ parameter of the non-central Rayleigh distribution

τ_a level crossing activity at threshold a

χ_p p-th percentile

CHAPTER 1

Introduction

1.1. Overview

Flashover of contaminated insulators in polluted areas has proven to be one of the most important factors influencing the operation of extra- and ultrahigh voltage transmission lines and substations [1, 4]. These are power-frequency flashovers on transmission lines without evidence of switching or lightning overvoltages and usually take place in wet weather conditions such as dew, fog, drizzle or light rain. Near industrial, agricultural or coastal areas, airborne particles are deposited on insulators and the insulator pollution builds up gradually. These deposits do not decrease the insulation strength when the insulators are dry. However, when fog or light rain wets the polluted insulator, a conductive layer is formed on the contaminated insulator surface, which initiates leakage current. The drying effect of leakage current produces dry-bands. The line voltage flashes over the dry-band and extension of the arc causes the insulator to flashover. In an operational system, several arcing periods precede actual flashover.

The prediction of approaching flashover is important for utilities.

Contamination-caused insulator flashovers result in expensive power outages. Utilities spend significant amounts of money on preventive maintenance, which includes insulator washing and cleaning. This expensive operation is scheduled by the subjective judgment of line engineers, based on historical experience or total hours of service since last washing.

Exact predictions of pollution build-up and identification of the time when the flashover is imminent has significant value to utilities. A condition-based maintenance program requires insulator washing only when specific diagnostic criteria indicate that such washing is warranted. Obviously, an accurate diagnostic criterion is needed to determine the condition of the insulator surface and to identify the possibility of flashover. Laboratory studies and industrial experience has shown that insulator surface leakage current, which is easily measurable, carries information about approaching flashover. Hence it is proposed to perform a comprehensive signature analysis of the leakage current, determine criteria appropriate for flashover prediction and to develop a monitoring system that alerts an operator about danger of flashover. The advantages of such a system over the traditional predetermined washing schedule are:

- the techniques for data acquisition and analysis are non-invasive and inexpensive
- unforeseen contamination-caused flashovers can be reduced since the insulator surface condition is constantly being monitored and diagnosed
- the washing cycles could be optimized, the overall operational costs reduced and transmission system made more reliable

The practical application and success of the leakage current sensor system depends on a reasonable understanding of the underlying contamination-caused insulator flashover mechanism, which is the subject of the following section.

1.2. Flashover Mechanism

1.2.1. Deposition of Contaminants

Outdoor insulators are generally exposed to contamination from a variety of sources. Insulators near coastal areas are contaminated by wind driven salt and those inland, by wind driven dust, agricultural and industrial pollution.

a) *Marine Pollution*. Most of the insulator contamination near coastal areas is due to airborne sea salts. Small water droplets are released from the tips of the ocean waves during stormy weather. These small droplets are blown away by winds, which evaporates the water of the small droplets to form even smaller droplets of brine. If the relative humidity is low enough, the water evaporates completely leaving a small, more or less dry, crytalline, salt particle. These salt particles are then deposited and stuck to the surface of the insulator. Insulators in regions extremely close to the sea can be exposed to direct salt water spray during periods of strong winds. The sun dries the water leaving a white salt layer on the surface of the insulator. The deposition of sea salt onto insulators is thus a function of wind velocity and distance from the sea.

b) *Inland Pollution*. The sources of insulator pollution include soil dust, fertilizer deposits, industrial emissions, fly ash, bird droppings, construction activities, etc.

Table 1. Typical sources of insulator pollution

Location	Source of Pollutant
Coastal areas	Sea salt
Rural areas	Soil dust, fertilizers, etc.
Desert	sand
Industrial	Fly-ash, industrial smokestacks
Highways	Road salt, smoke

Wind drives these airborne contaminant particles onto the insulator surfaces. Also, depending on proximity to highways and how the car traffic is, the wear of car tires produces a slick, tar-like carbon deposit on the insulator's surface. Road salts used on highways during the winter likewise play an important role during insulator surface pollution.

Insulators produce turbulence in airflow, which results in the aerodynamic 'catch' and deposition of particles on their surfaces [4]. The rate at which the insulator catches particles depends on the shape of the insulator, size and density of the particles and the speed of the airflow. The continuous deposition of these particles increases the thickness of these deposits. However, the natural cleaning effect of wind, which blows loose particles away, limits the growth of deposits. Occasionally, rain washes part of the pollution away and self-cleaning by airflow also removes some types of contaminant. The continuous depositing and cleaning produces a seasonal variation of the pollution on the insulator surfaces. After a long time (months, years) the deposits are stabilized and a thin layer of solid deposit will cover the insulator. Because of the cleaning effects of rain, deposits are lighter on the top of the insulators and heavier on the bottom. Table 1 summarizes the typical sources of insulator contamination.

1.2.2. Wetting of Contaminants

Porcelain and glass are easily wettable due to their high surface energy i.e., the surface exerts sufficient energy on a drop of water to cause it to spread out into a thin film.

a) *Sea Salt Pollution.* Condensation is the main source of wetting (even under conditions of fog and drizzle) near the ocean. The hygroscopic effect of the sea salt contamination causes condensation to begin at low levels of relative humidity. Condensation is also enhanced by radiative cooling of the insulator surface. Furthermore, wind drives salt water onto insulator surfaces very near the ocean, forming a conducting salt-water layer.

a) *Inland Pollution.* Moisture in the form of fog, mist, drizzle, light rain or dew impinging on the insulator surface wets the pollution layer, dissolving the salts and any soluble electrolytes to produce a thin conducting layer on the insulator surface. Wetting is dependent upon the amount of soluble salt in the contaminant, the nature of the insoluble material, time duration, surface conditions and the temperature difference between the insulator and its surroundings [1,4]. Ice accumulation on insulator surfaces also play a major role in wetting. In industrial areas, water may form ice due to water-dissolved industrial pollution e.g., ice formed from acid rain water. Ice deposits bridge the gaps in an insulator string and when the sun melts the ice, a conducting water layer together with a contamination coating will be formed on the insulator surface [1-4].

The bulk of the pollution on an insulator's surface is generally non-conducting

but moisture will intermittently render conductive, much of the soluble part of the pollution layer. The conductivity of the resulting thin conductive layer depends on the amount of moisture as well as the chemical composition of the contaminant. The severity (degree) of the pollution is characterized by the equivalent salt deposit density (ESDD). Equivalent Salt Deposit Density is measured by periodically washing down the pollution from selected insulators with distilled water and carefully collecting the water. The conductivity of the collected water is measured and the equivalent amount of salt, which produces the same conductivity is calculated. The obtained mg value of salt is divided by the cleaned area of the insulator to obtain the ESDD value. The calculation is done as follows [5]:

$$\sigma_{S20} = \sigma_{V20}\,[\,1 - 0.02277\,(T - 20)\,] \tag{1.1}$$

where

σ_{S20}	is the layer conductivity at a temperature of 20 °C (in S)
σ_{V20}	is the volume conductivity at a temperature of 20 °C (in S/m)
T	is the temperature of the insulator surface (°C)

The salinity, S_a in (kg/m^3), and the ESDD (mg/cm^2) are respectively given by

$$\begin{aligned} S_a &= (5.7\sigma_{S20})^{1.03} \\ \text{ESDD} &= \frac{S_a\,V}{A} \end{aligned} \tag{1.2}$$

where

V	is the volume of the cleaned water (in cm^3)
A	is the area of the cleaned surface (in cm^2)

Typical range of values of inland contamination levels provided by the Electric Power

Table 2. Typical ranges for inland pollution severity

Description	ESDD (mg/cm^2)
Very light	0-0.03
Light	0.03-0.06
Moderate	0.06-0.1
Heavy	≥ 0.1

Table 3. Typical ranges for marine pollution severity

Description	Salinity (kg/m^3)
Very light	0-10
Light	10-20
Moderate	20-40
Heavy	40-80
Severe	≥ 80

Research Institute [1] are listed in Table 2. Table 3 shows similar levels for marine pollution [4].

1.2.3. Leakage Current and Dry-band Formation

With voltage applied to a standard cap-and-pin ceramic insulator, wetting of the contamination layer starts the flow of leakage current. The soluble contaminant is first dissolved, forming a thin conductive layer on the surface of the insulator. Leakage current is then initiated and the current density depends upon the shape of the insulator's surface. Generally, the highest current density is around the pin. The current heats the conductive layer and evaporates the water at the areas with high current density. This leads to the development of dry bands around the pin. The dry bands modify the voltage distribution along the surface. Because of the high resistance of the dry bands, the system voltage is impressed across them. If the dry

bands cannot withstand the voltage, localized arcing develops and the dry bands will be spanned by discharges. When a discharge is initiated, the amplitude of the current is limited by the resistance of the series contamination layer.

The appearance of discharges also changes the current shape. The discharge generates short duration impulses superimposed on the 60 Hz current. However, in the beginning, the arc lasts only for a short time period. The extinction of the arc again changes the current shape. The dry-band is wetted again, which causes an increase in current. This leads to drying, which again produces surface arcing. Depending upon contamination levels, the arc length gradually increases, which ultimately leads to flashover.

The mechanism described above shows that heavy contamination and wetting may cause insulator flashover and subsequent service interruptions. This project proposes a mathematical signature analysis of the changes in insulator leakage current magnitude and shape, as a means of predicting contamination flashover of ceramic insulators.

1.3. Literature Review

B. F. Hampton investigated the voltage distribution along the wet, polluted surface of a flat insulating strip and the method of dry band formation, with subsequent growth of discharges on the polluted surface [2]. He deduced from his experiments, that an arc rooted on a cylinder having constant resistivity would propagate along the surface if the voltage gradient in the arc column is less than that along the

cylinder. Also, an arc propagating along a water surface burns in an atmosphere of steam, and measurements showed that the arc gradient in the steam is considerably higher than a similar arc burning in an atmosphere of air. However, the behavior of an arc rooted on a wet, polluted surface is complicated by the rapid changes in surface resistance which occur during a current surge; hence, Hampton's findings were not conclusive and further research was warranted to determine the conditions for flashover.

Obenaus [3] derived a relationship between the critical stress, E_c, and the maximum leakage current. His analysis was based on the assumption of a constant resistance in series with the arc discharge, an assumption that seems to be inconsistent with experimental results, which indicate a varying resistance. The work of Alson and Zoledziowski [6] deals with the arc development on a flat surface. By considering the source and the arc resistance and by adding an arc reignition condition under AC voltage, relations between current, arc length and voltage were established. They calculated a critical condition below which flashover is impossible. This can be shown to be the same as Hampton's results, if the same arc characteristics are used. They deduced analytically that flashover is impossible if the maximum current does not exceed $233{E_c}^{-1.31}$, where E_c is the critical applied voltage stress. The analytical results were compared to experimental results of naturally contamination insulators operated at 85 to 231 kV, with peak applied stress between 250 and 750 V/cm. There was good agreement between the analytical and experimental results indicating flashover may be predicted by the measurement of leakage current only.

Experimentally, numerous test methods have been devised to simulate natural conditions. Macchiaroli and Tuner [7], Naseer [8] and Kawai at project UHV [9] performed extensive series of tests to determine the performance characteristics of contaminated insulators and measured leakage current extensively to understand the insulators' performance. Because some parts of the leakage distance do not function during scintillations, Kawai introduced the concept of 'effective leakage distance' by using the results. Both Jolly [10] and McElroy [11] tested suspension insulators in salt fog to determine the effects of porous surface layers, salt fog concentrations, and surface conditions. To study the flashover phenomena they measured the leakage current continuously. Jolly derived a mathematical model, which gives the critical voltage if it is assumed that the discharge root will move forward whenever the field strength at the root exceeds some constant value. Rizk [12] proposed theories involving reignition. He reviewed and analyzed different flashover models and proposed a mathematical model for flashover. A presently proposed computational model to predict flashover voltage also uses the effect of field gradient and leakage current for the movement of an arc.

From the above studies it was established that leakage current is necessary to understand the flashover process. Verma observed that a flashover could be expected if a certain maximum leakage current is present. In fact, it has been shown that, for the failure of an insulator with a contamination layer, the peak value of the leakage current, I_{max}, immediately before a flashover is a characteristic parameter largely independent of the type of pollution. This finding he calls the 'I_{max}' approach. From

studies of current records up to complete flashover, Verma found that a critical peak current is reached, about 10 ms before complete flashover occurred, indicative of the imminence of flashover. If I_{max} is reached, flashover occurs, but if I_{max} is not reached, flashover cannot occur. But if the current exceeds I_{max} from whatever combination of circumstances, flashover is inevitable [13]. The practical applicability, and even the physical basis, of I_{max} has been criticized, but there is merit in leakage current measurement which leads to the flashover. Verma's later work refined the current measuring method. Such a technique was demonstrated in 1985 at FGH (High Voltage Research Institute, Mannheim) in Germany.

More recently, Mekhadi et al. [20] studied the conduction phenomena on polluted insulating surfaces under a.c. high voltages. From the experiments, they developed a theoretical arc model by treating the leakage current as a conduction current and the arc, a conducting channel that propagates between two concentric cylindrical electrodes. By solving the Laplace equation with the necessary boundary conditions, they obtained an expression for the leakage current, which effectively increased with applied voltage and/or pollution conductivity, as observed in practice. However, there was good correlation between the theoretical model and experimental data only for very small applied voltages (up to 9 kV). The model fails at high voltages because the assumption of concentric cylindrical electrodes is not valid in practice. Stathopulos and Topalis [21] used a stochastic model, manifested in the random formation of partial arcs at statistically random positions along the dry zones and also the random character of the dry-band width and number, to evaluate the surface flashover

characteristics of polluted insulators. From computer simulations using the proposed stochastic model, several useful quantities were evaluated including the flashover probability versus applied voltage, distribution function for the critical voltage, histogram for the leakage current path and the minimum, respectively maximum critical voltage versus the resistance per unit length for the pollution layer. The relationships obtained were critical in the dimensioning of the external insulation for overhead lines, but were not suitable for flashover prediction.

The work of Holtzhausen [26] consisted in using a set of parameters to best fit measured flashover voltage and leakage current data. Using a cylindrical insulator, he investigated the effects of variations in arc constants, reignition constants and arc root radius on parameter variations of the critical surface conductivity and the critical current. It was found that the solutions to the dynamic arc equations are particularly sensitive to variations in the reignition constants. Further work is needed for insulators with practical shapes. Rizk and Rezadada [27] and other researchers [28–30] updated the mathematical model for power frequency flashover of polluted insulators by incorporating the effects of reduced air density at high altitudes on the flashover voltage and critical leakage current of polluted high-voltage insulators. Rizk et al. also evaluated the effect of ambient pressure on the physical parameters of the dielectric recovery equation, effect of reduced pressure on the arc boundary radius and the combined effect of reduced humidity and reduced air density on the dielectric strength at ambient temperature. From the analysis, a new expression was derived for the reignition voltage, which included ambient pressure effects. The results indicated

that the critical AC withstand voltages of polluted simple-shaped insulators;

- vary approximately with the square root of ambient temperature
- the critical current is more sensitive to ambient pressure than the critical voltage
- the critical arc length amounts to about 65% of the leakage path, practically independent of pollution severity of ambient pressure

Accounting for insulator geometry, the paper also presented new altitude derating factors for polluted insulator performance and a new formula for the efficiency of leakage path utilization, but did not address the problem of flashover prediction.

Numerous studies have been conducted in the field of dynamic modeling of the arc characteristics in order to define criteria which allow prediction of polluted insulator flashover, and the results presented in recent publications [31–33]. Dhahbi-Megriche et al [31] used an analytical model which accounted for the configuration of insulator profile, the dynamic changes in the arc resistance and the instantaneous velocity of arc propagation. There was a satisfactory agreement between their results and the experimental and theoretical data reported by previous researchers. However, significant differences were also observed in the plots of leakage current vs. applied voltage for different conductivities, meaning the model needs to be improved. Danikis et al. [34] extended the Obenaus model to include the non-uniformity of the contamination of the insulator surfaces and also assumed that the boundaries of the dry bands are not parallel. With these considerations, the voltage distributions on the insulator surface as well as leakage current paths were computed. This model

only simulated some more realistic conditions but the results could not be used for flashover prediction. The findings of Holtzhausen [33] were that calculations of the flashover voltage of polluted insulators using 'basic arc constants' were inaccurate and that a general model to accurately predict insulator pollution flashover was not feasible.

Frequent occurrences of contamination related outages (especially near coastal areas), has resulted in the development of contamination monitoring and pollution severity assessment systems. Renowden et Richards [35] describe a remote contamination monitoring system (RCM) designed, fabricated, tested and deployed in Florida, with the ability to monitor contamination buildup and provide an actionable amount of warning for upcoming outages. The RCM has sensors, which measure leakage current and weather parameters like relative humidity, ambient temperature, insulator surface temperature, wind speed and direction, and the amount of rainfall. It also has a liquid water sensor (LWS) which measures amount of condensation and contamination level on an insulator surrogate. Preliminary results indicate that leakage current monitoring is an unreliable indicator of contamination level (except near pre-flashover levels) due to the fact that leakage current is a function of both water present and the amount of contamination. Similar contamination monitoring systems have been developed by NGK, which uses multiple leakage current detectors with Peltier modules [36]. The unit automatically measures contamination levels continuously without wiping them. Studies with such monitoring systems have also been conducted at sites in Korea and the Gulf of Mexico [37, 39].

Mizuno et al. [23] developed a computer model to dynamically simulate the risk of flashover of contaminated insulators under real-time change of the climatic environmental factors. By accumulating data from measurements of soluble and non-soluble contaminant deposits, cleaning by rain, wetting by moisture and other factors affecting the wetting of contaminated insulator surfaces, the risk of flashover of a ceramic insulator is calculated. This consequently is used to compute the resultant risk for a system of insulators connected in parallel and subjected to the same degree of pollution severity and wetting. There were several cases in which actual flashover events and the calculated results did not correlate well, indicating a necessity to improve the simulation model.

The literature review shows that no method exists for the accurate prediction of pollution-caused flashover for transmission lines.

1.4. Project Objectives

The objectives of this project are:

- Development of a theory that links the flashover mechanism to measurable quantities which are suitable for flashover prediction.
- Experimental validation of the theory of flashover prediction using signature analysis.
- Development of an electronic sensor system for flashover prediction and validation of system operation.

1.5. Structure of this Dissertation

This dissertation provides different aspects of leakage current signature analysis as a diagnostic tool for flashover prediction, with special focus on linear stochastic analysis.

Chapter 1 introduces the problem of contamination flashover on transmission lines and provides a brief review of current industry practices used for assessment of pollution severity.

Chapter 2 presents the concept of signature analysis of the leakage current. Several time-domain and frequency-domain techniques are presented.

Chapter 3 sets out the important theoretical relationships and numerical results of the linear stochastic analysis. The leakage current is predominantly random in nature and the statistical (probabilistic) and dynamic properties are evaluated in terms of level crossings, extreme value probability distributions and exceedances, of the leakage current envelope. It is worthwhile to mention that this analysis is novel and feedback would be greatly appreciated.

Chapter 4 reviews the dynamic arc modeling of the AC flashover. Surface discharges in the form of partial arcs precede contamination flashover and it is hoped that a computer model of the arc could aid in the understanding of the flashover process.

Chapter 5 describes an on-line leakage current monitoring system, which performs the signature analysis in real-time and warns operators of any ensuing flashovers.

Chapter 6 describes the conclusions of this project and also looks at the future of this project: improvements in the arc dynamic model, field testing of monitoring system on in-service insulators and also stochastic methods like Markov chains, Poisson point processes, higher order crossing analysis and stochastic integral and differential equations are all envisioned to be used for further signature analysis.

CHAPTER 2

Leakage Current Measurement and Signature Analysis

2.1. Introduction

As presented in the literature review, the measurement and analysis of the leakage current as a tool for condition-based monitoring of insulators has attracted a lot of research in the last few decades. However, due to the erratic changes in the leakage current, *rms* and *max* values alone could not be used to characterize the changes. This led to the notion of a comprehensive mathematical signature analysis of the leakage current, which is focus of the proposal for this dissertation. Another quantity that is candidate for signature analysis is the electric field and its distribution. The arc produces a high frequency field disturbance. Signature analysis of this quantity may also lead to proper identification and prediction. It was originally proposed to perform a systematic analysis of the waveforms of both electric field and leakage current to identify signature changes that can predict approaching flashover.

However, due a limitation imposed by available measurement equipment, only the leakage current signature analysis has been performed to date.

2.2. Flashover Tests and Leakage Current Measurement

The artificial contamination flashover tests considered were the clean-fog and salt-fog tests (both described later). The clean-fog pollution test reflects natural conditions where pollution occurs through a combination of conductive (e.g., salts or fertilizers) and non-conductive, airborne contaminants (soil, sand, minerals, etc.), typical of inland industrial regions. The salt-fog pollution test simulates natural conditions where contaminants are predominantly conductive (e.g., sea salts), typical of coastal areas.

The flashover tests are conducted in a laboratory fog chamber. The fog chamber is a 6 ft x 6 ft x 6 ft wood-frame structure, with a metallic tank as base and covered with polyethylene plastic. Fog is generated by evaporation of water from a steel tank containing two immersion heaters. The water tank is located on the floor at one corner of the fog chamber. The high voltage cable enters through a plastic bushing in side of the chamber, 3 ft above ground. Voltage is supplied from a 6.5 kVA 120/110000 V potential transformer, the primary side of which connected to a 50 kVA 120 V Powerstat variable autotransformer. With this, the mains supply voltage is varied form 0-120 V and stepped up. This supply has a short circuit current of about 30 A at 50 kV. The test insulators are suspended vertically from a wooden brace on

Figure 1. Hardware layout of fog chamber

the ceiling of the chamber, about 3 ft from the chamber wall. The flashover voltage is 12-15 kV/unit so that the nominal transformer secondary voltage is enough to supply the string. Also, the wooden brace can mechanically support this string. The whole fog-chamber is housed in a wire mesh enclosure 13 ft x 9 ft x 8 ft 5 in. Figure 1 shows a hardware layout of the fog chamber.

For protection of personnel, a contact-switch with a relay de-energizes the transformer whenever the door to the enclosure is opened. A red light-bulb visibly illuminates the room when the transformer is energized and danger signs are posted

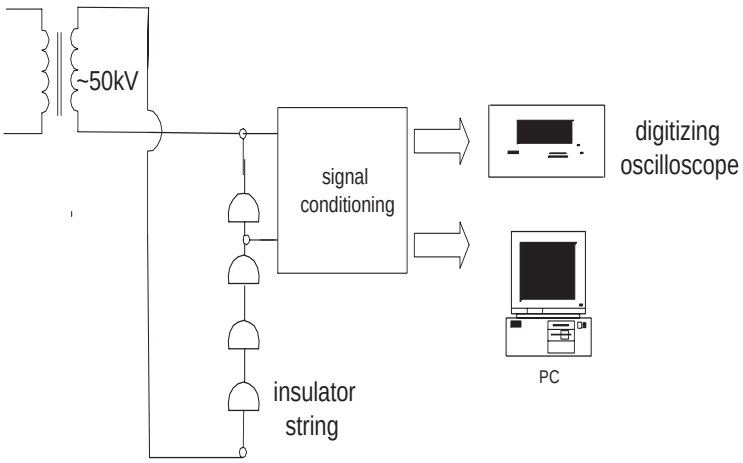

Figure 2. Experimental Setup

on the wire mesh to warn against unauthorized entry into the fog chamber. The measuring equipment was protected by three parallel stages; a metal oxide varistor (MOV), back-to-back zener diodes and a 20 A circuit breaker.

The leakage current is monitored by converting the current signal to voltage through the use of a 20 Ω power resistor. The shunt voltage across the 20 Ω resistor is fed to the analog inputs of a data acquisition (DAQ) system by a coaxial cable. In order to access the reliability of the DAQ system, a 60 MHz Hewlett Packard analog oscilloscope also provides visual display of the leakage current. Figure 2 shows a schematic of the experimental setup, Figures 3 and 4 respectively show a picture of the suspension-type cap-and-pin insulator and its cross-sectional view and Table 4 has some technical data of the insulator.

Figure 3. Standard cap-and-pin insulator

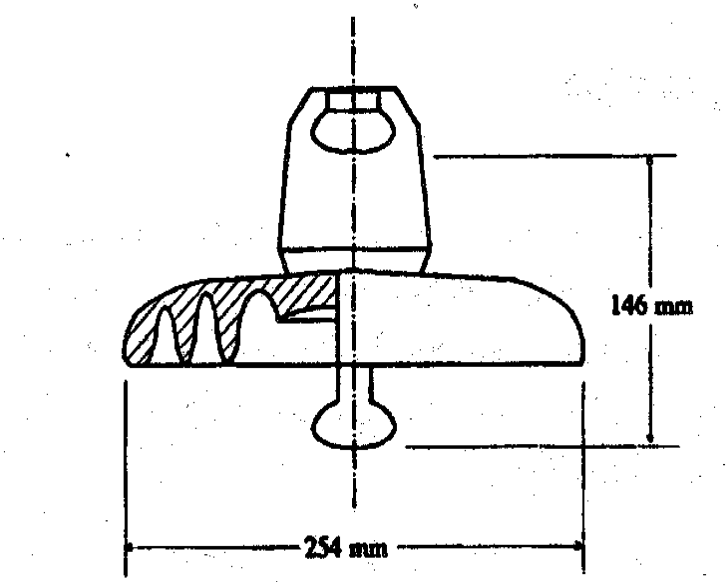

Figure 4. Layout of standard cap-and-pin insulator

Table 4. Technical data for standard cap-and-pin insulator

Shed diameter	254 mm
Unit spacing	146 mm
Leakage distance	305 mm
Top surface area	691 cm^2
Bottom surface area	908 cm^2

2.3. Test Procedure and Data Acquisition

The insulators used for the flashover tests were standard IEEE cap-and-pin porcelain insulators, which are readily available at ASU. This type of insulator has been used extensively on transmission lines and a tremendous amount of in-service performance data is documented. Also, their performance forms a basis against which the performance of other types of insulators are compared. Artificial contamination flashover tests are conducted periodically, with a duration of one to three hours. The tests are conducted in such a way as to reproduce the natural conditions.

Clean-Fog Tests: Firstly, the insulator surfaces are carefully cleaned by washing with detergent and rinsing thoroughly with clean water, in order to remove traces of dirt and grease. Next a contamination layer, consisting of a slurry of kaolin, sodium chloride and deionized water, is applied to the surface of each insulator. Contaminants which are non-conductive e.g., clay dust and conductive e.g., gypsum [1] are commonly found to be the materials adhering to naturally polluted insulators and these are reproduced here with kaolin and NaCl respectively. The slurry consists of 40 g kaolin per litre of water and NaCl is added. The salt concentration is adjusted to yield nominal contamination levels corresponding to about 0.05, 0.1 and 0.15 ESDD (Equivalent

Salt Deposit Density), briefly described in Chapter 1. The volume conductivity of the slurry is measured with a conductivity meter and compared to tabulated values to obtain the salinity [5]. There was a dispersion in ESDD of about ±12%. The insulators are dipped into the slurry and the contaminant mixture flooded over the surface of the insulators. One insulator is always kept for ESDD measurement only and not used in the flashover tests. After contamination the insulators are allowed to dry naturally in the sun and later transferred into the room to cool down before flashover tests.

The experiments are conducted in the laboratory fog chamber. The test insulators consists of a string of four suspension-type porcelain cap-and-pin insulators; the uppermost clean and used as a surrogate insulator for leakage current measurement, and the rest artificially contaminated. They are suspended vertically from ceiling of the chamber. Wetting of the insulators by steam-fog, produced by evaporation of water from an open tank. The tank has two fitted electrical immersion heaters (3 kW each) and it is covered until the water reaches boiling point, after which tank is uncovered and test voltage applied to the insulators. After an initial warm-up, the fog produced is equivalent to evaporation of about 10 liters of water per hour. Approximately 30 minutes is required to develop a heavy uniform fog and the temperature in the chamber rises 10 to 15°C. The steam fog duplicates the temperature differential between the ambient air and the insulator surface that exists during natural wetting. The supply voltage remains constant at about 50 kV for the total duration of the test.

Salt-Fog Tests: The insulator surfaces are thoroughly cleaned, wetted and suspended vertically in the fog chamber. Salt solution, consisting of NaCl and deionized water, with different salinities is then sprayed into the chamber through fog nozzles. Salinities of 10 kg/m^3, 30 kg/m^3 and 100 kg/m^3 were obtained by measuring the volume conductivity of the salt water and then looking up the corresponding salinity from [5]. The spray is formed from the salt solution and a stream of compressed air. The compressed air nozzle and the solution nozzle are at right angles to each other and both lie in the same plane. The salt solution is in a container located outside the fog chamber and the solution is pumped out through plastic tubes into the fog chamber using a submersible pump. A valve along the tube controls the flow rate. Air pressure is also adjusted between 80-90 psi. Two fog spray nozzles are placed diagonally and directed towards the center of the chamber. Voltage is applied simultaneously as the spraying starts.

Leakage current sampling and storage: With the insulators energized, the combination of contamination and wetting, initiates the flow of leakage current. The current is sampled at a rate of 2000-4000 samples/s, transferred to a data buffer and stored. The main components of the data acquisition system (to be described in a later chapter) are, a National Instrument AT-MIO-16E-2 DAQ plug-in board in a PC and LabVIEW^{TM} application software. The data is stored as both ASCII text files and binary files. This ensures that the LabVIEW^{TM} data could also be analyzed further using other software applications like MATLAB^{TM}.

The leakage current is recorded continuously until complete flashover occurs,

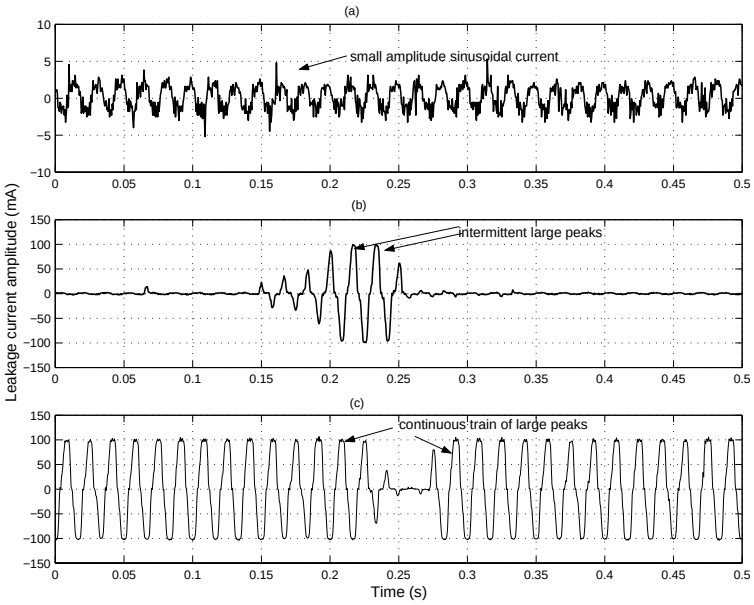

Figure 5. Typical leakage current waveforms (a) initial stages (b) mid-stages (c) final stages

or in the case of a withstand (non-flashover), until scintillation activity gradually disappears. The duration for both cases is usually one to two hours. Visual observation of the time trend of the leakage current on an oscilloscope shows that the current undergoes characteristic changes as the insulator surface goes from dry to a moistened and then to a completely wetted state. The three waveforms depicted in Figure 5 illustrate typical ensembles of the leakage current at various stages of the flashover process. The leakage current path of a dry contaminated insulator (or just immediately after fog application) is capacitive, the current magnitude very small and the shape is more or less sinusoidal (Figure 5a); distortion of the waveform is due to interference from radio waves, etc.

With the introduction of moisture, soluble contaminants are dissolved, a thin conductive layer is formed and the leakage current path becomes resistive and base

current magnitude increases. Heating effect of leakage current leads to dry-band formation and partial discharges across the dry-bands. The effect of these discharges is to create current surges and to modify the current waveshape; narrowing the width of the current wave. As wetting progresses, the dry-bands reabsorb moisture and more soluble contaminants are dissolved, hence the surface conductivity of the insulator increases, with a consequent increase in leakage current magnitude. The current magnitude depends on the level of contamination and the amount of moisture on the insulator surface. The increased current leads to further drying, which again produces localized surface arcing. Extinction and reignition of the local arcs also change the current shape; short duration impulses superimposed on the 60 Hz current. Depending upon contamination levels, the arc length gradually increases, which ultimately leads to flashover.

Flashover and Withstand Tests: The experiments included withstand tests and complete flashover tests. The leakage current waveforms for the two tests have some significant differences;

- During periods of maximum fog, there is very heavy scintillation activity and the peak current increases considerably. For the withstand tests (0.05, 0.1 ESDD), these large peaks occur intermittently, as shown in Figure 5b. With time, discharge activity which is strong at first, gradually disappears.

- The events leading to flashover are similar to the withstand case. However, the large peaks occur continuously and more frequently during several half cycles.

Figure 5c shows that, even though the maximum current is the same as in Fig. 5b (about 110 mA), there is a train of large peaks which may culminate in flashover of the insulator. Arcing is sustained until complete flashover. This is typical of the high contamination levels, 0.15 ESDD.

Salt-fog and Clean-fog Tests: There is no considerable difference in the shape or maximum leakage current for similar contamination levels using salt-fog or clean-fog. In general, heavy scintillation activity on contaminated insulators under salt fog tends to start quicker than under clean fog. This is probably due to the fact that deposition of high salt-density fog decreases the insulator surface resistance rapidly, the result of which is increased leakage current magnitude (compared to clean fog). The larger current more quickly develops dry-bands and stronger discharges are observed much earlier than in the case of clean fog.

2.4. Concept of Mathematical Signature Analysis

The previous section attests that, surface arcing precedes flashover. Arcing affects the magnitude and shape of the leakage current. Mathematical analysis and modeling leads to a nonlinear relationship between the leakage current time variation, arc length and pollution layer resistivity. The extension of the arc beyond a critical length further modifies the magnitude and shape of the current and may also cause flashover. Therefore, the current carries information, which could be identified and extracted for the prediction of imminent flashover. Obviously, observation of the peak and *rms* current is not sufficient. This leads to the concept of statistical signature

analysis of the current waveform. A systematic analysis will identify the parameter that best characterizes the features in the leakage current and indicates approaching flashover. Once a parameter is found, the philosophy is to detect deviations in the parameter of sufficient magnitude as to be considered outside the region of normal operation. The implementation of the signature analysis methodology involves four steps:

1. Selection of appropriate sensors for leakage current measurement, in this case a very simple measurement technique using a shunt resistor.

2. Extraction of features from the measurements using appropriate signature analysis techniques.

3. Determination of a reliable decision strategy, (by comparing extracted features with baseline data) in order to discriminate 'normal' conditions from abnormal.

4. Alerting an operator of possible danger if threshold limits are exceeded.

2.5. Preliminary Off-line Analysis

Signature analysis is a relatively new concept in high voltage engineering and an experimental study of leakage current signature analysis was carried out at ASU [11]. The previous study used FFT analysis of the leakage current to obtain the frequency signature. This preliminary investigation showed that other harmonics dominated, in particular the third harmonic, just prior to flashover. However, a threshold for the third harmonic for flashover to occur could not be established, probably due to

the spurious peaks encountered with FFT analysis. For the present analysis, several time-domain and frequency-domain digital signal analysis techniques were tested for applicability and accuracy. Digital signal processing methodologies examined included auto regressive (AR) modeling, spectral and cepstral analysis, and fitting of probabilistic models to the observed data. Basic signal descriptors such us the autocorrelation, zero crossing (level crossing) rate, and amplitude probability distribution functions were explored to detect trends which might indicate approaching flashover. An overview of the methods is presented in the following sections and subsequent chapters; the results have also been published in the technical literature (see Publications).

2.5.1. Time Domain Averaging (TDA) - Signal Averaging

Signal averaging is used extensively in different aspects of several of the analytical methods which follow. The primary reasons for averaging is to obtain statistically stable estimates or to even out spurious behavior. It consists of averaging N segments, the length of each segment being the basic period. The averaging of points separated by this period is given by

$$y(iT) = \frac{1}{N} \sum_{r=0}^{N-1} x(iT - rMT) \tag{2.1}$$

where $x(iT)$ and $y(iT)$ are the raw and averaged data, and M is the number of points per period. A recursive form of (2.1) is easily realized as

$$y(iT) = y_{r-1}(iT) + \frac{x_r(iT) - y_{r-1}(iT)}{r} \tag{2.2}$$

where r, the running index of the number of periods is updated at each recursion until $r = N$. This averaging technique is used in subsequent sections to average across windows, periodograms, biperiodograms etc., in order to obtain smooth and stable spectral estimates.

2.5.2. Time Domain Averaging (TDA) - Moving Average

The moving average is used to eliminate (or reduce) irregular fluctuations of data, $x(iT)$, by averaging values pertaining to adjacent points of $x(iT)$. In this way, the long-term trend in the data is captured. The general form is given by:

$$y(iT) = \sum_{j=-n}^{n} a_j x(iT + jT) \tag{2.3}$$

where a_j are weights satisfying $a_j = a_{-j}$. The coefficient a_j depend on the type of moving averaging e.g., simple, exponential, Spearman, etc. This averaging technique is used in the next section to obtain long term trends in data.

2.6. Spectral Analysis

Even though the leakage current signal is a function of time, it could be represented in the frequency domain, where the amplitude and phase are given with respect to frequency. Spectral analysis is a method that characterizes the frequency distribution of a measured signal. The Fourier transform (FT) is the mathematical foundation for relating a time or space signal to its frequency domain representation. However, due to certain shortcomings of the FT, notably spectral leakage and poor

resolution at the spectral peaks, it was proposed to use other high resolution digital spectral estimation techniques.

Different digital spectral analysis schemes were investigated, including the classical periodogram and correlogram, and also several time-series (autoregressive-moving average) models. Various autoregressive modeling algorithms, namely Burg's harmonic algorithm, covariance method and the modified covariance method, were used. All these methods compute the power spectral density (PSD). The mathematical background of these methods is summarized in appendix A1.

The leakage current was continuously digitized at a sampling rate of $T = 2000$ samples per second until complete flashover. The digitized samples were divided into frames, with blocks of data. The frame size is $N = 2048$ samples, representing about 60 cyles of the current. Digital spectral estimation methods were then applied successively to about hundreds of such frames, characterizing various stages of the flashover process. The basic idea was to establish trends in the spectral estimates, which might indicate the possibility of approaching flashover. As an illustrative example, the methods described above are applied to compute the power spectra of the leakage current waveforms in Figure 5.

2.6.1. Welch Periodogram

The periodogram power spectral density is given by

$$\hat{P}_W(f) = \frac{T}{N}\left|\sum_{n=0}^{N-1} x[n]\exp(-j2\pi fnT)\right|^2 \tag{2.4}$$

The procedure for computing the Welch periodogram is as follows:

- obtain N leakage current samples (sampling rate is T)
- subtract the means (DC level)
- select segment parameters; P segments of D samples each and overlap S between adjacent segments
- apply a Hamming window to each segment and compute the segment periodograms
- average the segment periodograms to yield the Welch periodogram
- do a *window closing* by adjusting the segment parameters for a variance/resolution trade-off

The segmentation ensures that statistically stable spectral estimates are obtained. The results are shown in Figure 6.

2.6.2. Blackman-Tukey Correlogram

The correlogram power spectral density is given by

$$\hat{P}_{BT}(f) = \sum_{m=-L}^{L} r_{xx}[m] \exp(-j2\pi f m T) \tag{2.5}$$

The Blackman-Tukey correlogram is obtained as follows:

- obtain N leakage current samples (sampling rate is T)
- subtract the means (DC level)
- select maximum lag (L) and form autocorrelation sequence(ACS) to lag L

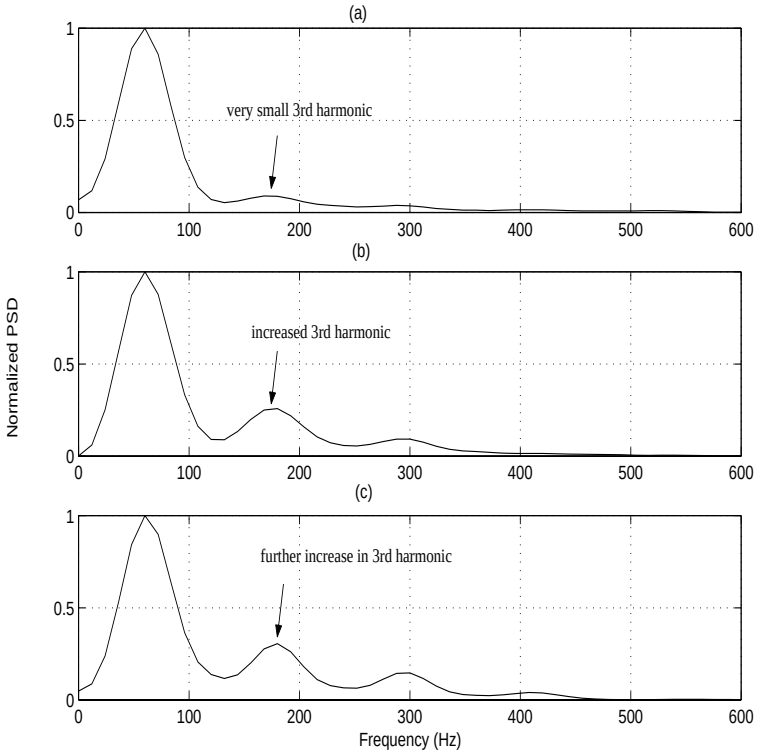

Figure 6. Welch periodogram: $N = 2048, D = 500, S = 250, P = 7$ (a) initial stages (b) mid-stages (c) final stages

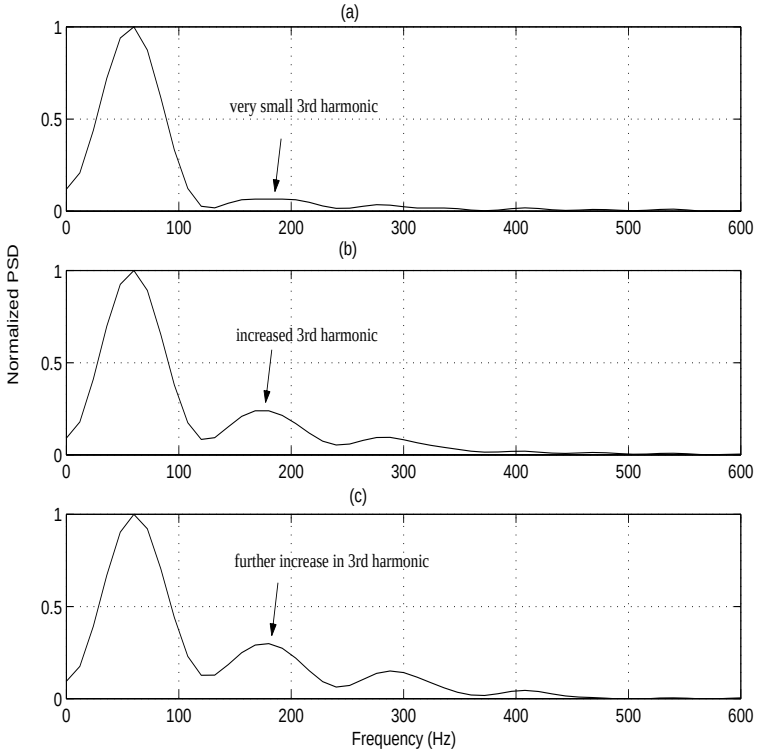

Figure 7. Blackman-Tukey correlogram: $N = 2048, L = 30$ (a) initial stages (b) mid-stages (c) final stages

- apply a Hamming lag window to the ACS and compute the Fourier transform to obtain correlogram

- do a *window closing* by adjusting the parameter L for a variance/resolution trade-off

A Hamming lag window was applied to the ACS in order to reduce leakage and also the bias in the spectral estimates. The results are displayed in Figure 7.

2.6.3. Autoregressive Spectral Estimation

The AR spectral estimation approach involves three steps. In step one, an appropriate time-series model is selected to represent the measured data. Step two consists in obtaining parameters of the model (AR coefficients). Several AR methods could be distinguished based on the algorithm used to estimate the AR coefficients from data samples. Here, three such methods are utilized: Burg's harmonic algorithm, the covariance method and the modified covariance method. In step three, the estimated parameters are inserted into the theoretical power spectral density expression to obtain the AR PSD. The AR power spectral density is given by

$$\hat{P}_{AR}(f) = \frac{T\hat{\rho}}{\left|1 + \sum_{n=1}^{p} \hat{a}[n] \exp(-j2\pi f n T)\right|^2} \tag{2.6}$$

where $\hat{a}[n]$ are the autoregressive coefficients and $\hat{\rho}$ is an estimate of the driving noise variance, also provided by all three methods.

The algorithm for AR spectral estimation is summarized below:

- obtain N leakage current samples (sampling rate is T)
- subtract the means (DC level)
- select AR model order parameter (p)
- estimate autoregressive coefficients using:
  - Burg's harmonic algorithm
  - the covariance and modified covariance methods

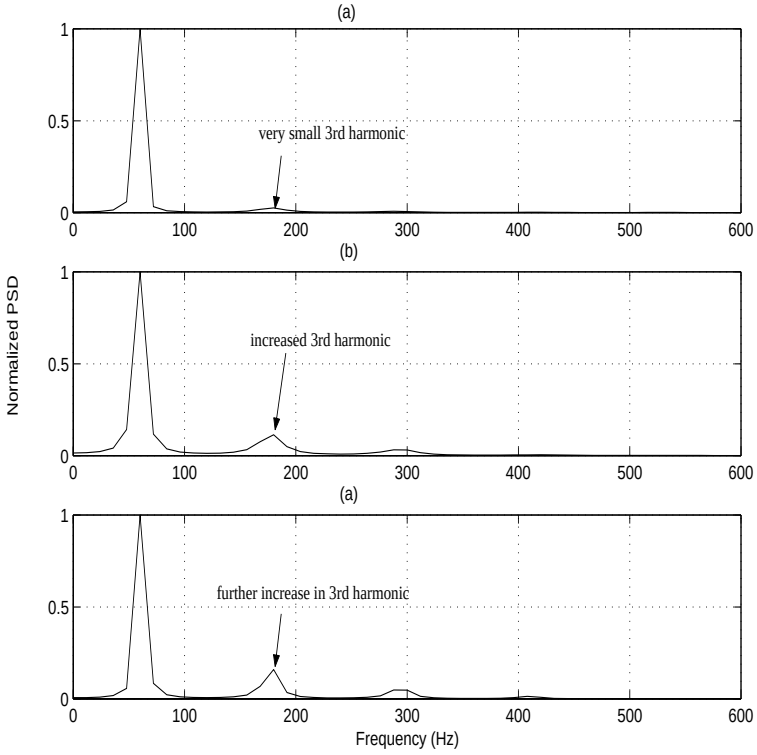

Figure 8. Burg's harmonic algorithm: $p = 20$ (a) initial stages (b) mid-stages (c) final stages

- compute AR PSD estimates
- do an *order closing* by adjusting the parameter p for a variance/resolution trade-off

Figures 8-10 show the results of the analysis for the three AR methods. A 20th-order AR process was chosen for all the three methods.

The spectral analysis methods presented above constitute basic tools for signal analysis. Each method has its own limitations, hence it was deemed extremely important to test each method's applicability to leakage current spectral analysis. All the spectral estimators performed adequately when applied to the measured leakage

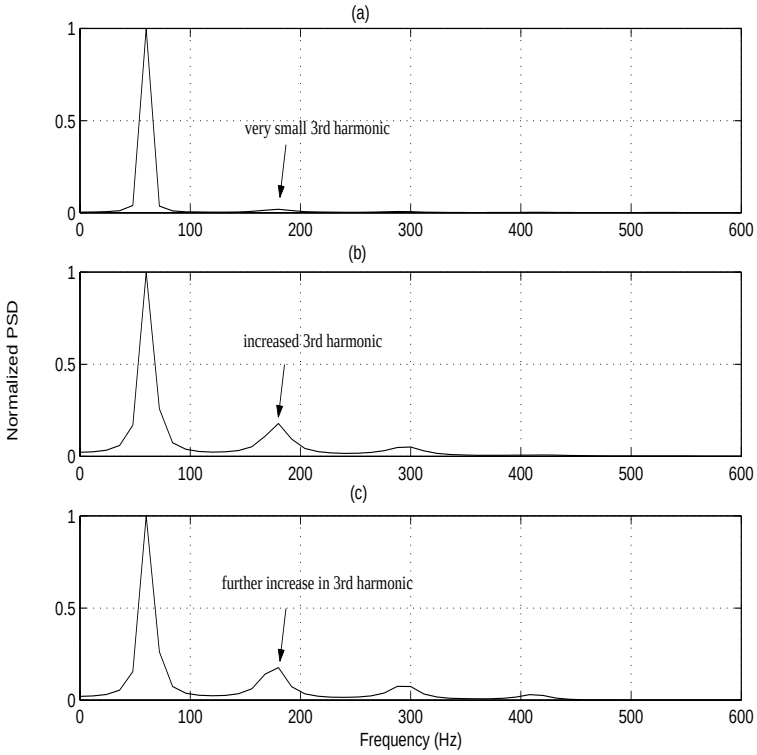

Figure 9. Covariance method: $p = 20$ (a) initial stages (b) mid-stages (c) final stages

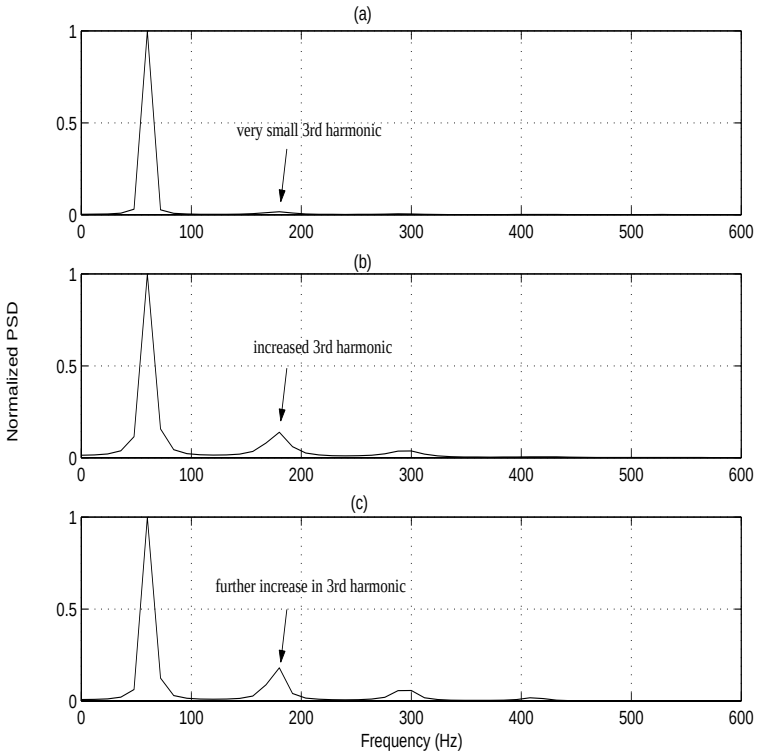

Figure 10. Modified covariance method: $p = 20$ (a) initial stages (b) mid-stages (c) final stages

current data. The superior behavior of the AR methods is manifested in the sharpness of the spectral peaks, as depicted by Figures 8-10. All the PSD curves clearly showed an emerging frequency signature as flashover is approached. They consistently showed an increase in the third harmonic content as flashover approached. The third harmonic content increased significantly just prior flashover. The ratio of the third harmonic content to fundamental, as computed by the classical methods, increased from almost zero during the initial stages to about 30% just prior to flashover. The AR estimators similarly computed a ratio of about 25%. Distinguishing features are presented below:

(i) The Welch periodogram produced very smooth spectral estimates and a small variance but the resolution at the spectral peaks was degraded due to the segmentation.

(ii) The correlogram was characterized by sidelobes, some of which produced negative PSD estimates (untrue PSD values). The PSD estimates were unbiased as the maximum lag L was increased. The resolution at the spectral peaks also increased with the maximum lag L, hence the performance depended very much on L.

(iii) All the AR methods were similar, typified by very sharp spectral peaks and a much more reduced variance in the PSD estimates (five times less than that of the periodogram).

Due to the small variance, high resolution at the spectral peaks and ease of computation, AR modeling and in particular, the Burg harmonic algorithm was fa-

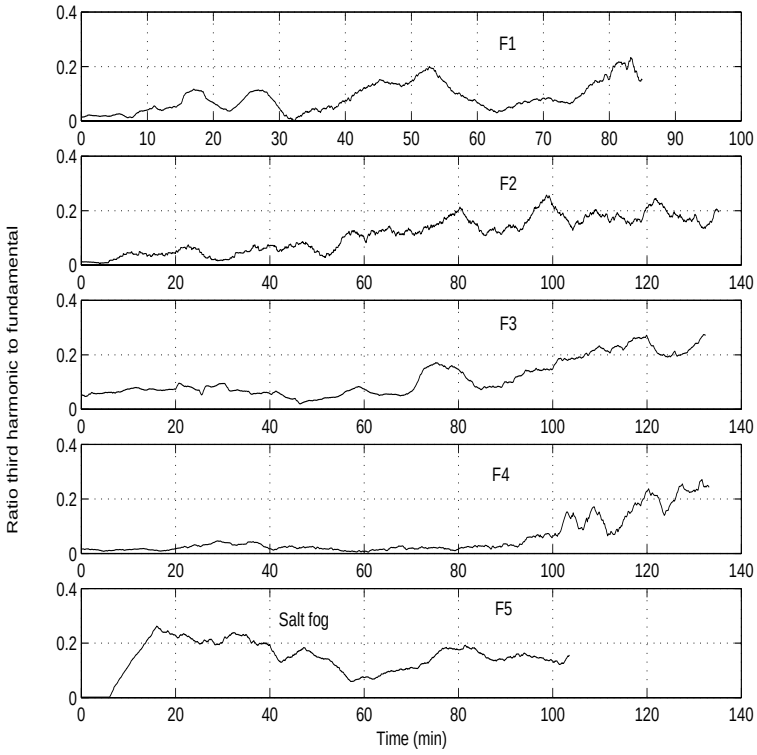

Figure 11. Temporal variation of ratio of third harmonic to fundamental for flashover cases

vored for subsequent power spectral analysis. This algorithm was used to estimate the time-trend of the ratio of third harmonic to fundamental for leakage current recorded during withstand and flashover tests. These temporal variations are shown graphically in Figures 11-14; the tests designated F1-F5 are for flashovers and W1-W5 are for withstands. Figures 13 and 14 show the flashovers and respectively, withstands superimposed on each other. F5 and W5 are salt fog tests and the rest clean fog. The displayed salt fog test had a heavy scintillation activity 20 minutes into the experiment; probably due to the very rapid decrease in the surface resistance of the insulator as a result of the high salt concentration. W4 is a very light naturally contaminated insulator.

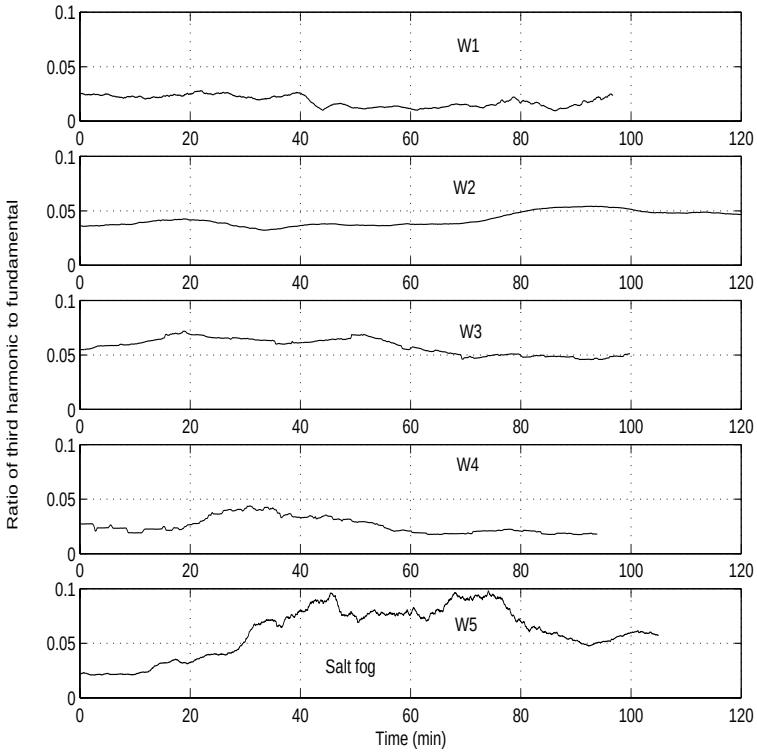

Figure 12. Temporal variation of ratio of third harmonic to fundamental for withstand cases

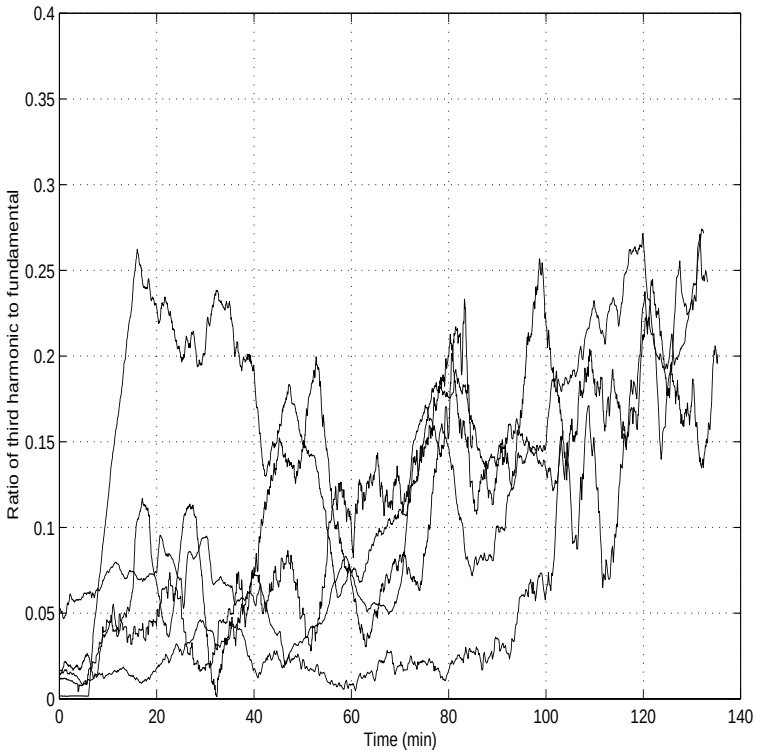

Figure 13. Temporal variation of ratio of third harmonic to fundamental for flashover cases (superimposed)

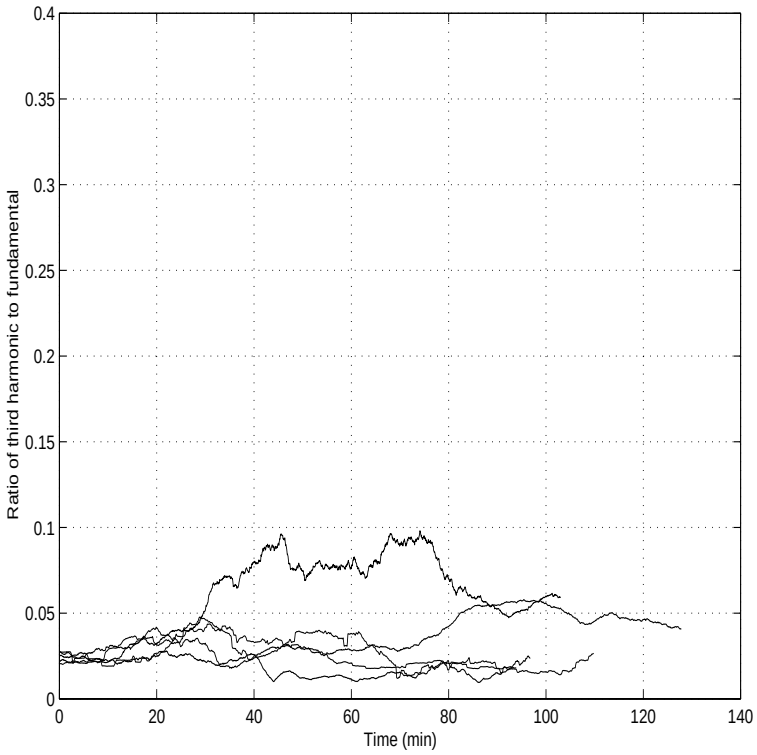

Figure 14. Temporal variation of ratio of third harmonic to fundamental for withstand cases (superimposed)

Observing the graphs of Figures 13-14, the individual points of the curves seem to exhibit random erratic fluctuations. These could be averaged out in order to expose the time-trend of the data, through use of a moving average. The technique used is a variation of the Holt-Winters method [56]. This averages P nearest neighboring points and the general formula is given by

$$\begin{aligned} y_0 &= x_1 + x_2 + ... + x_P \\ y_t &= \frac{1}{P}[y_{t-1} + (x_{P+1} - x_1) + (x_{P+2} - x_2) + ... + (x_n - x_{n-P})] \end{aligned} \tag{2.7}$$

where y is the trend and x is the raw data. A 50-point ($P = 50$) moving average is used to obtain general trends in the temporal variation of the ratio of third harmonic to fundamental. These are depicted in Figure 15 for both flashover and withstand cases. From the graphs, the effect of the smoothing is noticeable; the ratio tends to increase in the flashover case whereas in the withstand case, it peaks at some point and later decreases. For flashover, arcing is sustained and the continuous train of current peaks observed is rich in harmonics, hence this tendency.

2.7. Conclusions and Discussion

This chapter has presented the results of experimental measurement and analysis of leakage current obtained from artificially polluted insulators. A visual observation of a complete time-domain record of leakage current shows very erratic changes in peak current and also current waveshape. This prompts performing a comprehensive mathematical signature analysis of the current waveforms in order to capture trends which can be used to predict approaching flashover. Different digital spectral

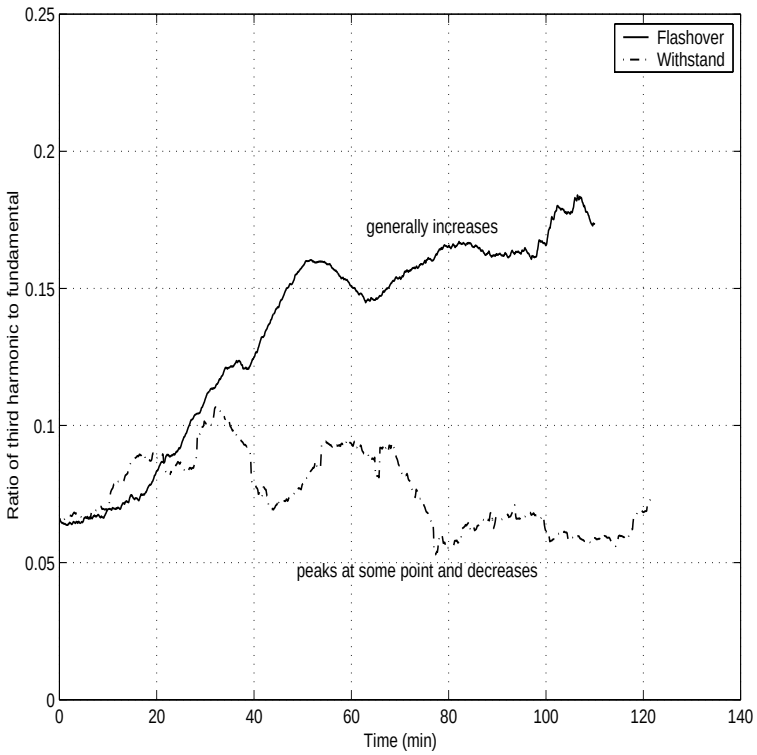

Figure 15. Time-trend of the ratio of third harmonic to fundamental using the Holt-Winters moving average

estimations techniques were employed to obtain the spectral content of the leakage current waveforms. This exploratory data analysis showed that the ratio of third harmonic to fundamental increases from almost zero at the start of the experiment to about 30% near flashover of the insulators. Even though the time-trend of this ratio varies, there is a considerable data reduction and this could facilitate the next phase of the signature analysis, of which spectral analysis is an intermediate phase.

In conclusion, the leakage current has random fluctuations in magnitude and shape, no two time histories are exactly the same and also the spectral content varies with time. This necessitates using statistical (probabilistic) signature analysis methods, which is the subject of a subsequent chapter.

CHAPTER 3

Linear Stochastic Analysis

3.1. Introduction

The experimental work in the previous chapter has shown that the measured leakage current of polluted insulators exhibits erratic changes in magnitude and shape. Numerous publications [21–25, 32] attribute this behavior to a flashover process that is non-linear and predominantly random in nature; the surface discharges are non-linear arcs, the contamination levels, wetting rate and also leakage current density are all non-uniform. Also the width and number of dry-bands, the formation of partial arcs and position of the partial arcs along the dry bands are all statistically random. Obviously, the underlying process is stochastic, and the magnitude of the leakage current at any chosen time cannot be precisely predicted. However, given a time history of leakage current, it could be characterized by statistical or probabilistic properties. Appropriately, the focus of this chapter is the evaluation of the stochastic properties of the leakage current in terms of the its level crossings and also a statistical characterization of its large peak values (extremes).

One of the traditional flashover prediction methods is the measurement of

leakage current peaks and prediction of the flashover when the peak current is larger than 100 mA [1, 13]. Another technique is to record the peaks of the leakage current for long periods and to use the statistical distribution of the peaks to make decisions about the pollution severity or approaching flashover. The reliability of both methods is questionable and these methods have found limited application. Observation of the leakage current profile on an oscilloscope shows that the current amplitude and shape vary randomly. However, variations in the leakage current envelope provide better information about insulator performance than just the instantaneous peak values.

Level crossing analysis [40–42] has been applied to study the dynamics of time-varying signals in different engineering fields including prediction of fatigue and failure. The motivation here is that, the leakage current has intermittent large peaks for withstand tests, whereas it has a continuous train of large peaks for the flashover case. Thus, the leakage current exceeding very high thresholds occurs only with intensive discharge activity and for only a very short interval may have hardly any deleterious effect, while a longer duration may cause flashover. In other words, the crossings and duration above very high thresholds play an important role in determining flashover. The level crossing problem is formulated in terms of mean crossing rates of the current envelope at specified high thresholds and the level crossing activity (LCA) at these high thresholds.

Extreme value theory is a well-established field used extensively to dimension structures that must withstand extreme environmental phenomena such as floods, earthquakes and sea waves [42–46, 59]. A major application is that if only the largest

events are considered from each of a number of equal time intervals, then the distribution of these largest events follows one of three asymptotic types (Gumbel, Weibull and Frechet). Here, extreme value distributions are used to the model the large excursions of the peaks of the leakage current envelope. Once the best fit is established, it is straightforward to further characterize the large peaks which occur rarely (low exceedance probability), but contribute substantially to flashover of the insulator. This is expressed in terms of an extreme value risk function (EVRF).

3.2. Analytic Envelope Process of the Leakage Current

The leakage current of the polluted insulator is continuously digitized till flashover. The procedure here is to perform a signature analysis of the current envelope due to the achievable data reduction. A common and very efficient analytic technique for envelope detection, obtained from the digitized samples of leakage current, is based on the Hilbert transform [55]. The current can be considered band-limited because the dominant harmonics are up to about the 7th harmonic (bandwidth is 500 Hz). For the band-limited current signal $i(t)$, the Hilbert transform is the convolution of the signal with the inverse of time and is given by

$$\tilde{i}(t) = \mathrm{H}[i(t)] = \frac{1}{\pi}\, i(t) \otimes \frac{1}{t} = \frac{1}{\pi} \int_{-\infty}^{\infty} \frac{i(\tau)}{t-\tau}\, d\tau \tag{3.1}$$

The Hilbert transform provides a 90 degrees phase shift to its input. The sum of the original leakage current and its phase shifted Hilbert transform form a complex analytic signal, $i_a(t)$. One of the properties of the Hilbert transform [55] is that the

modulus of this analytic signal gives the envelope of the leakage current, $i_{env}(t)$. The equation describing the envelope is given by (3.2).

$$\begin{aligned} i_a(t) &= i(t) + j\tilde{i}(t) \\ i_{env}(t) &= |i_a(t)| = \sqrt{i(t)^2 + \tilde{i}(t)^2} \end{aligned} \tag{3.2}$$

A simple method to calculate the Hilbert transform and the envelope is through the use of the FFT of the measured current. From (3.1), taking the FFT of both sides and noting that convolution in time equals multiplication in frequency,

$$FFT[\tilde{i}(t)] = FFT[i(t)] * FFT[1/\pi t] = I(f)[-j\text{sgn}(f)] \tag{3.3}$$

where $FFT(\cdot)$ represent Fast Fourier transform and $I(f)$ is the FFT of $i(t)$. Similarly, the FFT of the analytic leakage current signal is given by

$$FFT[i_a(t)] = FFT[i(t) + j\tilde{i}(t)] = I(f)[1 + \text{sgn}(f)] \tag{3.4}$$

hence

$$i_a(t) = FFT^{-1}\{I(f)[1 + \text{sgn}(f)] \tag{3.5}$$

The procedure for computing the envelope is:

- Obtain digitized samples of the leakage current.
- Divide into 1-minute segments. Figure 16 shows the leakage current and its envelope for part of a segment.
- Compute the Hilbert transform and envelope using the FFT as outlined above.

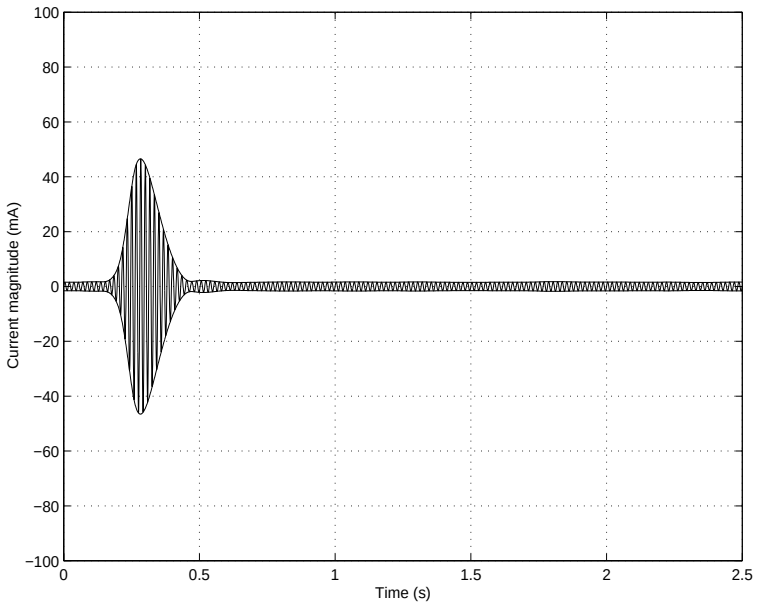

Figure 16. Section of the leakage current envelope for non-flashover case (0.1 ESDD)

Equation (3.3) gives the upper envelope curves of Figures 16 and 17. This is currently the procedure employed to compute the envelope from the measured leakage current. Unfortunately, this requires FFT calculations which is computationally expensive in real-time. Hence, a simpler and fairly accurate envelope detector, which utilizes a low-pass filtered version of a full-wave rectified leakage current, would be incorporated into our data acquisition system. The envelope so realized is a low frequency, slow-varying signal and a lower sampling rate could be used, resulting in an achievable data reduction.

3.3. Probability Density (Distribution) Function of the Envelope

In order to apply the statistical methods discussed above, a probability distribution (density) function of the envelope is required. The probability $P[E]$ of an event

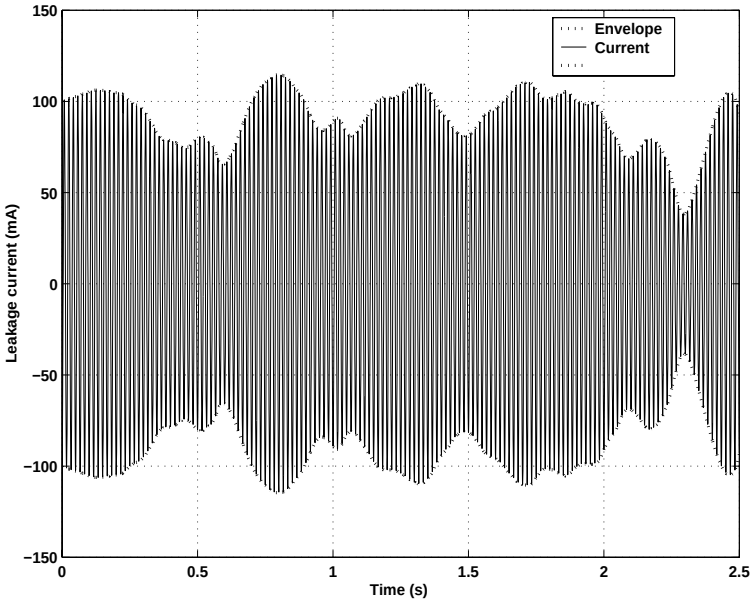

Figure 17. Section of the leakage current envelope for flashover case (0.15 ESDD)

E is defined as the number of times the event n_E occurs out a possible n repeated trials i.e.

$$P[E] = \lim_{n\to\infty} \frac{n_E}{n} \tag{3.6}$$

The probability distribution function (PDF) or cumulative distribution function (cdf), $F(x)$, of the random variable X is the probability of the event $X \leq x$ and is given by

$$F(x) = P[X \leq x] \tag{3.7}$$

The probability density function (pdf), $f(x)$, of the distribution function $F(x)$, is the derivative (if it exists) and is given by

$$f(x) = \frac{d\,F(x)}{dx} \tag{3.8}$$

The probability density function (pdf) of the underlying flashover process that generates the leakage current is unknown, due to the inherent complexity of the process. Since only digitized samples of the current are available, it is required to estimate the pdf from these observed data. The technique is to form the empirical (sample) distribution function using the histogram, apply different parametric models to the data and then using a statistical goodness-of-fit test, determine which model best fits the data. This was done using the Normal, Lognormal, Rayleigh, Gram-Charlier and Weibull distributions with both the chi-squared and the Kolmogorov-Smirnov goodness-of-fit tests. Using this technique, two competing models (Weibull and Gram-Charlier) were found to be superior. However, the modal values of the pdf were displaced by as much as 10 mA, hence it became imperative to use other methods as described below.

3.3.1. Non-Parametric Probability Density Estimate

The probability density function of the measured leakage current is not known and needs to be estimated from the sampled data. The histogram is one of the most common ways of representing the pdf from observed data samples. However, the general kernel density estimator is proven to be mathematically more efficient [49, 50] and has a smoothing effect. The kernel estimator provides a smoothed estimate of a pdf in analytical form as

$$\hat{f}(z) = \frac{1}{nh(n)} \sum_{i=1}^{n} K\left(\frac{z - z_i}{h(n)}\right) \tag{3.9}$$

where n is the sample size, K is a weighting function (kernel), $h(n)$ is a smoothing factor (also called window width or bandwidth). The idea behind these estimators is that each observed sample, z_i, is replaced by a function of z_i and the functions are summed up to yield the estimate of the density, $\hat{f}(z)$. The kernel, K, determines the shape of the functions while the window width, h, determines their width. The effect of varying the smoothing factor is to make the pdf very spurious for small h and to obscure all detail as h becomes large. There are also a lot of adaptive methods to adapt the amount of smoothing to the 'local' density of the data. In order for the pdf to be valid, $h(n)$ and $K(z)$ must satisfy

$h(n) > 0, \quad K(z) \geq 0, \quad \int_{-\infty}^{\infty} K(z) = 1$

The Epanechnikov kernel, with kernel function given by (3.10), has been shown to be optimal with respect to the *asymptotic mean square error*.

$$K_e(z) = \frac{3}{4\sqrt{5}}\left(1 - \frac{1}{5}z^2\right) \quad -\sqrt{5} \leq z \leq \sqrt{5}, \quad \text{zero} \quad \text{otherwise} \tag{3.10}$$

It is also asymptotically unbiased (3.11) and strongly consistent (3.12):

$$\lim_{n\to\infty} E[\hat{f}(z)] = f(z) \tag{3.11}$$

$$\lim_{n\to\infty} \hat{f}(z) = f(z) \tag{3.12}$$

where E denotes expectation and $f(z)$ is the true pdf. For subsequent analysis, comparisons and also for illustrative purposes, the Epanechnikov kernel pdf estimate is used to compute the pdf and via a numerical integration technique, the empirical distribution function (PDF) is obtained.

3.3.2. Parametric Density Estimate

An approximate parametric description of the pdf of the envelope can be obtained by using (3.2). The probability density of the envelope, $i_{env}(t)$, is calculated as a function of two random variables; the measured current and its Hilbert transform i.e., $i(t)$ and $\tilde{i}(t)$, respectively. Assuming that $i(t)$ and $\tilde{i}(t)$ are Gaussian processes with equal variance ν^2 and means m_1 and m_2 respectively, the joint distribution function of the random variables $i(t)$ and $\tilde{i}(t)$ is:

$$f(i,\tilde{i}) = \frac{1}{2\pi\nu^2}\exp\left[-\frac{1}{2}\left\{\left(\frac{i-m_1}{\nu}\right)^2 + \left(\frac{\tilde{i}-m_2}{\nu}\right)^2\right\}\right] \tag{3.13}$$

With the change of variables

$i = z\cos\Theta, \quad \tilde{i} = z\sin\Theta, \quad \lambda^2 = m_1^2 + m_2^2, \quad z > 0, \quad 0 \le \Theta \le 2\pi,$

the Jacobian of the transformation is z (the dependence on t has been dropped for convenience). By definition, the marginal distribution of z is calculated by integrating over all Θ:

$$F(z) = \frac{1}{\nu^2}\exp\left[\frac{1}{2}\left(\frac{\lambda}{\nu}\right)^2\right] \int_0^z dz\; z\exp\left[\frac{1}{2}\left(\frac{z}{\nu}\right)^2\right] I_0\left(\frac{\lambda z}{\nu^2}\right) \tag{3.14}$$

Noting that $z = \sqrt{i^2+\tilde{i}^2} = i_{env}$ and observing the integrand above, the probability density function of the envelope is given by

$$f(z) = \frac{z}{\nu^2}\exp\left(-\frac{z^2+\lambda^2}{2\nu^2}\right) I_0\left(\frac{z\lambda}{\nu^2}\right), \quad z > 0 \tag{3.15}$$

where

$I_0(x) = \frac{1}{2\pi}\int_0^{2\pi} e^{x\cos\Theta}\, d\Theta$

is called the zero order modified Bessel function of first kind. The parameters λ and ν can be estimated from data using the method of moments as described in Appendix B. These parameters are related to the second and fourth moments by the polynomials

$$E[z^2] = 2\nu^2 + \lambda^2 \tag{3.16}$$

$$E[z^4] = 8\nu^4 + 8\nu^2\lambda^2 + \lambda^2 \tag{3.17}$$

Hence the estimates are given by

$$\hat{\lambda}^2 = \sqrt{E^2[z^2] - E[z^4]} \tag{3.18}$$

$$\hat{\nu}^2 = E[z^2] - \hat{\lambda}^2 \tag{3.19}$$

As later sections will show, the data is generally multi-modal and only a mixed distribution (probably both discrete and continuous distributions) will provide a global best fit. However, for all intents and purposes, this unimodal non-central Rayleigh distribution worked very well especially for data samples greater than 20 mA. Figure 18 shows probability density functions for using non-central Rayleigh and Epanechnikov kernel (smoothing parameter $h(n) = 30$) for the waveform of Figure 16.

3.4. Numerical Results

Several flashover tests were conducted on a string of four artificially contaminated ceramic insulators, energized at 50 kV, in a laboratory fog chamber. The contamination levels were from 0.05, 0.1 and 0.15 ESDD. The insulators were energized and wetted by fog for 1-2 hrs or until flashover of a withstand occurred. During

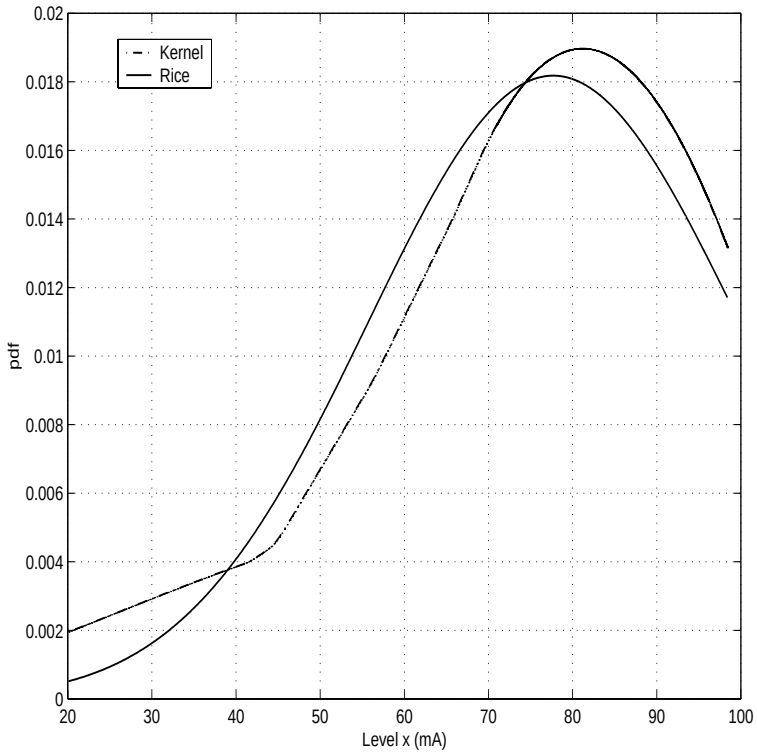

Figure 18. Epanechnikov kernel pdf estimate (dotted) and non-central Rayleigh pdf estimate (solid) for waveform of Figure 16

this tests the leakage current was continuously recorded with the data acquisition system. Using the digitized samples of leakage current, the analytic envelope is computed through the Hilbert transform, over one-minute segments. Here, z represents the samples of the envelope, $i_{env}(t)$, obtained through the Hilbert transform. In the following pages, sample calculations are rendered to illustrate the application of the stochastic analysis to the leakage current envelope. Since several leakage current recordings were obtained, the calculations are done for one time history and similar calculations for all others tabulated for comparison. The leakage current considered is for a string of four insulators, contaminated to a level of 0.15 ESDD and energized at 50 kV.

3.4.1. Level Crossing Analysis of the Envelope

The level crossing problem deals the expected number of times a trajectory crosses an arbitrarily level in a prescribed time [40–42]. In particular, this analysis estimates the mean crossing rate (upcrossing and downcrossing) of the leakage current envelope $z(t)$ at a fixed level a in time T. The mean number of crossings per unit time of the level $z = a$ by the envelope of the leakage current is given by the Rice equation [40]:

$$E[N_a] = \int_{-\infty}^{\infty} |\dot{z}|\ f(z, \dot{z})\ |_{z=a}\ d\dot{z} \tag{3.20}$$

where $f(z, \dot{z})$ is the joint probability density function of the envelope $z(t)$ and its derivative process, $\dot{z}$, at equal moments in time t.

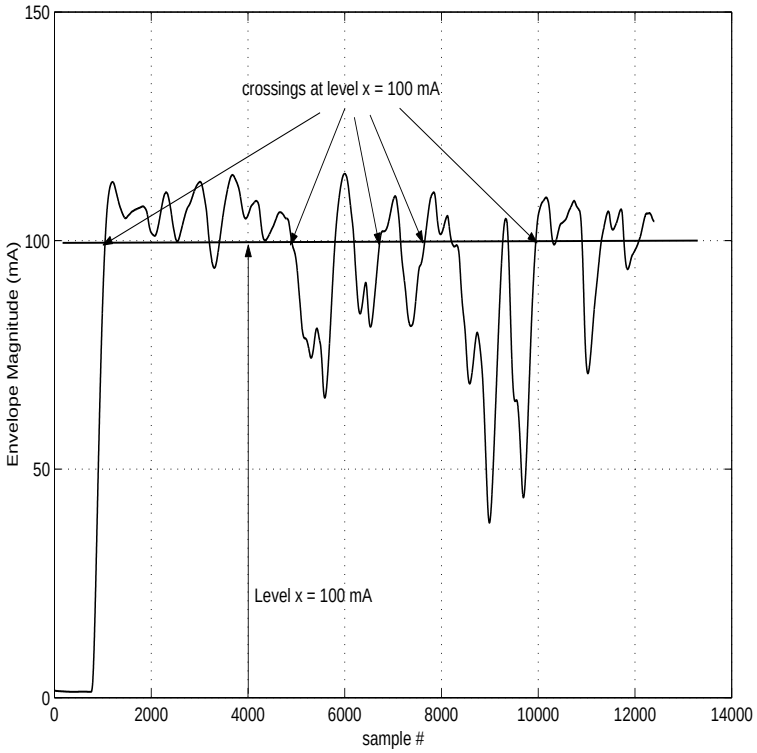

Figure 19. Illustration of level crossings of the leakage current envelope at z = 100 mA.

Figure 19 illustrates the crossing rate of the envelope at a level, $z = 100$ mA. A simple oscillation count will show that there are 9 upcrossings (crossings with positive slope) and 8 downcrossings (crossings with negative slope) giving a total of 17 crossings of the level, $z = 100$ mA. Since the total duration represents 10 seconds of data, the mean crosssing rate is 1.7 s^{-1}.

The motivation here is that, there is a considerably increase in the leakage current magnitude, with the increase in intensity of arcing activity. However, the leakage current for the withstand (non-flashover) has intermittently large peaks whereas the flashover case exhibits a continuous train of large peaks. Obviously, the mean crossing rate at high thresholds (large peaks) will be much higher for the continuous train than

the intermittent. The fluctuations in the envelope are invariably nondeterministic, however with this analysis, it is hoped that minimum crossing rates at specified high levels could be established which might indicate the imminence of flashover.

For this analysis, the mean crossing rate is computed using:

(i) cycle counts to form the empirical crossing spectrum (exact method)

(ii) a closed form functional relationship involving the pdf (approximate method).

3.4.2. Empirical Crossing Spectrum (ECS)

The empirical crossing spectrum $N(a)$ is defined as the number of times the envelope $z(t)$ crosses the level $z = a$ as a function of a. The ECS is formed using a counting distribution as defined below:

$$N(a) = \sum_i I_{(m,n)}(a) \tag{3.21}$$

where the indicator function $I_{(m,n)}(a) = 1$ if $m < a < n$, and zero otherwise. Obviously, the crossing spectrum is a stepwise constant discontinuous function.

A closed-form expression can also be obtained for the crossing rates by using the Rice equation of (3.20) and the probability density function derived in the previous section. Considering the envelope process to be a wide-sense stationary (WSS) differentiable random process, assume that the process and its derivative process are statistically independent, then the joint density function is given by

$$f(z, \dot{z}) = f(z) f_1(\dot{z}) \tag{3.22}$$

where $f(z)$ is the probability density function of the envelope from (3.15) and $f_1(\dot{z})$ is the pdf of the derivative. The pdf of the derivative is assumed Gaussian:

$$f_1(\dot{z}) = \frac{1}{\sqrt{2\pi\nu_{\dot{z}}^2}} \exp\left(-\frac{\dot{z}^2}{2\nu_{\dot{z}}^2}\right) \tag{3.23}$$

With this assumption, the mean crossing rate is

$$\begin{aligned} E[N_a] &= \int_{-\infty}^{\infty} |\dot{z}|\ f(z,\dot{z})\ |_{z=a}\, d\dot{z} \\ &= f(z)\,|_{z=a} \int_{-\infty}^{\infty} |\dot{z}|\ f_1(\dot{z})\ d\dot{z} \\ &= \frac{2}{\sqrt{2\pi}}\lambda\nu_{\dot{z}} \exp\left(-\frac{a^2+\lambda^2}{2\nu^2}\right) I_0\left(\frac{z\lambda}{\nu^2}\right) \end{aligned} \tag{3.24}$$

where

$$\nu_{\dot{z}}^2 = -\frac{d^2R(\tau)}{d\tau^2}\bigg|_{\tau=0} \tag{3.25}$$

is the variance of the derivative process and $R(\tau)$ is the correlation function of the digitized leakage current envelope. The variance of the derivative process can also be obtained using moments of the power spectrum.

Figure 20 shows a typical empirical crossing spectrum of the envelope (0.1 ESDD, time duration-2 hrs). The graph shows a lot of crossing at smaller thresholds (understandably, this is due to the sinusoidal nature of the leakage current variation), which masks the effects of the crossings at higher levels. Hence, Figures 21-23 only show crossing rates above 40 mA. Figures 21 and 22 depict crossing rates for withstand and flashover tests respectively. The crossing rates for thresholds above 60 mA drop off more rapidly for the withstand cases, than those for flashover. Inherently, sustained arcing which may lead to flashover creates a continuous train of

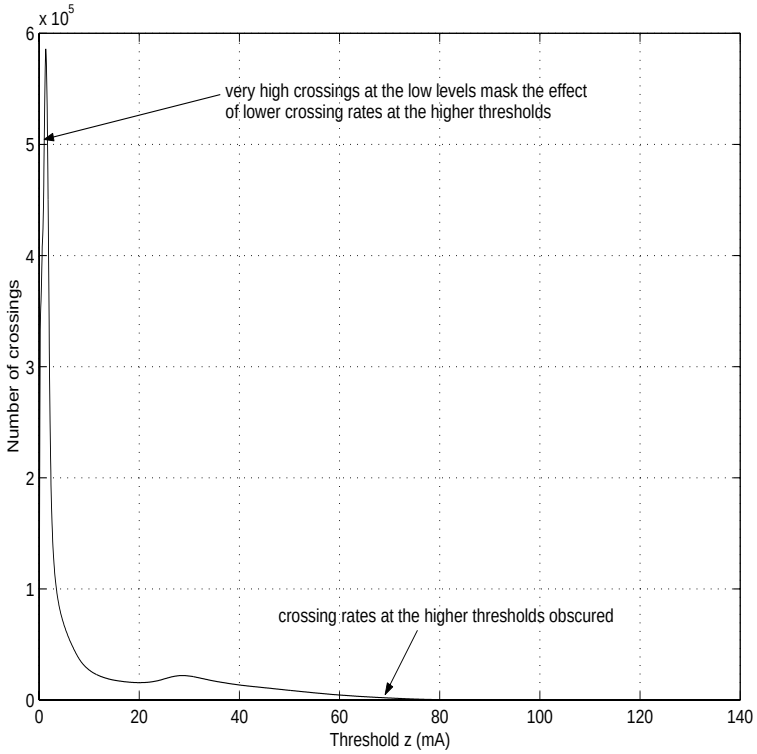

Figure 20. Empirical crossing spectrum for the whole range of current magnitude, 0.1 ESDD

large current peaks; consequently the higher crossing rates at these high peaks. In the case of a withstand, disruptive discharges intermittently produce large current peaks albeit fewer than the flashover case and this explains the more rapid fall off in crossing rates at the higher thresholds.

3.4.3. Extreme Value Analysis of the Envelope

Extreme value (EV) analysis primarily deals with asymptotic distributions of the maxima and minima of random variables. Here, EV modeling is applied to the right tails of the distribution functions describing envelope in order to access its extremal behavior, especially during periods when there is intensive arcing leading to

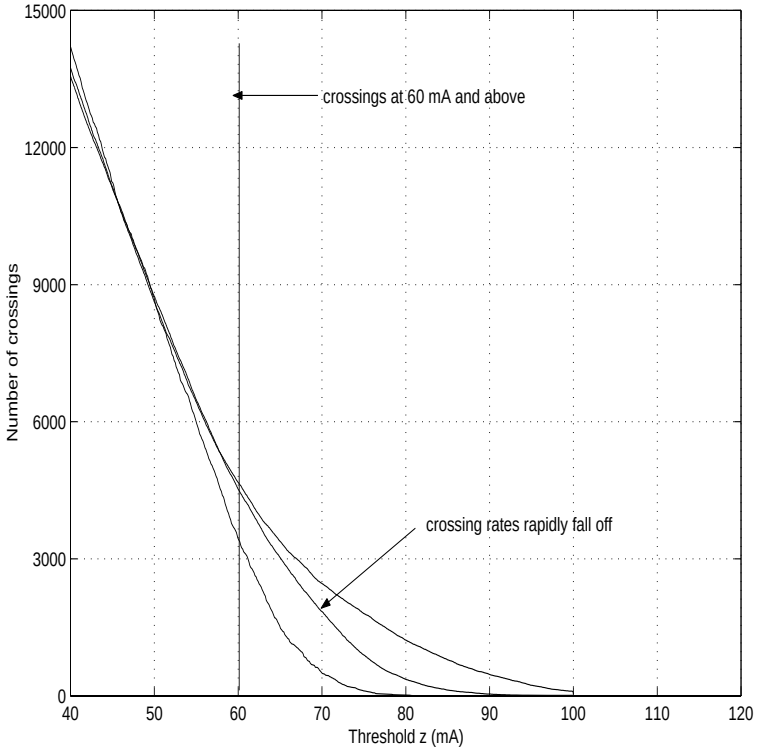

Figure 21. Empirical crossing spectrum for withstand cases, 0.1 ESDD

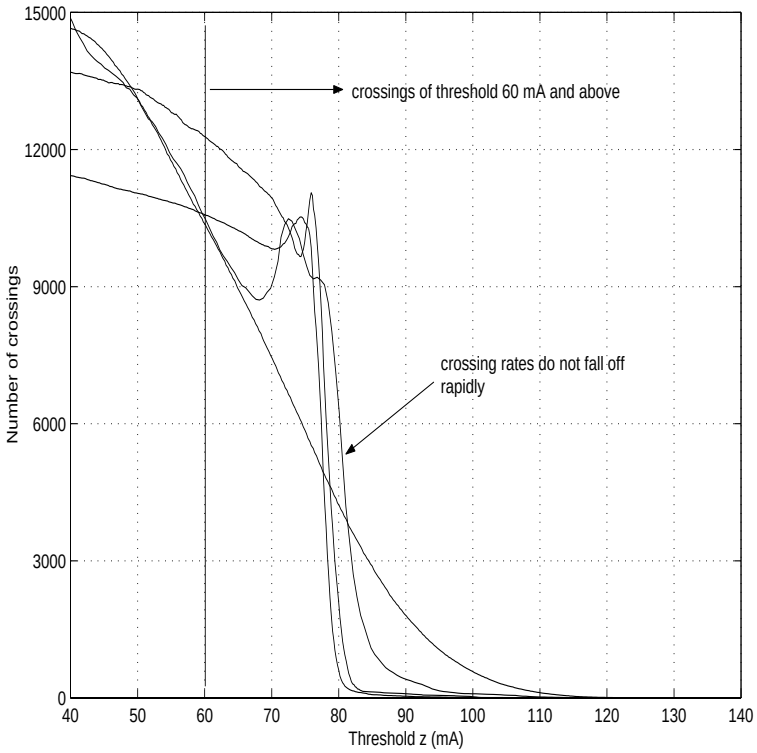

Figure 22. Empirical crossing spectrum for flashover cases, 0.15 ESDD

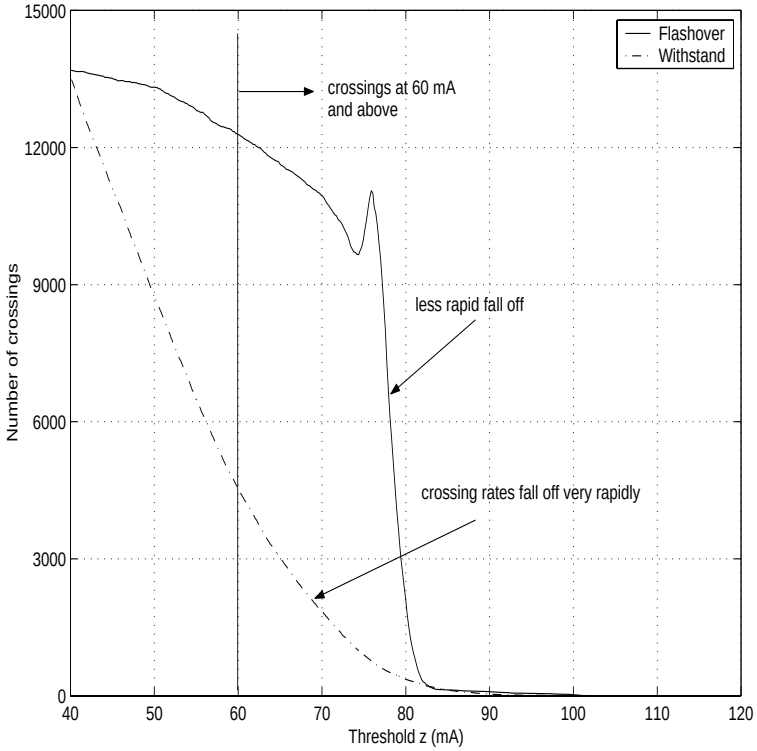

Figure 23. Comparison of mean crossing rates for flashover and withstand cases

flashover. This entails using EV analysis to assess the probable largest value to occur in a specified time, to predict amplitudes which occur with low exceedance probability and also to calculate a measure of the severity of these characteristic large peaks. The principal issues in considering this type of analysis include:

- there are very few observations in the tail of the distribution
- given one time history, estimates are required to be predicted beyond z_{max}, the largest observed data value
- standard distributions fit well where the data has greatest density and can be severely biased in estimating tail probabilities

The probability density function of the envelope follows the general class of exponential distributions. Thus it belongs to the domain of attraction of the Asymptotic Type I Extreme Value Distribution (Gumbel distribution) with density and distribution functions given by

$$\begin{aligned} g(z) &= \alpha \exp[-\alpha(z-u) - e^{-\alpha(z-u)}] \\ G(z) &= \exp[-e^{-\alpha(z-u)}] \end{aligned} \tag{3.26}$$

The parameters of the Gumbel distribution, α (called the scale parameter) and u (location parameter), can estimated from data using maximum likelihood estimation (MLE) techniques, outlined Appendix B. First, the peak value of the envelope is sampled every second and the data parameterized over one-minute segments to obtain EV distribution parameters. To calculate the EV parameters, a threshold value needs to be set, above which data samples are considered extreme. A critical issue is the

appropriate selection of this threshold: setting this threshold too high means there might not be enough data to obtain good estimates of α and u. However, a small value will also bias the estimates. A combination of two methods was employed:

- subsample of data which exceed the 95^{th}-percentile of the empirical distribution [45]
- $20\sqrt{n}$ (n = data size) top values when data is arranged in descending order [47]

Both gave a threshold value close to 104 mA, hence all values larger than 104 mA are considered extreme. Figure 24 displays the Gumbel density and distribution functions compared to the Epanechnikov kernel estimator (empirical), conditioned on $z > 104$ mA. Using only the extreme values, the maximum likelihood estimates of the parameters of the Gumbel distribution are $\alpha = 0.4814$ mA^{-1} and $u = 106$ mA. The interpretation is that, the most probable largest magnitude of the envelope (a random variable) is $u = 106$ mA and the mean value of this largest magnitude is $mean = u + 0.5772/\alpha = 107.2$ mA, with $variance = \pi^2/6\alpha^2 = 9.38$ mA^2. The 95% confidence interval is [106.8 mA,107.6 mA].

3.5. Flashover Prediction Techniques

3.5.1. Level Crossing Activity (LCA)

Several time histories of leakage current exhibit a typical behavior: with arcing appear isolated peaks, the frequency of appearance of the peaks increases with increase in the intensity of arcing activity. Just prior to flashover, the current modifies

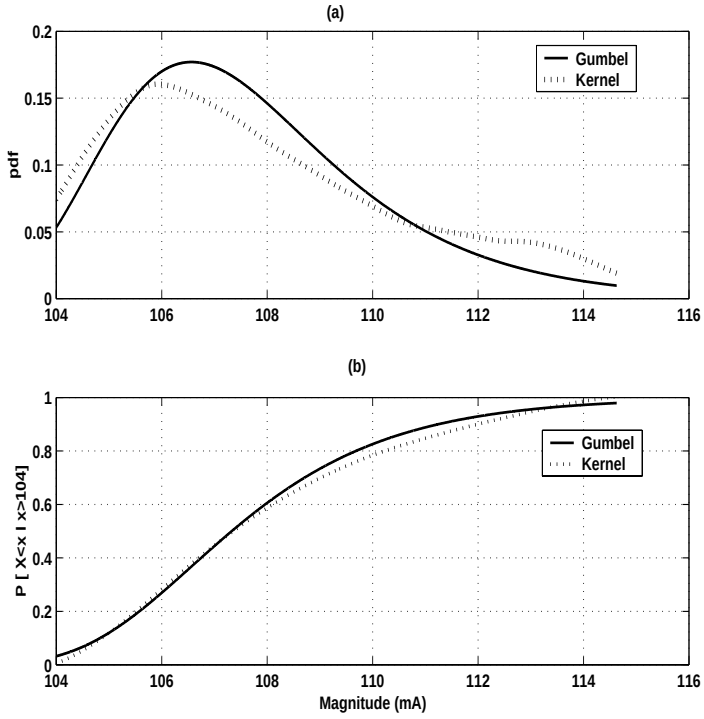

Figure 24. Comparison of fitted Gumbel distribution (solid) to empirical (dotted) for extreme peaks of the envelope, conditioned on $z > 104$ mA (a) probability density function (b) probability distribution function

to a train of peaks with a distributed character. The relative magnitude of the peaks also increases significantly near flashover. Thus, the crossings at high levels occur most frequently with upcoming flashover and hence, the mean time spent (denoted by τ_a) above a specified high threshold is candidate for flashover prediction. Here, τ_a, is formulated as the mean time between successive crossings of the same level a and is called the level crossing activity (LCA). The bigger the value of the LCA, the greater the risk of flashover. The LCA is defined as the ratio of the probability that the leakage current envelope is above the level a to the mean crossing rate at that level i.e.,

$$\tau_a = \frac{P[z(t) > a]}{E[N_a]} \tag{3.27}$$

The original proposal was to perform a multi-level crossing analysis, whereby crossings of different levels are obtained and a statistical mean calculated. However, since the ultimate goal is to implement a real-time system, CPU time is determining factor. Evidently, a single level crossing analysis algorithm requires less CPU time than the multi-crossing. In order to reliably determine which level a to use for the crossing analysis, a simple procedure involving the probability density function was employed. A period of intense arcing with no flashover results in a pdf with modal value μ_1 (say). The onset of flashover shifts the modal value to another value different from μ_2. Figure 25 demonstrates the procedure, with plots of the two pdfs and a decision boundary, arbitrarily set as the intercept of the two pdfs. This method gave a level $a = 92$ mA, thus the level crossing activity at 92 mA, τ_{92}, is the flashover

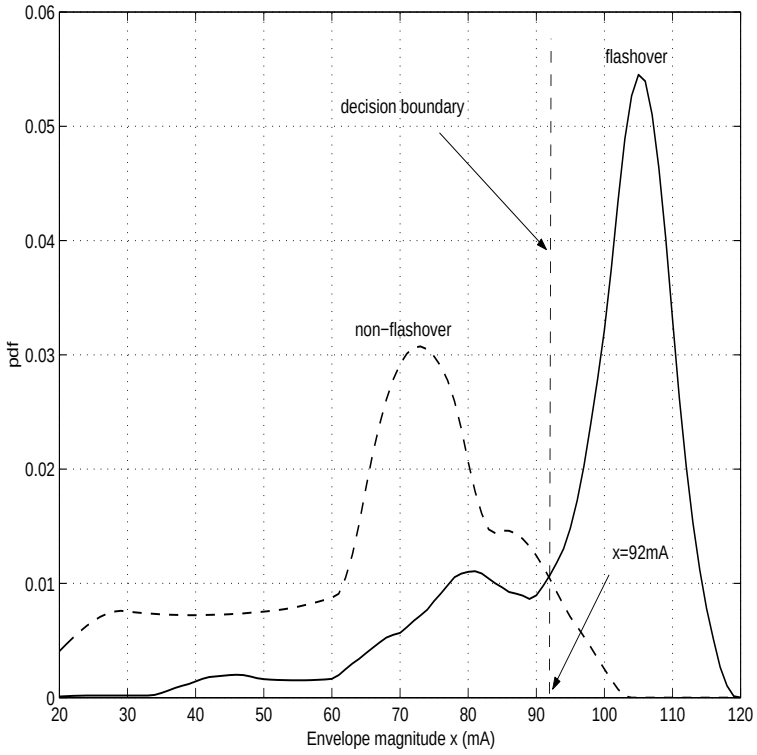

Figure 25. Determination of arbitrary level for crossing analysis using pdf for non-flashover envelope (dotted) and pdf for flashover (solid)

prediction criterion:

$$LCA = \tau_{92} = \frac{P[z(t) > 92]}{E[N_{92}]} \tag{3.28}$$

Results for LCA calculations are tabulated in Table 5. The inference from the flashover cases is that, the mean time duration for which the leakage current envelope staying above 92 mA will sufficiently cause flashover, is 100 ms. The algorithm for calculating the LCA is as follows:

1. Obtain digitized samples of the current envelope.

2. Using frames of 1-minute duration, compute the numerator using the Epanechnikov

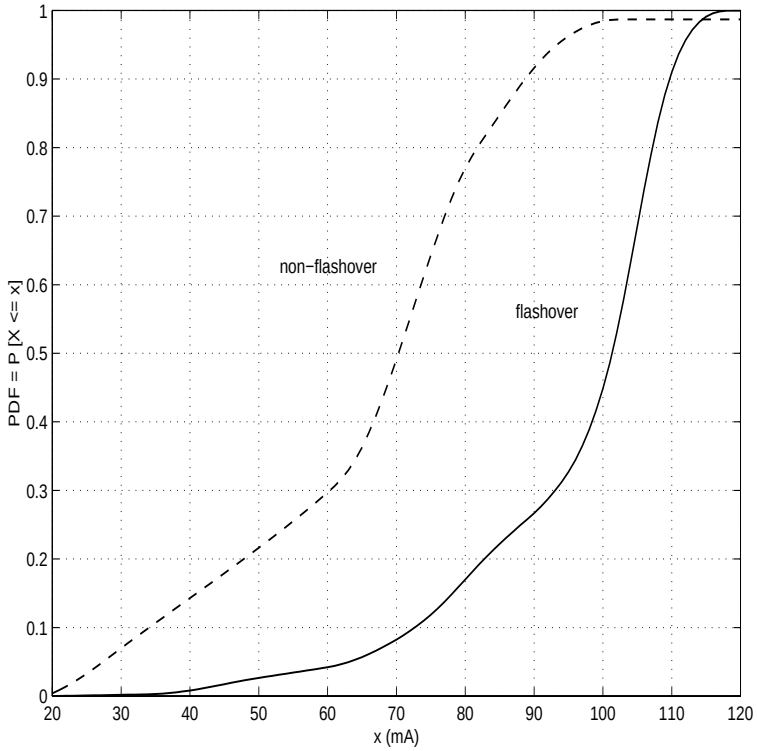

Figure 26. Cumulative distribution functions for pdfs in Figure 25

Table 5. Calculated values of τ_{92} for different ESDD levels

ESDD (mg/cm^2)	τ_{92} (ms)	Effect
0.15	100	Flashover
0.15	115	Flashover
0.15	120	Flashover
0.15	108	Flashover
0.15	116	Flashover
0.10	50	Withstand
0.10	64	Withstand
0.10	77	Withstand
0.10	53	Withstand
0.10	80	Withstand

kernel density estimate. This is done for periods in which at least one current peak exceeds 92 mA.

3. Compute the denominator using the empirical crossing spectrum.

4. Calculate the LCA and determine the mean values near flashover. For withstand tests, determine the maximum values attained.

3.5.2. Extreme Value Risk Function

The extreme value risk function (EVRF) attempts to quantitatively characterize the risk associated with rare, large events which occur with low probability but have a high damage level. Here, the rare events are the large current peaks and the damage is flashover of the insulator. Even though the frequency of occurrence of large peaks is small (low exceedance probability), the cumulative effects may indeed be substantial (high consequence) because if flashover indeed occurs, this is very undesirable. This risk analysis is done in the framework of probabilistic risk analysis using the partitioned multiobjective risk method (PMRM), outlined in [59, 60]. The PMRM is an analytical method for making risk-related policy decisions, with previous applications including dam and nuclear safety, groundwater and air pollution and aerospace technologies.

The methodology lies in generating a risk measure for extreme excursions of the leakage current envelope - low probability/high consequence events. In a previous section, the large peaks of the current envelope were modeled with the extreme value probability density and distribution functions, $g(z)$ and $G(z)$. The *exceedance*

probability of z is defined as the probability that the random variable Z is observed to be greater than or equal to z, and is equal to one minus the PDF evaluated at z, $1 - G(z)$. The p-th percentile of the distribution is the value $\chi_{p/100}$ defined by

$$P[z \leq \chi_{p/100}] = p/100 \tag{3.29}$$

This implies that $p\%$ of the individual samples of the population have a value less than or equal to $\chi_{p/100}$.

PMRM normally partitions risk into three ranges; events with

- High exceedance probability and low consequence.
- Moderate exceedance probability and moderate consequence.
- Low exceedance probability and high consequence.

Only the last range is considered because it has the most adverse effects on the underlying process; flashover of the insulator. In order to assess the risk of extreme current peaks on insulator flashover, a risk (or damage) function, R, defined as the conditional expected value given that events with cumulative probability greater than or equal to p occur, is introduced. The probability p is called the partitioning probability and is chosen very high (consequently, the low exceedance probability). The 95^{th} and 99^{th} percentile point ($p = 95/100$ and $99/100$) are used for this analysis. The mathematical background of the method is presented below:

$$\begin{aligned} g(z) &= \alpha \exp[-\alpha(z-u) - e^{-\alpha(z-u)}] \\ G(z) &= \exp[-e^{-\alpha(z-u)}] \end{aligned} \tag{3.30}$$

With the partitioning probability p given, its percentile point χ_p) is given by

$$\begin{aligned} p &= P[z \leq \chi_p] \quad = \quad G(\chi_p) \quad \Rightarrow \\ \chi_p &= G^{-1}(p) \\ &= u - \alpha^{-1}[\ln(-\ln(p))] \end{aligned} \tag{3.31}$$

$$R(\chi_{\mathrm{p}}) = \frac{\int_{\chi_p}^{\infty} z\, g(z)\, dz}{\int_{\chi_p}^{\infty} g(z)\, dz} = \frac{1}{1-p}\int_{\chi_p}^{\infty} z\, g(z)\, dz \tag{3.32}$$

By substituting $g(z)$ in (3.32), a straightforward calculation yields an approximate expression for the risk function;

$$R(\chi_p) \;=\; u_t + \frac{1}{\alpha_t} \tag{3.33}$$

where

$$\begin{aligned} u_t &= u - (1/\alpha)\ln\{\ln[t/(t-1)]\} \\ \alpha_t &= \alpha(t-1)\ln[t/(t-1)] \\ t &= 1/(1-p) \end{aligned} \tag{3.34}$$

Tables 6 and 7 shows MLE parameter estimates, percentile points and associated risk measures calculated for leakage current recordings at different contamination levels.

In order to assign a physical interpretation to the risk function, consider the percentile point χ_p, with probability p, the reciprocal of the exceedance probability is often termed the return period (the recurrence interval) and given by

$$T(\chi_p) = \frac{1}{1-p} \tag{3.35}$$

Table 6. MLE parameter estimates, percentile points and associated risk measures for partitioning probability $p = 0.95$

ESDD	α	u	$\chi_{0.95}$	$R(\chi_{0.95})$
0.15	0.431	104.3	111.2	113.6
0.15	0.458	104.2	110.8	113.0
0.15	0.420	106.0	113.1	115.5
0.15	0.481	104.3	111.8	113.9
0.15	0.492	108.9	114.8	117.0
0.10	0.983	100.0	103.0	104.1
0.10	0.760	68.8	72.7	74.1
0.10	0.840	90.1	93.6	94.9
0.10	0.773	87.5	91.3	92.7
0.10	0.668	85.2	89.6	91.2

Table 7. MLE parameter estimates, percentile points and associated risk measures for partitioning probability $p = 0.99$

ESDD	α	u	$\chi_{0.95}$	$R(\chi_{0.95})$
0.15	0.431	104.3	115.0	117.3
0.15	0.458	104.2	114.2	116.4
0.15	0.420	106.0	117.0	119.3
0.15	0.481	104.3	115.2	117.3
0.15	0.492	108.9	118.2	120.3
0.10	0.983	100.0	104.7	105.7
0.10	0.760	68.8	74.9	76.2
0.10	0.840	90.1	95.6	96.8
0.10	0.773	87.5	93.5	94.8
0.10	0.668	85.2	92.1	93.6

Utilizing the 95^{th} and 99^{th} percentile points for illustration; at 0.15 ESDD, $T(\chi_{.95}) = 20$, $\chi_{0.95} = 111.2$ mA, $R(\chi_{.95}) = 113.6$ mA and similarly, $T(\chi_{.99}) = 100$, $\chi_{0.99} = 115.0$ mA, and $R(\chi_{.99}) = 117.3$ mA. This means that there is a 5% probability (5 chances in 100) that the current will exceed 111.2 mA but when this happens then it is expected that at least one peak will exceed 113.6 mA every 20 seconds until flashover occurs. Similarly, there is a 1% probability that the current will exceed 115.0 mA but when this happens then it is expected that at least one peak will exceed 117.3 mA every 100 seconds until flashover occurs. In this respect, the risk function provides a deterministic measure of the severity of the underlying process. Selection of different partitioning probabilities changes the values but does not change the overall results.

To summarize the overall procedure:

- Obtain samples of the envelope, either analytically or through the use of an envelope detector, in equal intervals of time T.
- Based on only data samples exceeding the 95^{th}-percentile, calculate the location (u) and scale (α) parameters of the extreme value distribution.
- Define the partitioning probability u, compute the quantile χ_p, the return period $T(\chi_p)$ and also the value of the risk function $R(\chi_p)$.

3.6. Discussion and Conclusions

This chapter has submitted the results of applying level crossings and extreme value models to the analysis of the probabilistic dynamics of polluted insulator leakage current. The aim was to analyze the current envelope continuously until flashover in order to establish trends, which might indicate the imminence of flashover. At specified high levels (large peaks) of the envelope, the frequency of finite crossings of, and the time duration above these levels play an important role in determining approaching flashover. The notion of level crossing activity (LCA) of the envelope is introduced and a measure of the LCA is proposed. This measure is related to the mean distance between successive crossings of the envelope at the prescribed level. Also, a risk function which provides information about the extreme current peaks is presented.

At this point, a comparison of the analytical methods is in order:

1. Spectral analysis of the leakage current has shown a strong fundamental component of 60 Hz, with little or no harmonics under normal conditions. Under arcing conditions, the harmonic content increases with a dominant third harmonic. The ease of computation (CPU computation time, number of operations and data storage) is very light, the method is very well-developed and easily implemented in real-time. However, the changes in spectral content of the leakage current show some degree of fluctuation, which may be difficult to interpret. It may predict flashover about fifty percent of the time. This technique is recommended for early warning of incipient flashover or simply, a means for flagging a degradation in the performance of the insulator.

2. Level crossing analysis takes into consideration the statistical properties of the leakage current. It deals with crossing rates at large current peaks hence averages out the bias caused by smaller peaks. This technique may be most accurate for predicting flashover; high crossing rates are indicative of periods of intensive arcing activity and lower rates correspond to the background (non-arcing) activity. It will predict flashover almost nine out of ten times, however it is computationally most intensive and approximate methods of calculation are needed for on-line application.

3. Extreme value analysis also considers statistical properties of the leakage current, deals with large peaks and evens out the bias due to smaller current peaks. The calculations are straightforward and can easily be implemented on-line. It is currently the most reliable method, with respect to ease of computation and success

Table 8. Comparison of analytical methods

Method	Parameter	Critical	Marginal	Negligible
Spectral Analysis	P_{180}/P_{60}	≥ 0.25	0.1-0.25	0-0.1
Level Crossing	τ_{92} (ms)	≥ 100	20-100	0-20
Extreme Value	$R(\chi_{0.95})$ (mA)	≥ 105	90-105	0-90

rate. It is also the recommended analytical technique for real-time signature analysis of polluted insulator leakage current.

Table 8 summarizes the flashover criteria for the various analytical techniques under the specific operating conditions of 12.5 kV/unit insulator, 0.1-0.15 ESDD and artificial pollution of the insulators. Critical values mean incipient flashover, marginal means close monitoring required and negligible, the events can be ignored. It is envisioned that combinations of the analytical methods presented here will be used to develop technologies for on-line monitoring of actual service insulators. This will provide an independent means of assessing situations that are most likely manifestations of approaching flashover of contaminated ceramic insulator.

CHAPTER 4

Dynamic Arc Modeling

4.1. Introduction

Laboratory studies and industrial experience show that surface discharges in the form of partial arcs precede insulator flashover. The physical processes involved are numerous and very complex [54], however it is hoped that a simple mathematical model of the arc could aid substantially in understanding the flashover phenomenon. Much progress has been made in recent years in the physical analysis of the arc, resulting in a set of elaborate partial differential equations. Of more practical use is the treatment of the arc as a purely electrical circuit element; a non-linear resistor. The arc current is then a function of the voltage, arc length and properties of the surrounding medium. Several models have been proposed for static and dynamic arc modeling and also AC and DC voltages [2–4, 6, 10, 11, 13, 16, 25, 26]. A dynamic model is presented here which takes into account the instantaneous changes in the arc parameters. For a given insulator profile, supply voltage and pollution severity, the model calculates the time variation of arc current, arc length, arc resistance, etc.

4.2. Static Arc Model

The voltage balance equation using a static arc model of an arc in series with pollution layer is represented by

$$\begin{aligned} V(t) &= V_a + V_c + V_{arc}(t) + I_{leak}R_{poln} \\ V_{arc}(t) &= AL_{arc}I_{leak}^{-n} \end{aligned} \tag{4.1}$$

where A and n are arc constants. The symbols are listed in table 9. Based on this static model, empirical formulae for critical values of arc length and electric stress can be derived, in order for flashover to occur [6, 12]:

$$\begin{aligned} L_c &= \frac{L}{1+n} \\ E_c &= A^{1/(1+n)} r_p^{n/(1+n)} \end{aligned} \tag{4.2}$$

The static model is very well documented and simulations using this model will not be repeated here.

4.3. Concept of AC Dynamic Arc Model

A review of recent mathematical models, describing the flashover phenomenon indicates that they are mostly static models and for direct current. In order to develop a model which can predict AC pollution flashover, the model must take into consideration the real, albeit complex processes that lead to pollution flashover. A dynamic model which accounts for all the rapidly changing arc parameters (voltage, current, length, resistance, etc) could foster better understanding of the flashover process.

AC flashover deviates considerably from the DC case, principally due to the natural current zeros of the AC voltage. When a current zero occurs, the arc is extinguished. The conditions under which arc reignition might take place following a current zero must be accounted for. For flashover to occur, the arc needs to propagate until the insulator electrodes are bridged. The criterion for arc propagation under AC voltage needs to be included. Furthermore, due to the alternating voltage, there is no defined anode or cathode as they constantly interchange. Also, because of energy storage in the arc associated with its conductance and finite rates of energy flow, the arc is characterized by a 'time constant', which depends on the electrical inertia of the arc [52]. The time constant for low current arcs (which is representative of insulator surface arcs) is of the order of 100 μs.

All these factors are combined to develop a theoretical model that calculates arc parameters, as presented in the following sections.

4.4. Analytical Calculation of Leakage Current

A simplified dynamic arc model devised from the more elaborate physical considerations and the external electric circuit is that of an arc resistance in series with a pollution resistance, supplied by a sinusoidal voltage. The arc is a single dominant arc and the pollution resistance represents the pollution layer of the unbridged portion of the insulator. The arc is assumed only to move along the surface of the insulator and the pollution layer is assumed uniform. Also, the source impedance is neglected. This is very simplified in the sense that there might be multiple arcs, the pollution layer is

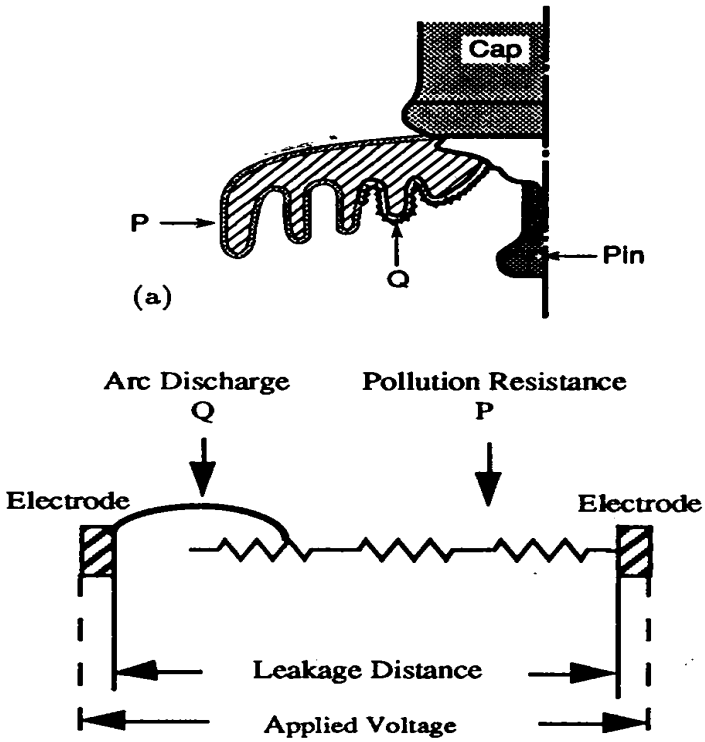

Figure 27. The arc as a circuit element - arc resistance in series with pollution resistance.

non-uniform, wetting of the insulator surface is non-uniform and other processes (e.g. thermal) are not accounted for. Figure 27 depicts the polluted insulator along with its dry band arc. During the arcing period the leakage current can be calculated using the model proposed by Obenause [3] and mathematically developed by Rizk [12]. This model contains arcs and surface resistance connected in series. The equation for the sinusoidal supply voltage $V(t)$ and arc voltage is given by:

$$\begin{aligned} V(t) &= V_a + V_c + V_{arc}(t) + I_{leak}R_{poln} \\ V_{arc}(t) &= R_{arc}L_{arc}I_{leak} \end{aligned} \tag{4.3}$$

The arc resistance per unit length is obtained dynamically from Mayr's equa-

Table 9. List of symbols and arc parameters

Symbol	Description	Unit
$V(t)$	sinusoidal supply line to neutral	V
V_m	peak supply voltage	V
V_a	anode voltage drop	V
V_c	cathode voltage drop	V
V_{arc}	arc voltage	V
R_{arc}	arc resistance per unit length	Ω/cm
L_{arc}	arc length	cm
R_{poln}	pollution resistance	Ω
R_p	pollution resistance per unit length	Ω/cm
E_{arc}	electric field in arc	V/cm
E_p	electric field in pollution layer	V/cm
I_{leak}	leakage current	A
I_a	arc current	A
σ_s	surface conductivity of pollution layer	μS
L	insulator creepage length	cm
τ	arc time constant	s
υ	velocity of arc propagation	cm/s
μ	arc mobility	5 to 50 cm^2/V.s
A	static arc parameter	63 $VA^{0.5}$/cm
n	static arc parameter	0.5
Q_o	arc energy content constant	0.16 W/cm
N_o	arc heat conduction loss constant	1000 W/cm.s
V_{ig}	arc ignition voltage	V

tion. The resistance of the arc channel per unit length, R_{arc}, is given by

$$R_{arc} = \alpha e^{-Q/Q_o} \tag{4.4}$$

where Q is the energy content per unit length of arc channel and α and Q_o are constants. Taking the time derivative of (4.4)

$$\frac{dQ}{dt} = -\frac{Q_o}{R_{arc}}\frac{dR_{arc}}{dt} \tag{4.5}$$

The rate of change of energy content/unit length is also given by the net power input i.e.,

$$\frac{dQ}{dt} = E_{arc}I_{arc} - N_o \tag{4.6}$$

where E_{arc} and I_{arc} are the electric field in the arc and arc current, respectively and N_o is the heat conduction loss (convection and radiation losses neglected), shown by Mayr to be constant. Combining (4.5) and (4.6)

$$\begin{aligned} -\frac{Q_o}{R_{arc}}\frac{dR_{arc}}{dt} &= E_{arc}I_{arc} - N_o \\ -\frac{Q_o}{R_{arc}}\frac{dR_{arc}}{dt} &= R_{arc}I_{arc}^2 - N_o \\ \frac{dR_{arc}}{dt} &= \frac{R_{arc}}{\tau}\left(1 - \frac{R_{arc}I_{arc}^2}{N_o}\right) \\ \tau &= \frac{Q_o}{N_o} \end{aligned} \tag{4.7}$$

The expression for the leakage current from these equations is given by

$$I_{leak} = \frac{V(t) - V_a - V_c}{R_{arc}L_{arc} - R_{poln}} \tag{4.8}$$

The pollution resistance is calculated from the form factor, as

$$\begin{aligned} R_{po\ln} &= \frac{1}{\sigma_s}\int_{Larc}^{L}\frac{dl}{2\pi r(l)} \\ R_p &= \frac{R_{poln}}{L - L_{arc}} \end{aligned} \tag{4.9}$$

where

l is the distance from the upper electrode (cap) on the insulator surface

$r(l)$ is the radius of the insulator at a distance of l from the upper electrode.

4.4.1. Arc Reignition

The arc re-ignition voltage can be calculated by an empirical formula given in [9]. The same formula is used as the extinction voltage even though this may not be the case for real arcs. After the supply voltage passes through the natural current zeros, the arc re-ignites the the exceeds this value.

$$V_{ig} = 23\ R_p^{0.4} \tag{4.10}$$

4.4.2. Arc Propagation

The arc will only propagate (arc length increases) if the electrical field is lower in the arc than in the pollution layer ($E_{arc} < E_p$). This is Hampton's criterion for propagation. The general perspective is that, when E_{arc} exceeding E_p, any physical extension of the arc will lead to a decrease in current, with a further increase in E_{arc},

since arcs show a falling characteristic of stress against current. The electric fields in the arc and pollution layer are respectively given by

$$E_{arc} = 63 I_{leak}^{-0.5} \qquad \text{and} \qquad E_{poln} = 63^{2/3} R_p^{1/3} \tag{4.11}$$

If the condition for propagation is satisfied, then the velocity of propagation is accordingly given by

$$\upsilon = \mu E_{arc} \tag{4.12}$$

4.5. Computer Simulation

The above equations form a system of coupled differential-algebraic equations:

$$\begin{aligned} \frac{dR_{arc}}{dt} &= \frac{R_{arc}}{\tau}\left(1 - \frac{R_{arc} I_{arc}^2}{N_o}\right) \\ \frac{dL_{arc}}{dt} &= \mu E_{arc} \end{aligned} \tag{4.13}$$

$$V(t) = V_a + V_c + R_{arc} L_{arc} I_{leak}(t) + I_{leak} R_{poln} \tag{4.14}$$

The system is solved on a Pentium PC using Matlab routines. A flowchart of the routine is displayed in Figure 28. The creepage length of the insulator was L = 30.5 cm. The main parameters monitored are the temporal evolution of leakage current, arc resistance and arc length, for different values of supply voltage. The numerical analysis shows that the peak value and the duration of the current increases with increase in arc length. The flashover occurs when the arc bridges the insulator chain, with L_{arc} approximately equal to $0.9L$. When $L_{arc} = L$, short circuit occurs and the current increases to the system short circuit current.

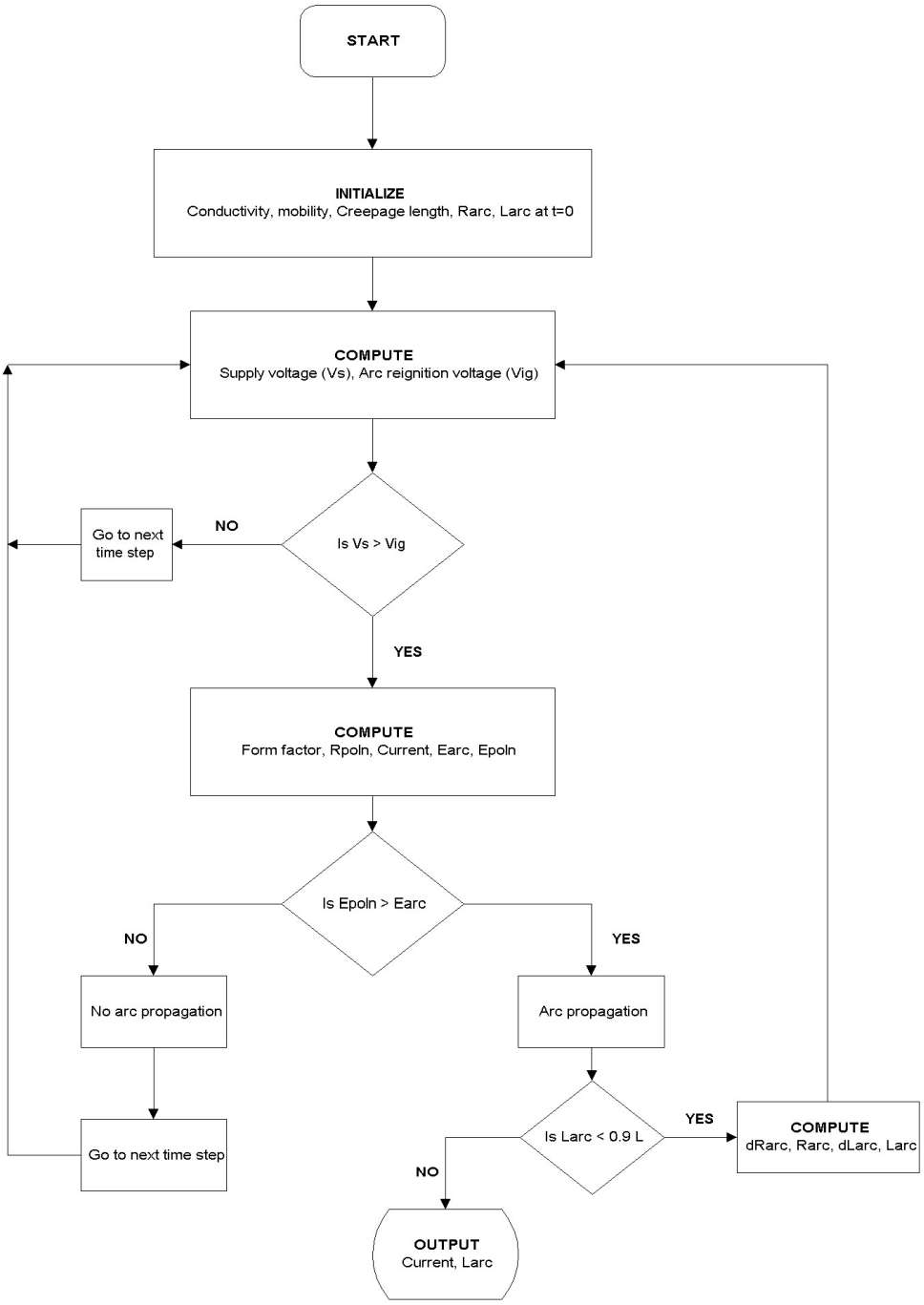

Figure 28. Flowchart of routine for calculating analytic leakage current

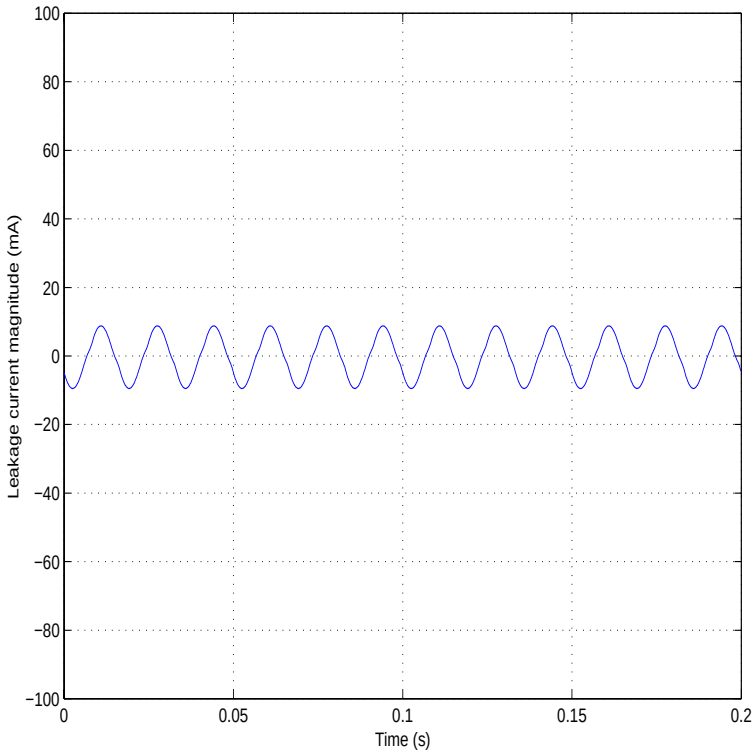

Figure 29. Analytically calculated leakage current for non-flashover case current (σ_s = 5 μS)

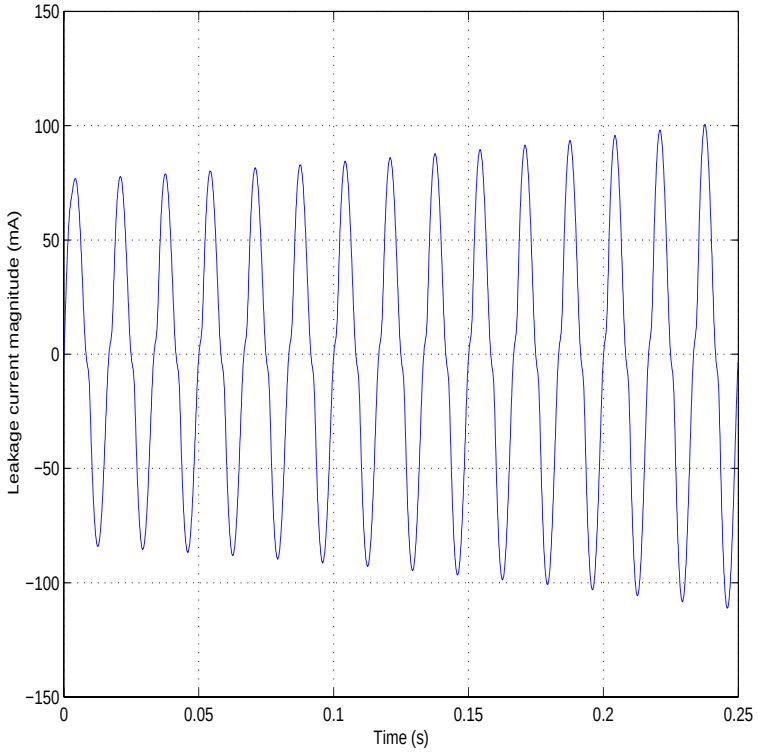

Figure 30. Analytically calculated leakage current for flashover case ($\sigma_s = 15\ \ \mu$S)

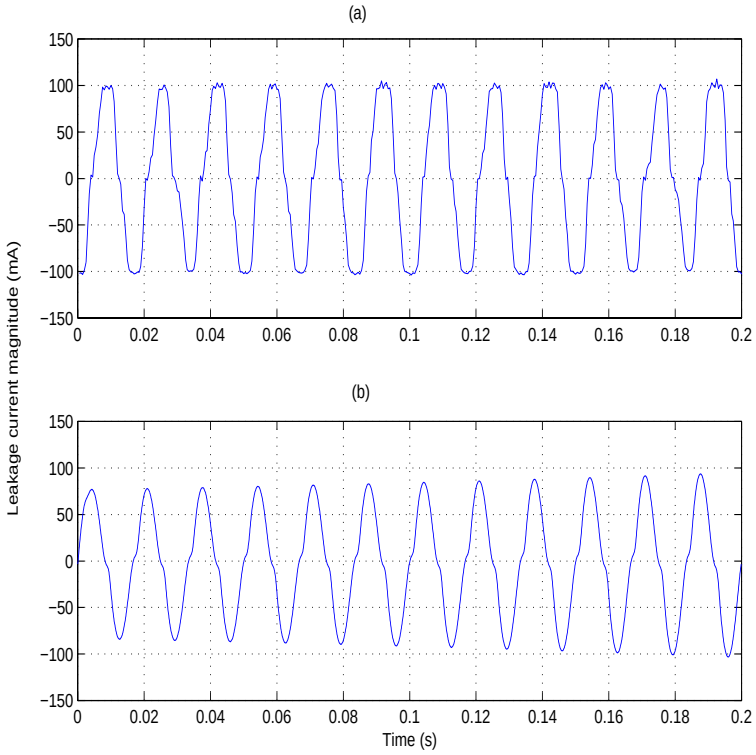

Figure 31. Comparison of measured and calculated pre-flashover leakage current (a) measured (b) calculated

4.6. Validation of Model

In order to validate the model, the results of the simulation are compared to similar results obtained from the experimental work described in Chapter 2 and also to empirical models presented in the literature. Since the experiments involved measuring leakage current at different pollution levels for a string of insulators energized at constant voltage, the comparison is done for a similar insulator profile at different conductivities. There is a simple equivalence between the conductivity, σ_s (μS) and pollution level, ESDD (mg/cm^2) [4] given by

$$\sigma_s = 100 * ESDD \tag{4.15}$$

The voltage applied to the insulator string is 50 kV hence the voltage per unit insulator is 12.5 kV. Figures 29 and 30 show the analytically calculated leakage current using the equations above for a non-flashover (σ_s = 5 μS, about 0.05 ESDD, and supply voltage 12.5 kV rms) and a flashover case (σ_s = 15 μS and supply voltage 12.5 kV rms). The calculated is indeed truly representative of real measured leakage current. A comparison of pre-flashover leakage current for measured and calculated leakage currents is provided in Figure 31. The measured current is for a string of four insulators energized at 50 kV (12.5 kV/unit), at a contamination level of about 0.15 ESDD. Peak currents obtained from both analytical model and experimentally are also compared against critical flashover currents derived empirically. Results are tabulated in Table 10. The expressions for the critical current derived from static arc

Table 10. Comparison of peak currents for analytical, experimental and empirical models

ESDD (mg/cm^2)	σ_s (μ S)	R_p (Ω/cm)	I_{pe} (mA)	I_{pm} (mA)	I_{cz} (mA)
0.05	5	27240	10	8	56
0.1	10	13620	100	80	56
0.15	15	8840	112	98	56

considerations by Zoledziowski (I_{cz}) are given by:

$$\begin{aligned} I_{cs} &= (A/R_p)^{1/(n+1)} \\ I_{cz} &= 233E_c^{-1.31} \end{aligned} \tag{4.16}$$

Peak stress E_c is simply computed as V_m/L. Here, I_{pe} is the peak current obtained experimentally and I_{pm} is the analytically calculated peak current.

The peak current from the dynamic model is within 10% of the experimental. Both analytical and dynamic peak currents are about twice the empirical. The difference between the analytical and the empirical is mainly due to the fact that most empirical models were derived form static considerations and different authors have the tendency to use different arc constants. The difference between analytical and experimental is due to inherent limitations in the models used:

1. Non-uniformity of conductivity and also pollution layer thickness. The initial conductivity (assumed constant in the dynamic model) varies continuously and irreversibly during the progress of a flashover test.

2. The arc may not necessarily follow the surface of the insulator and also physical processes in the arc may create propagation speeds much higher than that used in the model.

4.7. Conclusions

Flashover tests to evaluate the performance of insulators under polluted conditions are time consuming and require expensive laboratories. Even though the model presented above still needs modifications, the extent of agreement between both current magnitude and waveshape for the analytical and experimental cases is satisfactory. Hence, the principal application of this theoretical modeling would be to help simulate as much as possible the practical conditions under which insulators perform. In this way, fairly accurate results could be obtained, eliminating the need for site testing. It could also be incorporated into the design of high voltage devices which must operate under polluted conditions.

CHAPTER 5

Online Leakage Current Signature Analysis System

5.1. Brief Overview of Online Signature Analysis System

The system presented is a PC-based data acquisition system that monitors leakage current of polluted insulators during flashover tests in a laboratory fog chamber. The system simultaneously acquires the leakage current, performs a signature analysis of the current in real-time, and depending on any emerging signatures, ascertains if threshold limits have been exceeded. An alarm is send out to operating personnel if there is danger of flashover.

To obtain accurate and timely data, the system uses a National Instruments plug-in DAQ board and LabVIEW^{TM} software. LabVIEW^{TM} is a powerful, simple, and flexible development system that met all of our requirements for data acquisition, data analysis, cost and time required for development. The interactive graphical user interface (GUI) and visual presentation were also important factors governing the choice of LabVIEW^{TM}. The system consists of a PC running Windows 95, equipped with a plug-in DAQ board (AT-MIO-16E-2) and LabVIEW^{TM} software. The software automatically performs data acquisition and analysis and data streaming to the

hard drive with a high rate of effectiveness and reliability. A GUI gives a graphical representation of the instantaneous leakage current and other relevant plots.

5.2. Purpose of Online Signature Analysis System

The aims of the real-time signature analysis system are:

1. To monitor insulator surface contamination build-up in real-time through the leakage current.

2. To perform a real-time (online) mathematical signature analysis of the measured leakage current and to monitor the time-trend of a pre-defined performance index.

3. To trigger an alarm and warn operating personnel if the threshold limits of the index are exceeded, for appropriate action to be taken.

5.3. Concept

The mechanism of insulator contamination flashover clearly attests that the leakage current undergoes magnitude and shape changes, leading to flashover. Preliminary off-line analysis (presented in Chapter 2) revealed that the frequency signature of the leakage current might be a good indicator of approaching flashover. There is a significant increase in the third harmonic component, relative to the other harmonics, just prior to flashover. Conceptually, the real-time system continuously monitors the leakage current, computes the ratio of third harmonic to fundamental and determines if a threshold has been exceeded. The basic philosophy is that the signature changes

Table 11. Technical specifications for AT-MIO-16E-2 DAQ board

Number of channels	16 single ended, 8 differential
Maximum sampling rate	500 kS/s
Resolution	12 bits, 1 in 4096
Streaming-to-disk rate	1.25 MS/s
FIFO buffer size	8192 samples
Relative accuracy	±0.5 LSB
Bandwidth	1.6 MHz
Input voltage range	±5 V, 0 to 10 V
Input coulping	DC or AC
Input impedance	100 GΩ
Input bias current	±200 pA
Input offset current	±100 pA

in the leakage current might cause deviations in this ratio, of sufficient magnitude to be considered outside the region of normal operation. The other signature analysis methods presented in previous chapters can equally well be programmed and updated as new techniques become available.

5.4. National Instrument DAQ Hardware

The basic considerations for selecting the AT-MIO-16E-2 DAQ plug-in board were versatility, ruggedness, data throughput to hard drive and also cost. The analog input and output specifications give information on both the capabilities and the accuracy of the DAQ board and these are displayed in Table 11. The number of channels, sampling rate, resolution, and input range were satisfactory for our application.

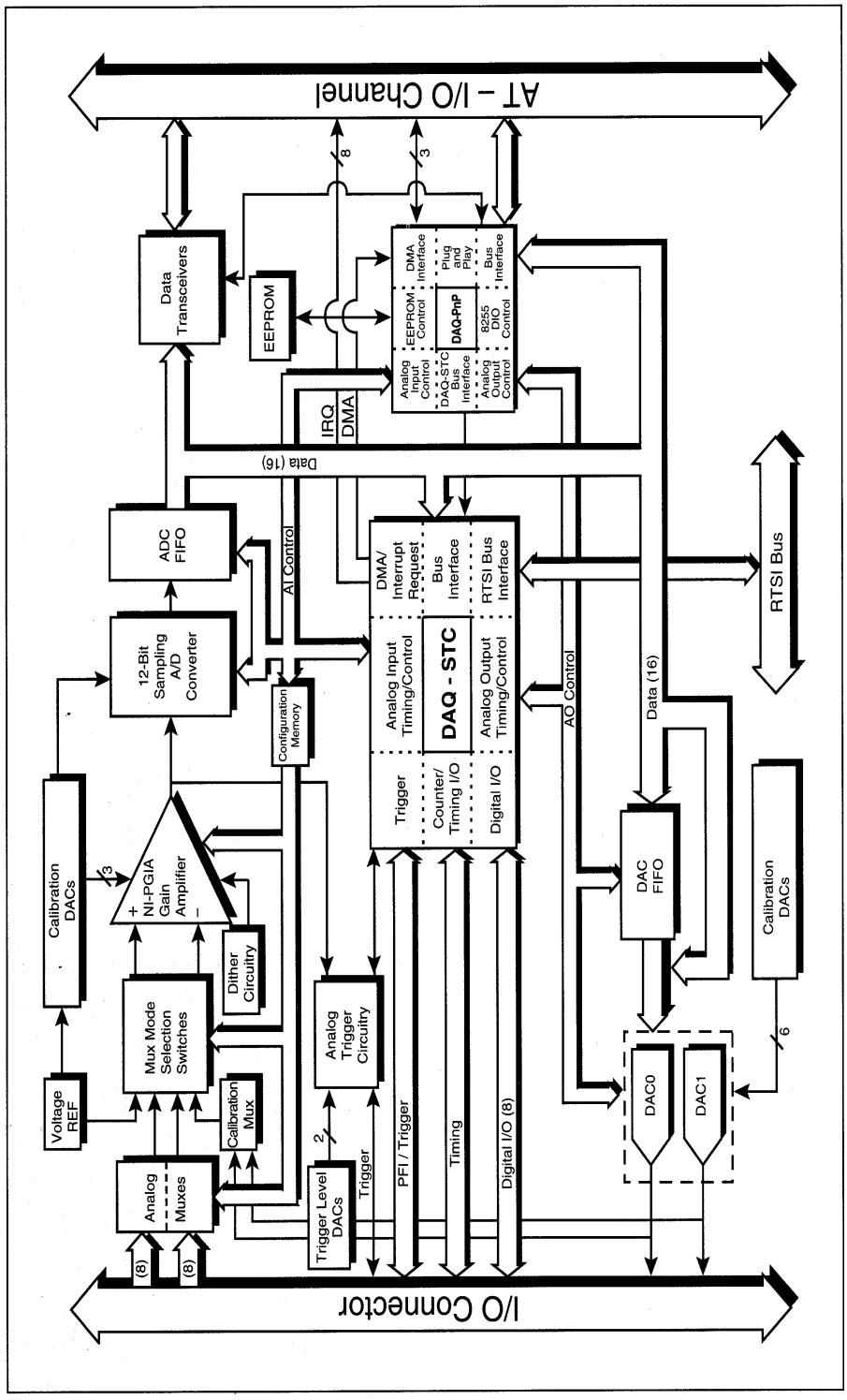

Figure 32. Hardware block diagram of DAQ system

5.5. Data Acquisition and Analysis

The various stages involved in the data acquisition and analysis include leakage current acquisition, digital filtering, data windowing, computation of power and frequency estimates and also sending out an alarm if thresholds are exceeded. The flow chart of Figure 34 illustrates the process, which is shown programmatically in Figure 35.

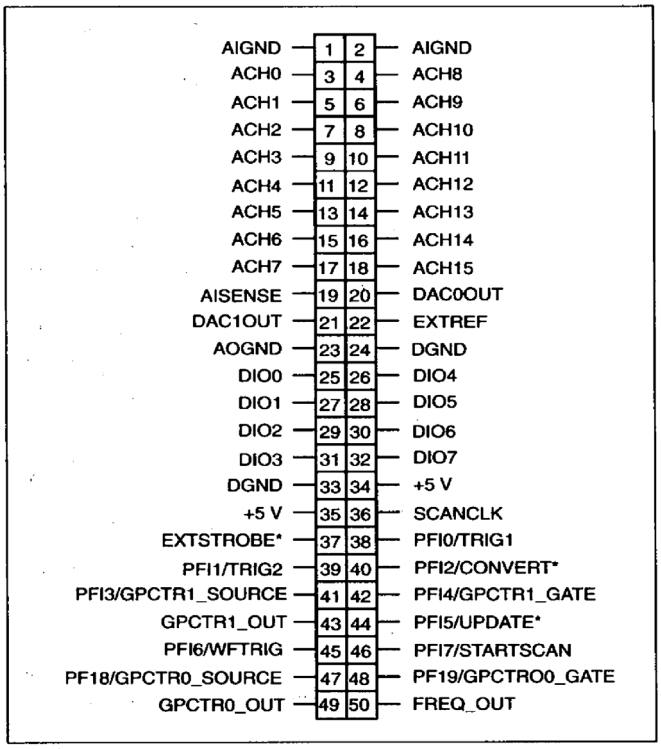

Figure 33. I/O connector showing terminals

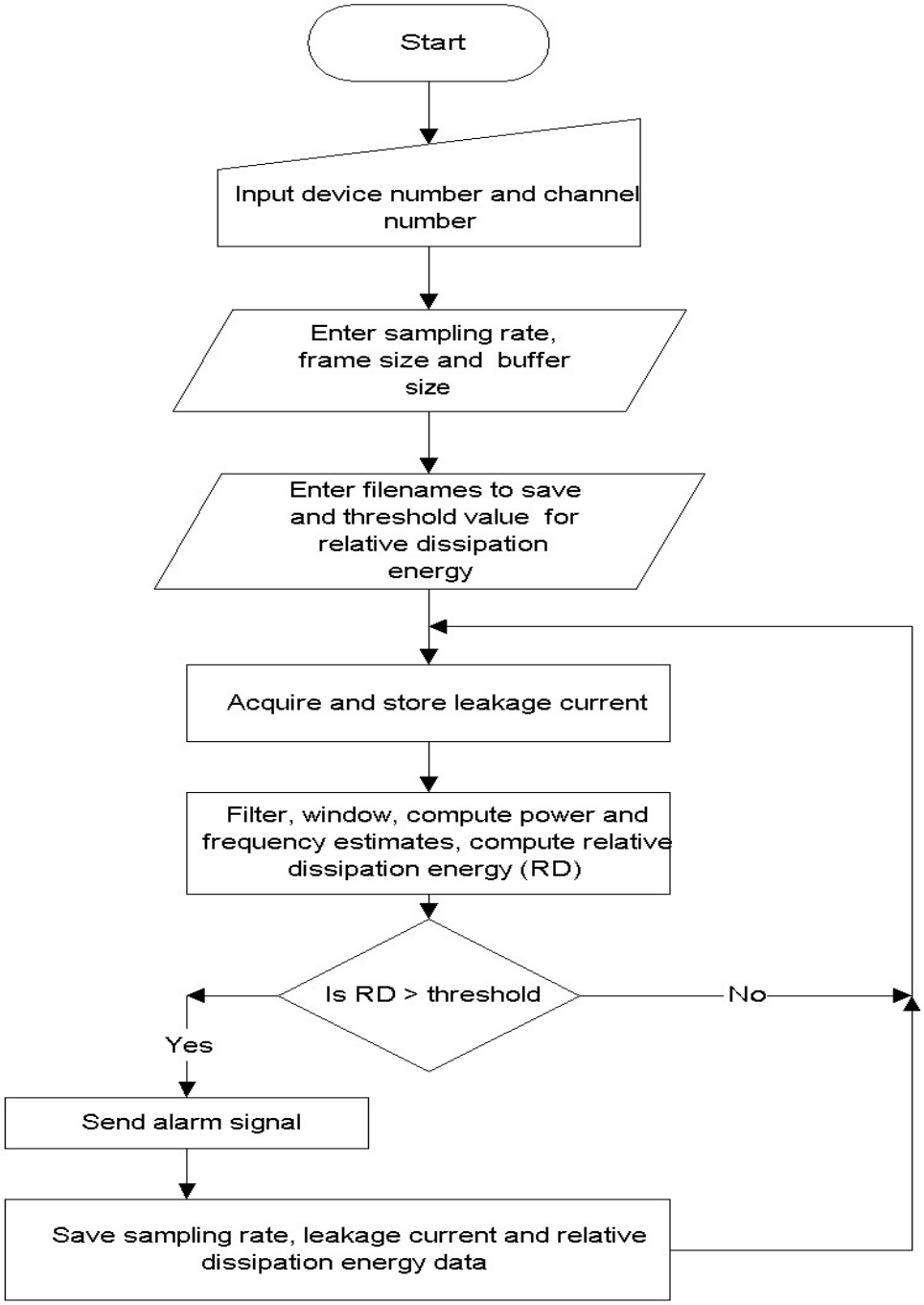

Figure 34. Flow chart of data acquisition and analysis

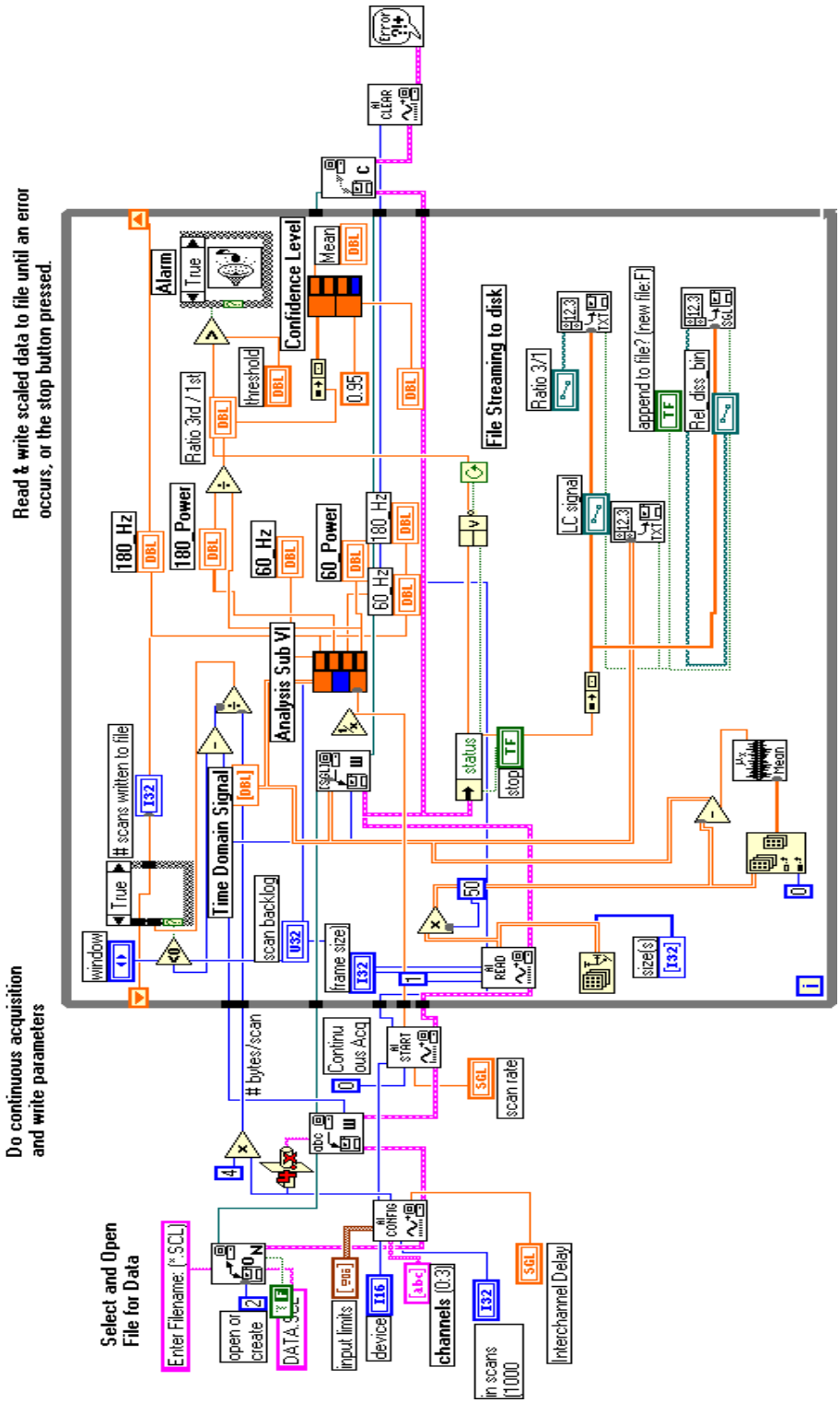

Figure 35. LabVIEW^{TM} block diagram for leakage current acquisition and storage

In the following sections, the operation of the system and explanation of the various parameters will be illustrated with sample acquisitions and analysis .

5.5.1. Connections and Configuration

The leakage current is measured across a surrogate insulator as described in Chapter 2. The current is first converted to a shunt voltage through the use of a shunt resistor. A coaxial cable then feeds the shunt voltage to any of the analog input channels of the **I/O** connector block as single-ended inputs, shown in Figure 36. The inputs are normally connected between **channel 0** and analog input ground (AIGND). The I/O connector is coupled to the plug-in DAQ board through a shielded cable assembly.

5.5.2. Data Analysis Virtual Instrument (VI)

The data analysis VI is displayed in Figure 37 and the more important parameters of the block diagram shown on the front panels of Figures 38-40.

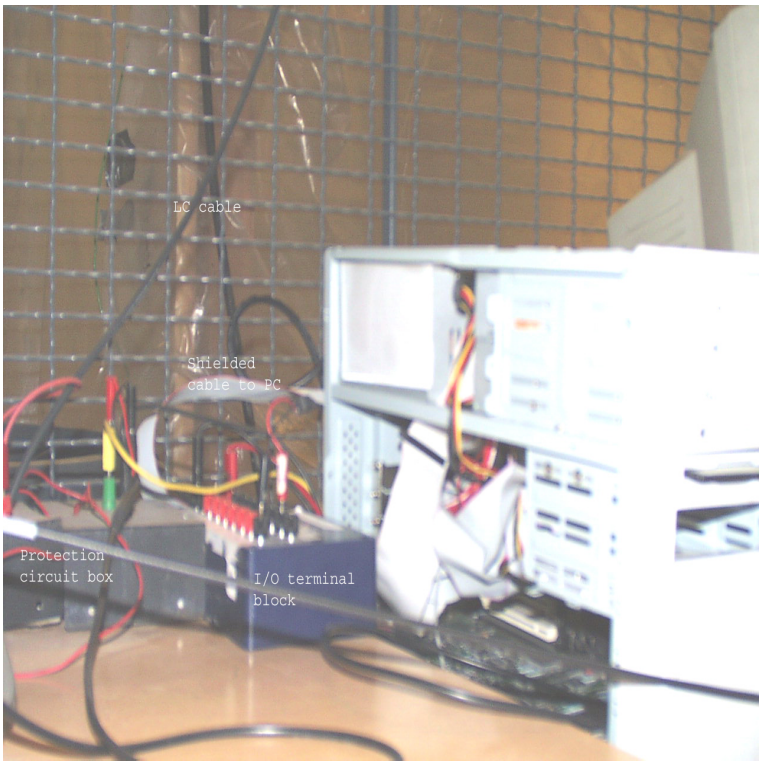

Figure 36. Connection of I/O terminal block and cable to PC

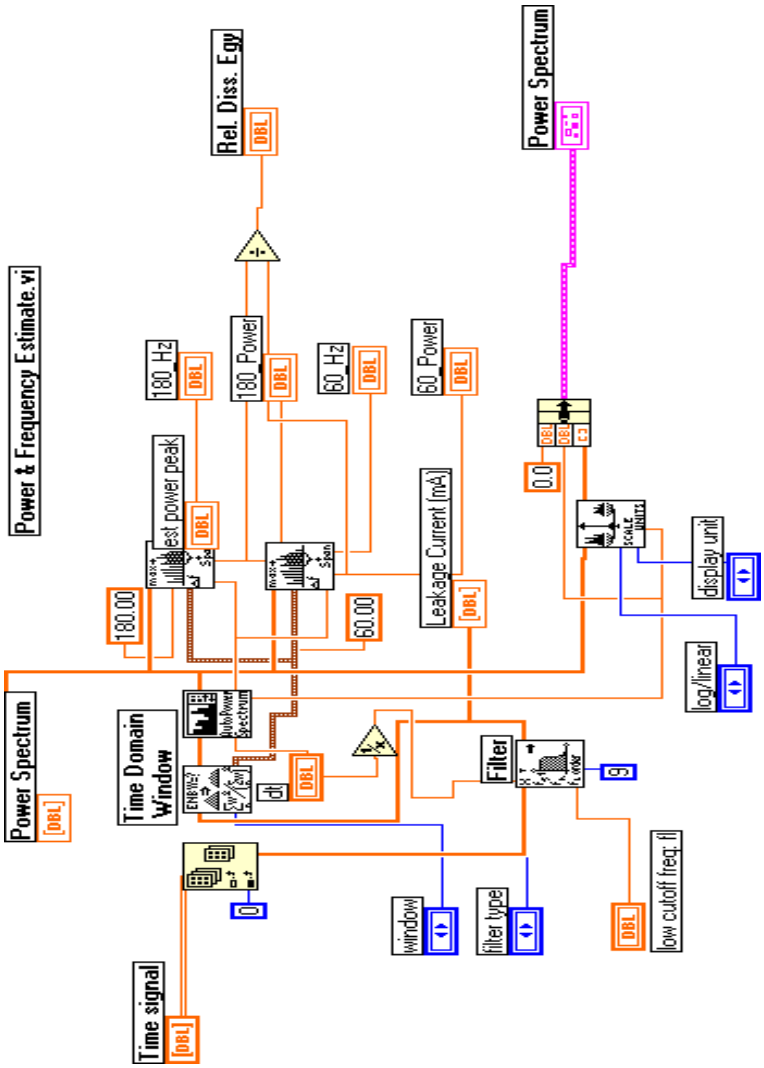

Figure 37. LabVIEW^{TM} sub VI block diagram for leakage current analysis

On the front panel, **device 1** and **channel 0** refer to the DAQ board and input channel, respectively. **Scan rate** determines the rate at which the leakage current is sampled. The sampling rate chosen is 2000 samples/s. The acquired data is temporarily stored in a buffer, the size of which is given by the **buffer size**. The number of samples to be transferred from the buffer at a time for processing is set by the **frame size**, usually a power of 2. Both buffer and frame sizes are the same, 2048 samples, representing 1.024 seconds of data. The input voltage limits of the acquisition channel is set to ± 5 V because the shunt voltage of the leakage current is expected to be about ± 2 V. Also, both the raw leakage current and the processed data are stored on the hard drive by streaming to disk and saving the data to a user supplied filename. A two-hour recording takes about 100 MB of hard disk space if saved as ASCII text file and 20 MB as a binary file. The acquisition, analysis and streaming to disk are performed until complete flashover when the user presses the stop button. Alternatively, if an error occurs in a part of the process, the acquisition automatically stops and the error outputted to a log file.

The acquired data is shifted in and out of the buffer for processing. It is first filtered to remove unwanted high frequency noise using a digital filter. The filtering is done with a **lowpass** Butterworth filter with a **cutoff** frequency of 600 Hz. The preliminary off-line analysis has shown that the dominant harmonics are up to about the seventh. The filtered data is then windowed for further processing. Windowing minimizes the transition edges of the truncated waveforms, thus reducing spectral leakage. The default window is **Hamming**.

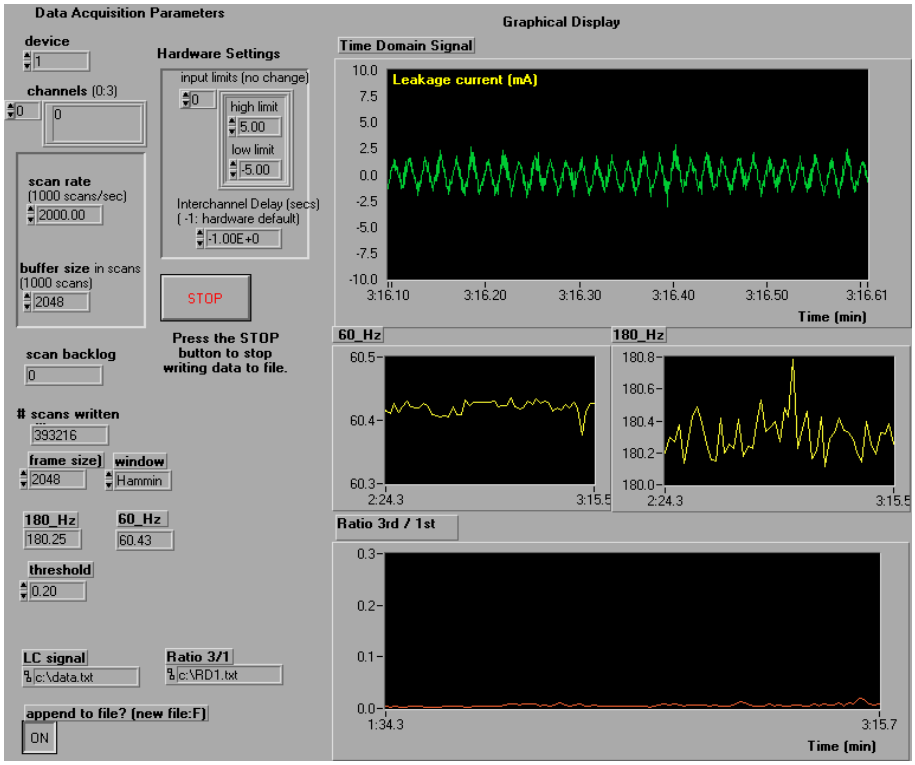

Figure 38. LabVIEW^{TM} VI front panel showing acquired leakage current during first three minutes

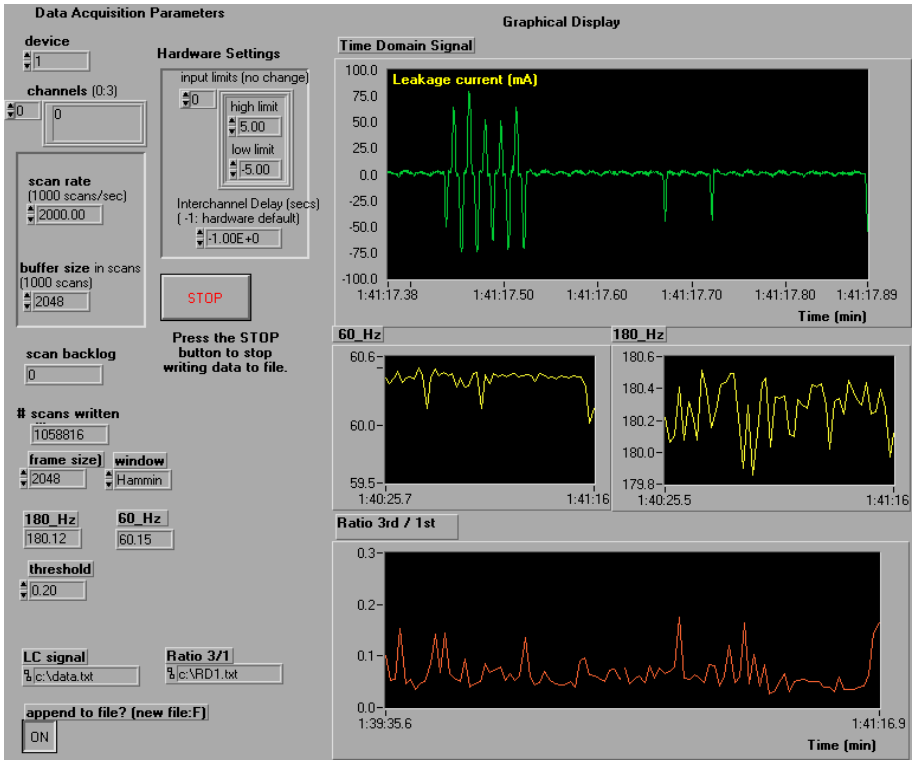

Figure 39. LabVIEW^{TM} VI front panel showing acquired leakage current

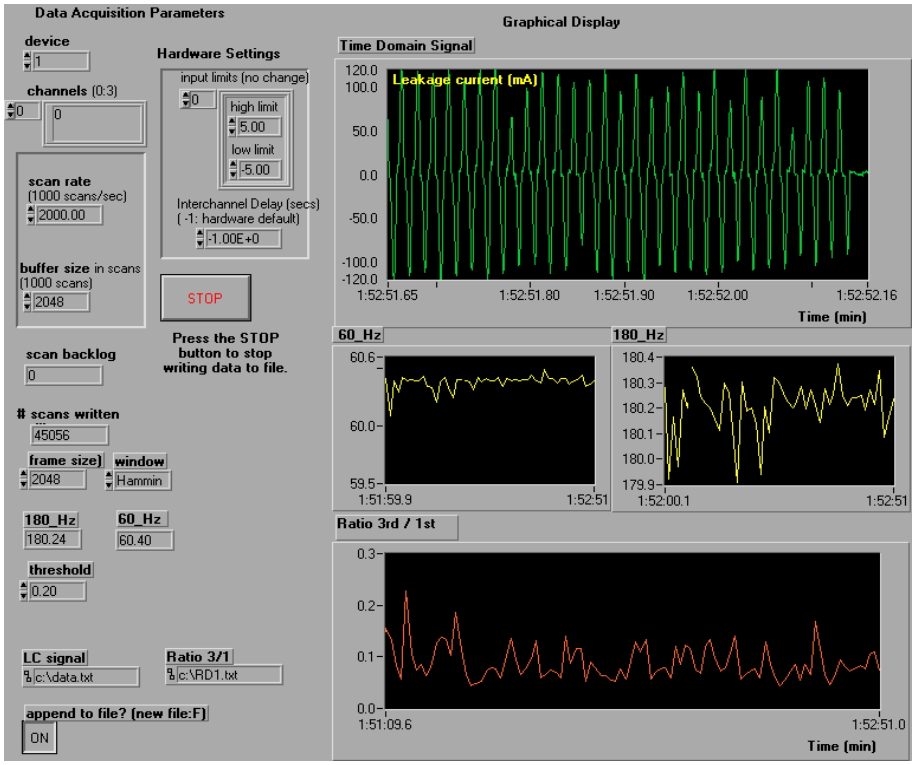

Figure 40. LabVIEW^{TM} VI front panel showing acquired leakage current after two hours

After windowing, the VI then computes the single-sided, scaled auto power spectrum of the resulting time-domain signal. The power spectrum is computed as

$$PowerSpectrum = \frac{FFT(X) * FFT(X)}{N^2} \tag{5.1}$$

where N is the number of samples (2048) in the leakage current signal array $X(t)$. Power Spectrum is the single-sided power spectrum in volts squared per hertz. From the already computed power spectrum, simultaneous estimates of the 60 Hz (**60_Hz**) and 180 Hz (**180_Hz**) frequencies, and also the power around these frequencies are made. The graphical display on the Figures 38-40 include these power and frequency estimates and also the temporal variation of the ratio of third harmonic to fundamental (**Ratio**), denoted by $R31$ and defined as:

$$R31 = \frac{P_{180}}{P_{60}} \tag{5.2}$$

where P_{180} is the estimated peak power around 180 Hz and P_{60} is the estimated peak power around 60 Hz. From the graphs, the maximum bias in the 60 Hz estimate is 0.6 Hz and 1 Hz for the 180 Hz estimate, hence the computations are fairly accurate.

5.5.3. Alarm

The alarm is realized by signaling through the speaker in the PC. The instantaneous value of the ratio of third harmonic to fundamental is compared to the threshold (0.25) and if greater (Logical TRUE), a beep is sounded.

To guard against false alarm due to measurement equipment failure or malfunctioning, computation errors, noise through the acquisition channels, etc., the sub

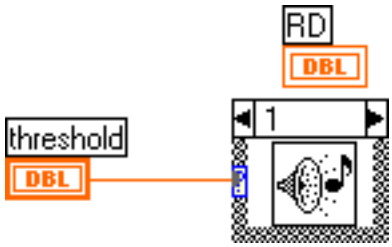

Figure 41. LabVIEW^{TM} realization of alarm signal

Table 12. Threshold limits for flagging an alarm

Activity	Current Shape	Threshold value	Flag
No arcing	Sinusoidal	$0 - 0.1$	Ignore
Intermittent arcing	Short bursts + sinusoidal	$0.1 - 0.25$	Warning
Sustained arcing	Pulsating + sinusoidal	> 0.25	Danger

VI of Fig. 42 uses the spectral estimates (ratio of 3^{rd} harmonic to fundamental) to compute confidence intervals of the estimates at a preselected level of significance, $\alpha_L = 0.05$. In this way, data samples that do not fall within the computed confidence interval are identified and discarded as outliers.

5.6. Conclusions and Discussion

A PC-based real-time leakage current monitoring and diagnostic system that provides engineers with the information they require to initiate insulator washing has been presented. This low-cost system can be permanently installed or made portable. Once connected, the system automatically monitors, records and transmits collected data to substation engineers for interpretation.

This application could be incorporated into a SCADA system, to report alarms to operating personnel; this will help minimize unplanned outages due to insulator

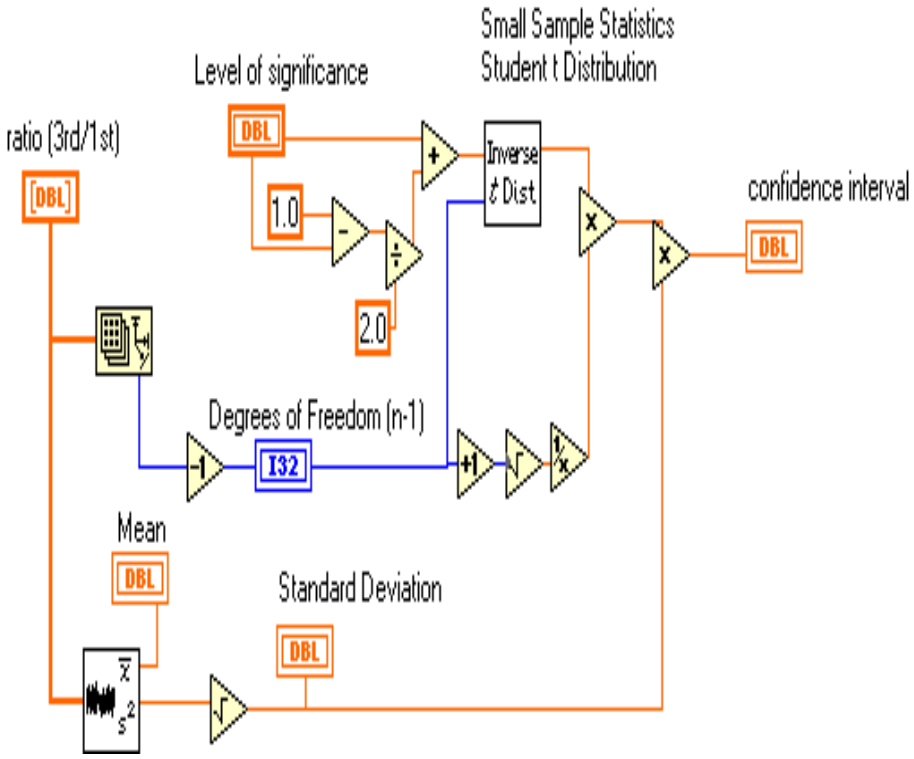

Figure 42. LabVIEW^{TM} subVI to identify and discard outliers

pollution flashover and also optimize the washing cycles of insulators. It could equally well be an integral part of a utility system's preventive maintenance capabilities; resulting in safer, less costly and more reliable operation of the system.

CHAPTER 6

Future Research

6.1. Concluding Remarks

Contamination flashover of outdoor porcelain insulators results in outages, equipment damage and potentially, catastrophic fires. Additionally, the reliability of the electric transmission system is seriously compromised. Hence the prediction of approaching flashover is very beneficial to utilities, and this is the subject matter of the this dissertation.

The project objectives were to identify measurable quantities which are suitable for flashover prediction, to perform a signature analysis of this quantity and also to develop an online monitoring system that will alert operators of any ensuing insulator flashovers. This dissertation has described the signature analysis of the easily measurable insulator leakage current, as a means of predicting flashover. Also, this concept of signature analysis of the leakage current has been evolved to create an online computer-based diagnostic system.

Experimentally, both the clean-fog and salt-fog tests, methods that reflect contamination mechanisms primarily in industrial and coastal areas respectively, were

conducted. The results indicate that, there is no considerable difference in the shape or maximum leakage current for similar contamination levels using salt-fog or clean-fog. However, heavy scintillation activity tends to start quicker under salt fog conditions than under clean fog. This may be due to the more rapid decrease in surface resistance of the insulator with the deposition of high salt-density spray. The higher the ESDD value (conductivity) of the pollution layer, the more likelihood of a flashover and the lower the value, the better chances for an insulator withstand.

The major findings of the signature analysis of the leakage current include:

1. Visual observation of a complete time-domain record of leakage current indicates very erratic changes in peak current and also current waveshape. The leakage current for a withstand (non-flashover) has intermittently large peaks whereas the flashover case exhibits a continuous train of large peaks.

2. Spectral analysis of the leakage current has shown a strong fundamental component of 60 Hz, with little or no harmonics under normal conditions. Under arcing conditions the harmonic content increases, with a dominant third harmonic.

3. Level crossing and extreme value analysis are novel statistical techniques in leakage current signature analysis. They offer further insight into the probabilistic dynamics of polluted insulator leakage current. The inference from the level crossing analysis is that crossing rates for thresholds above 60 mA drop off more rapidly for the withstand cases, than those for flashover. Sustained arcing which may lead to flashover creates a continuous train of large current peaks; consequently there're more crossings at these high peaks.

Extreme value analysis calculates the risk function, a deterministic measure of the severity of the underlying process which will sufficiently cause flashover e.g., at 0.15 ESDD with clean-fog wetting, there is a 5% probability that the leakage current will exceed 111.2 mA but when this happens then it is expected that at least one peak will exceed 113.6 mA every 20 seconds until flashover occurs.

4. A real-time leakage current monitoring system has been developed. The basic philosophy is to continuously sample the leakage current, perform a spectral analysis to obtain the ratio of third harmonic to fundamental, and determine if deviations in this ratio are of sufficient magnitude to be considered outside the region of normal operation. A threshold of 25% has been established and the system flags an alarm when this threshold is exceeded.

6.2. Future Work

The end product of this project will be a methodology for predicting flashover of polluted insulators; a computer-based diagnostic system that can be used in a substation to acquire the necessary baseline and trending leakage current, analysis software to evaluate the data and a means of flagging appropriate alarms. The project, and subsequent use of the developed methods, is also expected to produce an increased understanding of the effects of contamination and other system conditions on the performance of ceramic insulators. In this respect, the future of this project may include;

1. Field tests of the diagnostic system using in-service insulators; longer insulator strings and higher voltages. This will help correlate values obtained from laboratory tests with those obtained from real operating systems in order to enhance the interpretation of results.

2. Research to improve the physical and mathematical models as well as appropriate equivalent circuit models for the generation, evolution, extinction and re-ignition of flashover arcs. Provision will be made for more accurate modeling of non-uniform pollution layer, insulator geometry and atmospheric conditions. Also, the conditions under which the arc column travels in the surrounding medium and not the surface of the insulator (observed with heavy contamination levels) will be more thoroughly investigated.

3. Extension of the stochastic analysis to cover Markov chains, Poisson point processes, higher order spectral analysis (already in the developmental stages) and higher order crossing analysis.

References

[1] K. J. Lloyd and H. M. Schneider, "Insulation for Power Frequency Voltage," Transmission Line Reference Book (345 kV and above), Electric Power Research Institute, Palo Alto, California, USA, 1982.

[2] B. Hampton, "Flashover Mechanisms of Polluted Insulation," *IEE Proceedings*, Vol. 111, pp. 985-990, 1964.

[3] F. Obenaus, "Kriechweguberschlag von Isolatoren mit Fremdschichten," *Elektrizitatsirtschaft*, Heft 24, pp 878-882, 1960.

[4] T. J. Looms, *Insulators for High Voltage*, Peter Peregrinus Ltd., London, United Kingdom, 1988.

[5] IEEE Std 4-1995, *IEEE Standards Techniques for High Voltage Testing*, 1995.

[6] L. Alston and S. Zoledziowski, "Growth of Discharges on Polluted Insulation," *IEE Proceedings*, Vol. 110, pp. 1260-1266, 1963.

[7] B. Macchiaroli and F.J. Turner, "A New Contamination Test Method," *IEEE Transactions on Power Apparatus and Systems*, Vol. PAS-88, pp. 1400-1411, September 1969.

[8] E. Nasser, "Some Physical Properties of the Electrical Discharges on Contaminated Surfaces," *IEEE Transactions on Power Apparatus and Systems*, Vol. PAS-87, pp. 957-963, April 1968.

[9] M. Kawai, "Research at Project UHV on the performance of Contaminated Insulators Part II: Application to Practical Design," *IEEE Transactions on Power Apparatus and Systems*, pp. 1111-1120, May/June 1973.

[10] D. Jolly, "Physical Processes in the Flashover of Insulators with Contaminated Surfaces," Ph. D. Thesis, Dept. of Electrical Engineering, MIT, 1971.

[11] A. McElroy, "Flashover Mechanisms of Insulators with Contaminated Surfaces," Ph.D Thesis, Dept. of Electrical Engineering, MIT, 1969.

[12] F. A. M. Rizk, "Mathematical Models for Pollution Flashover," *Electra*, pp. 71-103, 1981.

[13] M. P. Verma, H. Nicklasch, W. Heise, H. Lipken, G. G. Luxa and H. Schreiber, "The Criterion for Pollution Flashover and its Applications," *CIGRE 33-09*, 1978.

[14] G. G. Karady and M. Shah, "Flashover Voltage Phenomena on Contaminated Non-ceramic and Glass Insulator Surfaces," *Proceedings on Non-ceramic Outdoor Insulation*, Paris, France, 1993.

[15] R. G. Holugate, D. A. Swift, "Composite Rod Insulators for AC Power Lines:

Electrical Performance of Various Designs at a Coastal Testing Station," *IEEE Transactions on Power Delivery*, Vol. 5, No. 4, pp. 1944-1955, October 1990.

[16] R. Sundarajan and R. S. Gorur, "Dynamic Arc Modeling of Pollution Flashover of Insulators under DC Voltage," *IEEE Transactions on Electrical Insulation*, Vol. 28, No. 2, pp. 209-218, April 1993.

[17] Stanislav B. Kesler, *Modern Spectrum Analysis II*, IEEE Press, 1988, USA.

[18] C. K. Yuen, D Fraser, *Digital Spectral Analysis*, Pitman, East Melbourne, Australia, 1979.

[19] Peter Sydenham, *Signal Processing for Industrial Diagnostics*, Elsevier, London, 1996.

[20] A. Mekhadi, S. Bouazabia, "Conduction Phenomena on Polluted Insulating Surfaces under AC High Voltages," *Ninth International Symposium on High Voltages*, Subject 3, Paper No. 3174, Graz, Austria, September 1995.

[21] I. A. Stathopulos, F. V. Topalis, "A Stochastic Model for the Evaluation of the Surface Flashover on Polluted Insulators," *Ninth International Symposium on High Voltages*, Subject 3, Paper No. 3195, Graz, Austria, September 1995.

[22] Y. Mizuno, H. Nakamura, K. Naito, "Dynamic Simulation of Risk of Flashover of Contaminated Ceramic Insulators," *IEEE Transactions on Power Delivery*, Vol. 12, No. 3, pp. 1292-1298, July 1997.

[23] Y. Mizuno, K. Naito, W. Naganawa, "A Study on Probabilistic Assessment of Contamination Flashover of High Voltage Insulators," *IEEE Transactions on Power Delivery*, Vol. 10, No. 3, pp. 1378-1383, July 1995.

[24] J. Bogucki, J. Chojcan, A. Kaluzny, "The Numerical Modeling of the Exposure of High Voltage Insulators to Contamination," *Sixth International Symposium on High Voltages*, Paper No. 47-21, New Orleans, USA, September 1989.

[25] N. Dhahbi-Megriche, A. Beroual, "Flashover Dynamic Model of Polluted Insulators under AC Voltage," *IEEE Transactions on Dielectrics and Electrical Insulation*, Vol. 7, No. 2, pp. 283-289, April 2000.

[26] J. P. Holtzhausen, "The Relationship between the Parameters Affecting the AC Pollution Performance of a Cylindrical Insulator," *Ninth International Symposium on High Voltages*, Subject 3, Paper No. 3233, Graz, Austria, September 1995.

[27] F. A. M. Rizk, A. Q. Rezazada, "Modeling of Altitude Effects on AC Flashover of Polluted High Voltage Insulators," *IEEE Transactions on Power Delivery*, Vol. 12, No. 2, pp. 810-817, April 1997.

[28] H. P. Mercure, "Insulator Pollution Performance at High Altitude: Major Trends," *IEEE Transactions on Power Delivery*, Vol. 4, No. 1, pp 1461-1468, January 1989.

[29] H. Chaofeng, G. Zhicheng, Z Renyu, "Influence of Air Pressure on AC Flashover

Voltage of Polluted Post Insulators," *8th International Symposium on High Voltage Enigineering*, Paper No. 46.01, Yokohama, Japan, 1993.

[30] V. M. Rudakova, N. N. Tikhodeev, "Influence of Low Air Pressure on Flashover Voltages of Polluted Insulators: Test Data, Generalization Attempts and Some Recommendations," *IEEE Transactions on Power Delivery*, Vol. 4, No. 1, pp 607-613, January 1989.

[31] N. Dhahbi-Megriche, A. Beroual, L. Krahenbuhl, "Dynamic Model of Polluted Insulators Flashover," *10th International Symposium on High Voltage Enigineering*, Montreal, Canada, August 1997.

[32] J. P. Holtzhausen, "AC Pollution Flashover Models: The Relationship between Characteristic Parameters," *10th International Symposium on High Voltage Enigineering*, Montreal, Canada, August 1997.

[33] J. P. Holtzhausen, "AC Pollution Flashover Models: Accuracy in Predicting Insulator Flashover," *10th International Symposium on High Voltage Enigineering*, Montreal, Canada, August 1997.

[34] M. G. Danikas, I. Karafyllidis, D. Agoris, "The Problem of Flashover on Insulator Surfaces: An Extension of the Obenuas Model," *10th International Symposium on High Voltage Enigineering*, Montreal, Canada, August 1997.

[35] C.N.Richards, J.D.Renowden, "Development of a Remote Insulator Contamination Monitoring System," *IEEE Transactions on Power Delivery*, Vol. 12, No. 1, pp. 389-397, January 1997.

[36] K. Iwai, Y. Hase, "Development of a New Apparatus for Contamination Measurement of Overhead Transmission Line Insulators," *IEEE Transactions on Power Delivery*, Vol. 13, No. 4, pp. 1412-1417, October 1998.

[37] S. Matsui, N. Nakashima, "State of the Art in Semiconductor Glazed Insulators for Transmission Lines in Heavily Contaminated Areas," *Proceedings of the 1997 5th International Conference on Properties and Applications of Dielectric Materials*, Part 2, Seoul, South Korea, May 1997.

[38] Ziyu Zhao, Hengkun Xie, Zongren Peng, "A Newly Developed Leakage Current Monitoring System for the Assessment of Insulator Pollution Severity," *Proceedings of the 1995 International Symposium on Electrical Insulating Materials*, Tokyo, Japan, September 1995.

[39] Minesh Shah, K. Mackevich, L.Mazeika, "Coastal Insulator Performance Monitoring and Countermeasure," *10th International Symposium on High Voltage Enigineering*, Montreal, Canada, August 1997.

[40] S.O. Rice, "Mathematical Analysis of Random Noise," *Bell Systems Tech Journal*, July 1945.

[41] Ephraim Suhir, *Applied Probability for Engineers and Scientists*, McGraw-Hill, NY, 1997.

[42] M. R. Leadbetter, Georg Lingren, Holger Rootzen, *Extremes and Related Properties of Random Sequences and Processes*, Springer-Verlag, NY, 1983.

[43] Enrique Castillo,*Extreme Value Theory in Engineering*, Academic Press, San Diego, CA, 1991.

[44] R. D. Reiss, M. Thomas, *Statistical Analysis of Extremes*, Birkhauser Verlag, Basel, Switzerland, 1997.

[45] Janos Galambos, James Lechner, E. Simiu, *Extreme Value Theory and Applications*, Kluwer Academic Publishers, Netherlands, 1994.

[46] J. Tiago de Oliveira, *Statistical Extremes and Applications*, D. Reidel Publishing Co., Dordretcht, Netherlands, 1984.

[47] Jan Beirlant, Jozef Teugels, Petra Vynckier, *Practical Analysis of Extremes*, Leuven University Press, Leuven, Belgium, 1996.

[48] Mircea Grigoriu, *Applied Non-Gaussaian Processes*, Prentice Hall PTR, Englewood Cliffs, New Jersey, 1995.

[49] B. W. Silverman, *Density Estimation*, Chapman and Hall, New York, 1986.

[50] David Scott, *Multivariate Density Estimation - Theory, Practice and Visualization*, John Wiley & Sons, New York, 1992.

[51] L. J. Slater, *Confluent Hypergeometric Functions*, Cambridge University Press, London, 1960.

[52] Thomas Browne, *Circuit Interruption - Theory and Practice*, Marcel Dekker, Inc., New York, 1984.

[53] J. M. Somerville, *The Electric Arc*, Methuen & Co. Ltd., London, 1959.

[54] R. L. Boxman, D. M. Sanders, P. J. Martin, *Handbook of Vacuum Arc Science and Technology*, Noyes Publications, New Jersey, 1995.

[55] S. Braun, J.K. Hammond, "Additional Techniques," Mechanical Signature Analysis, Academic Press, London, 1986.

[56] T. Ratinger, "Seasonal Time Series with Missing Observations," *Applications of Mathematics*, Vol. 41, No. 1, pp. 41-55, 1996.

[57] George Karady, Felix Amarh, Raji Sundararajan, "Dynamic Modeling of AC Insulator Flashover Characteristics," *11th International Symposium of High Voltage Engineering*, Vol. 4, pp. 107-110, London, England, August 1999.

[58] George Karady, Felix Amarh, "Signature Analysis for Leakage Current Waveforms of Polluted Insutors," *IEEE Transmission and Distribution Conference*, Vol. 2, pp. 806 - 811, New Orleans, April 1999.

[59] Per-Ola Karlsson, Y. Haimes, "Risk-Based Analysis of Extreme Events," *Water Resources Research*, Vol. 24, No.1, pp. 9-20, January 1988.

[60] J. Pannullo, D. Li, Y. Haimes, "Posterior Analysis in Assessing Risk of Extreme Events: A Conjugate Family Approach," *Reliability Engineering and System Safety*, Vol. 40, pp. 101-110, January 1988.

APPENDIX A

DIGITAL SPECTRAL ESTIMATION TECHNIQUES

A.1 Welch Periodogram

A data record of N samples, sampling interval T, is divided into P segments of D samples each. With a shift of S samples between adjacent segments ($S \leq D$), the maximum number of P is given by the integer part of $(N - S)/S + 1$. The weighted pth segment will consist of the samples

$$x^{(p)} = w[n]\, x[n + pS] \tag{A.1}$$

for $0 \leq n \leq D - 1$. The index range of segments is $0 \leq p \leq P - 1$. The sample spectrum of the weighted pth segment is given by

$$\tilde{P}_{xx}^{(p)}(f) = \frac{1}{UDT} \left| X^{(p)}(f) \right|^2 \tag{A.2}$$

over the frequency range $-1/2T \leq n \leq 1/2T$, where $X^{(p)}$ is the discrete-time Fourier transform of the pth segment

$$X^{(p)}(f) = T \sum_{n=0}^{D-1} x^{(p)}[n]\, e^{-j2\pi fnT} \tag{A.3}$$

and U is the discrete-time window energy

$$U = T \sum_{n=0}^{D-1} w^2[n] \tag{A.4}$$

The average of the windowed segment periodograms yields the Welch periodogram estimate,

$$P_W(f) = \frac{1}{P} \sum_{p=0}^{P-1} \tilde{P}^{(p)}(f) \tag{A.5}$$

A Hamming window is used as the data window:

$$w[n] = 0.54 + .46 \cos\{2\pi[n - (N-1)/2]/(N-1)\},\ 0 \leq n \leq N - 1 \tag{A.6}$$

A.2 Blackman-Tukey Correlogram

The PSD is defined as the discrete-time Fourier transform of the autocorrelation sequence

$$P_{xx}(f) = T \sum_{m=-\infty}^{\infty} r_{xx}[m]\, e^{-j2\pi fmT} \tag{A.7}$$

The correlogram method of PSD estimation substitutes a finite sequence of autocorrelation estimates for the infinite sequence of unknown true autocorrelation values

$$P_{BT}(f) = T \sum_{m=-L}^{L} r_{xx}[m]\, e^{-j2\pi fmT} \tag{A.8}$$

where the autocorrelation estimates,$r_{xx}[m]$, have been computed to maximum lag indices $\pm L$and $-1/2T \leq n \leq 1/2T$. L is typically much less than N. The autocorrelation sequence (ACS) is given by

$$r_{xx}[m] = \frac{1}{N} \sum_{n=0}^{N-m-1} x[n+m]\, x^*[n] \tag{A.9}$$

To reduce the effect of leakage of the implicit rectangular window, and hence the bias in the estimate, an odd-length $(2L+1)$-point Hamming lag window $w[m]$ over the interval $-L \leq n \leq L$ and symmetric about the origin is applied.

A.3 Autoregressive Modeling

This class of spectral estimators devise a parametric description of the second-order statistics by assuming a time-series model of the random process. The output processes are completely described in terms of the model parameters and the variance of the white noise process [19]. The AR model consists of a set of parameters which could be used for either prediction or spectral estimation. The pth order AR linear

predictor is given by

$$x[n] = -\sum_{k=1}^{p} a[k]\, x[n-k] \quad + \quad u[n] \tag{A.10}$$

where $x[n]$ is the output of a causal filter that models the observed data, $a[k]$ are the AR parameters and $u[n]$ is a zero mean white Gaussian distributed process with variance σ^2. The spectral estimate (Power Spectral Density) is given by

$$P_{AR}(f) = \frac{\sigma^2}{1 + \sum_{k=1}^{p} a[k]\; e^{-j2\pi kf}} \tag{A.11}$$

There are several techniques which may be used to determine the AR parameters. The methods considered in this dissertation are the Burg harmonic algorithm, covariance and modified covariance methods. The forward linear predictor and the forward linear prediction error (on the basis of the previous p samples) for the nth sample are respectively given by

$$\begin{aligned} \hat{x}_p^f[n] &= -\sum_{k=0}^{p} a_p^f[k]\; x[n-k] \\ \hat{e}_p^f[n] &= x[n] - \hat{x}_p^f[n] \\ &= x[n] \; + \; \sum_{k=0}^{p} a_p^f[k]\; x[n-k] \end{aligned} \tag{A.12}$$

where the $a_p^f[k]$ are the forward linear prediction coefficients for order p. Similarly the backward linear predictor and prediction error (based on the proceeding $n-p$ samples) $\hat{x}_p^b[n]$,$\hat{e}_p^b[n]$, respectively may be defined as

$$\begin{aligned} \hat{x}_p^b[n] &= -\sum_{k=0}^{p} a_p^b[k]\; x[k+p] \\ \hat{e}_p^b[n] &= x[n-p] - \hat{x}_p^b[n-p] \\ &= x[n-p] \; + \; \sum_{k=0}^{p} a_p^b[k]\; x[n-p+k] \end{aligned} \tag{A.13}$$

where $a_p^b[k]$ are the backward linear prediction coefficients for order p.

The covariance method chooses the AR parameters such that the forward linear prediction squared error is minimized. The relationship between the forward linear prediction errors and linear prediction coefficients may be expressed in matrix notation as

$$\mathbf{e}_p^f = \mathbf{X_p} \begin{bmatrix} 1 \\ \\ \mathbf{a}_p^f \end{bmatrix} \tag{A.14}$$

in which the Nx$(p+1)$ Toeplitz data matrix $\mathbf{X_p}$, the $(N-p)$-element error vector $\mathbf{e}_p^f$, and the p-element linear prediction coefficient vector $\mathbf{a}_p^f$ are defined as

$$\mathbf{X_p} = \begin{bmatrix} x[p+1] & \dots & x[1] \\ \ddots & \ddots & \vdots \\ x[N-p] & & x[p+1] \\ \vdots & \ddots & \vdots \\ x[N] & \dots & x[N-p] \end{bmatrix}, \ \mathbf{e}_p^f = \begin{bmatrix} e_p^f[p+1] \\ \vdots \\ e_p^f[n] \end{bmatrix}, \ \mathbf{a}_p^f = \begin{bmatrix} a_p^f[1] \\ \vdots \\ a_p^f[p] \end{bmatrix}$$

The squared error at order $p$is given by

$$\rho_p^f = \sum_{n=p+1}^{N} \left| e_p^f[n] \right|^2 = \left(\mathbf{e}_p^f\right)^T \mathbf{e}_p^f \tag{A.15}$$

The normal equations that minimize the squared error are determined by least squares analysis to satisfy

$$\mathbf{X_p}^T \mathbf{X_p} \begin{bmatrix} 1 \\ \\ \mathbf{a}_p^f \end{bmatrix} = \begin{bmatrix} \rho_p^f \\ \\ \mathbf{0_p} \end{bmatrix} \tag{A.16}$$

This is the method employed by the covariance method to obtain the AR parameters. Minimizing the average of the forward and backward prediction error power (squared

magnitude) as given by

$$\begin{aligned} \rho_p^{fb} &= \frac{1}{2}\left(\frac{1}{N}\sum_{n=p+1}^{N}\left|e_p^f[n]\right|^2 + \frac{1}{N}\sum_{n=p+1}^{N}\left|e_p^b[n]\right|^2\right) \\ &= \left(\mathbf{e}_p^f\right)^T\left(\mathbf{e}_p^f\right) + \left(\mathbf{e}_p^b\right)^T\left(\mathbf{e}_p^b\right) \end{aligned} \tag{A.17}$$

leads to the set of normal equations

$$\left(\mathbf{X_f}^T\mathbf{X_f} + \mathbf{X_b}^T\mathbf{X_b}\right)\ \mathbf{a}_p^f = \mathbf{X_f}^T\mathbf{x_m} + \mathbf{X_b}^T\mathbf{x_n} \tag{A.18}$$

where

$$\mathbf{X_f} = \begin{bmatrix} x[p] & \cdots & x[1] \\ \vdots & \ddots & \vdots \\ x[2p] & & x[p+1] \\ \vdots & \ddots & \vdots \\ x[N-1] & \cdots & x[N-p] \end{bmatrix} \quad \mathbf{X_b} = \begin{bmatrix} x[1] & \cdots & x[p] \\ \vdots & \ddots & \vdots \\ x[p] & & x[2p] \\ \vdots & \ddots & \vdots \\ x[N-p] & \cdots & x[N-1] \end{bmatrix}$$

$$\mathbf{x_m} = \begin{bmatrix} x[p+1] \\ x[p+2] \\ \vdots \\ x[N-1] \end{bmatrix} \quad \mathbf{x_n} = \begin{bmatrix} x[1] \\ x[2] \\ \vdots \\ x[N-p] \end{bmatrix}$$

The Burg algorithm minimizes the error power with respect to only the reflection coefficients which must satisfy the Levinson recursion

$$a_m[p] = a_m[p-1]\ +\ k_p a_{p-m}[p-1] \tag{A.19}$$

where k_p is the pth reflection coefficient, $a_m[p]$ and $a_m[p-1]$ are the$m$th AR parameter estimates computed at the pth and the previous $(p-1)$th steps respectively.

For the purposes of fitting an autoregressive model, it is assumed that the prediction error is a whitened process, permitting the autoregressive parameters to be equated to the linear prediction coefficients.

APPENDIX B

MAXIMUM LIKELIHOOD ESTIMATION

B.1 Parameter Estimates of the Gumbel Distribution

The probabability density function of the asymptotic type I extreme value distribution is given by

$$f(x) = \alpha \exp[-\alpha(x-u) - e^{-\alpha(x-u)}] \tag{B.1}$$

The likelihood function may be written as

$$L = \alpha^n \exp\left[-\sum_{i=1}^{n} \alpha(x_i - u) - \sum_{i=1}^{n} e^{-\alpha(x_i-u)}\right] \tag{B.2}$$

The solution of the two equations $\frac{\partial}{\partial u} \ln L = 0$ and $\frac{\partial}{\partial \alpha} \ln L = 0$ gives the following maximum likelihood estimators for u and α:

$$\begin{aligned} \frac{1}{n}\sum_{i=1}^{n} e^{-\hat{\alpha}(x_i-\hat{u})} &= 1 \\ \bar{x} &= \frac{1}{\hat{\alpha}} + \hat{u} + \frac{1}{n}\sum_{i=1}^{n} x_i e^{-\hat{\alpha}(x_i-\hat{u})} - \frac{\hat{u}}{n}\sum_{i=1}^{n} e^{-\hat{\alpha}(x_i-\hat{u})} \end{aligned} \tag{B.3}$$

The eliminitant of the above two equations gives

$$\bar{x} = \frac{1}{\hat{\alpha}} + \hat{u} + \left(\sum_{i=1}^{n} x_i e^{-\hat{\alpha}x_i}\right)\left(\sum_{i=1}^{n} e^{-\hat{\alpha}x_i}\right)^{-1} \tag{B.4}$$

$$\hat{u} = -\frac{1}{\hat{\alpha}} \ln\left(\frac{1}{n}\sum_{i=1}^{n} e^{-\hat{\alpha}x_i}\right) \tag{B.5}$$

The estimator $\hat{\alpha}$ can first be evaluated from (B.3) using an iteration method and providing an arbitrary assigned starting value. On estimating $\hat{\alpha}$, $\hat{u}$ can then be determined from (B.4).

B.2 Parameter Estimates of the Non-Central Rayleigh Distribution

The parameters of the non-central Rayleigh distribution can be determined using the method of moments because even order moments have closed form expressions as polynomials in ν and λ. Any arbitrary moment of this density function can be written as

$$\begin{aligned} E[z^n] &= \int_0^\infty z^n f(z)\, dz \\ &= \int_0^\infty \frac{z^{n+1}}{\nu^2} \exp\left(-\frac{z^2+\lambda^2}{2\nu^2}\right) I_0\left(\frac{\lambda z}{\nu^2}\right)\, dz \end{aligned} \tag{B.6}$$

Using the definition of confluent hypergeometric function [51], the above expression evaluates to

$$E[z^n] = (2\nu^2)^{n/2}\, {}_1F_1\left[-\frac{n}{2}; 1; -\frac{\lambda^2}{2\nu^2}\right] \tag{B.7}$$

where ${}_1F_1\left[a; b; c\right]$ is the confluent hypergeometric function. For some particular moments (when $n/2$ is an integer), the confluent hypergeometric function is a polynomial in its argument. Thus the second and fourth moments can be evaluated as

$$\begin{aligned} E[z^2] &= 2\nu^2 + \lambda^2 \\ E[z^4] &= 8\nu^4 + 8\nu^2\lambda^2 + \lambda^2 \end{aligned} \tag{B.8}$$

Closed form estimates of ν and λ can thus be obtained from (B.8). Hence the parameters can be calculated in terms of the second and fourth order moments which can be estimated from data samples of the leakage current envelope.

APPENDIX C

PUBLICATIONS

[1] George Karady, Felix Amarh, Raji Sundararajan, "Dynamic Modeling of AC Insulator Flashover Characteristics", *11th International Symposium of High -Voltage Engineering*, Vol. 4, pp 107-110, London, England, August 1999.

[2] George Karady, Felix Amarh, "Signature Analysis for Leakage Current Waveforms of Polluted Insulators", *IEEE Transmission and Distribution Conference*, Vol. 2, pp 806 - 811, New Orleans, April 1999.

[3] George Karady, Felix Amarh, "Flashover Prediction of Polluted Insulators by Real-Time Signature Analysis of Leakage Current", *30th North American Power Symposium*, pp 353 - 356, Cleveland, October 1998.

[4] George Karady, Felix Amarh, Manuel Reta et al, "Enhanced Methods for Transformer Failure Investigation", *3rd International Association of Science and Technology for Development Conference*, pp 370 - 374, Las Vegas, November 1999.

[5] Felix Amarh, George Karady, "Extreme Value Analysis of Leakage Current Envelope Process", *IEEE PES Summer Meeting*, Vol. 4, pp 2531-2535, Seattle, WA, USA, July 2000.

[6] George Karady, Felix Amarh, Manuel Reta et al, "Improved Techniques for Transformer Failure Investigation', *IEEE PES Summer Meeting*,Vol. 4, pp 2412-2416, Seattle, WA, USA, July 2000.

[7] Felix Amarh, George Karady, "Level Crossing Analysis of Leakage Current Envelope Process",*IEEE Power Engineering Letters*, Accepted for Publication.

[8] Felix Amarh, George Karady, Raji Sundararajan, "Linear Stochastic Analysis of Leakage Current Envelope Process", *IEEE Transactions on Power Delivery*, Submitted for Publication.

APPENDIX D

COMPUTER PROGRAMS

```
%PROGRAM TO COMPUTE TEMPORAL VARIATION OF RATIO OF THIRD
%HARMONIC POWER TO FUNDAMENTAL USING THE BURG ALGORITHM
s = input('Enter name of data-file: ','s');
x = x(:);
n=length(x);
nwind=2048;        %Number of samples per segment
olap=nwind/2;      %Number of samples to overlap
nseg=fix((n-olap)/(nwind-olap)); %Number of frames
ORDER=30;          %Autoregressive model order
ind=1:nwind;       %Size of sliding window

  for j=1:nseg;

     xx=x(ind);
     NFFT=2^nextpow2(xx);
     Pxx = PBURG(xx-mean(xx),ORDER,NFFT);
     k1=round(NFFT*60/2000);k3=round(NFFT*180/2000);
     P1=max([Pxx(k1-2) Pxx(k1-1) Pxx(k1) Pxx(k1+1) Pxx(k1+2)]);
     P3=max([Pxx(k3-2) Pxx(k3-1) Pxx(k3) Pxx(k3+1) Pxx(k3+2)]);
     r(j)=P3/P1;

         ind=ind+(nwind-olap); %Move to next window
```

```
end
plot(r(:));

%MOVING AVERAGE SMOOTHING TO ESTABLISH TRENDS
% Synopsis: MA(Y,WIND) is the moving average smoother of Y with
%           window width WIND.  Default for WIND is 5.

function s = ma(y,wind)
 y = y(:);
 if nargin < 2, wind = 5; end;
[m n] = size(y);
if m < wind, disp('Window wider than sample');
return; end;

s = cumsum( [sum(y(1:wind)); y(wind+1:m)-y(1:m-wind)] )./wind;

function data=gumbplot(x,nr1,nr2);

% GUMBPLOT Estimates the parameters in the Gumbel distribution function
%
%                    -(x-b)/a
%       F(x) = exp(-e        ),   x>0
```

```
%  Synopsis: [a,b] = gumbplot(x,nr1,nr2)
%             data = a two column matrix containing the parameters in the
%                    Gumbel distribution function for each column in  x.
%                    The first column contains  a:s  and the second  b:s,
%             x    = a vector with data, or a matrix with data from
%                    several groups, one group per column.

if (size(x,1)==1)
  x=x';
end

[n,m]=size(x);
x=sort(x);
X=((1:n)'-1/2)/n;
Y=-log(-log(X));

levels=[.001 .01 .1 .2 .3 .5 .7 .8 .9 .95 .97 .98 .99 .995 .9975 .999 ];
lev=-log(-log(levels));

clf
data=zeros(2,m);
beta=zeros(2,m);
```

```
predvalue=zeros(2,m);
for i=1:m
  A=[ones(n,1) x(:,i)];
  beta(:,i)=A\Y;
  data(:,i)=[1;-beta(1,i)]/beta(2,i);
  predvalue(1,i)=beta(1,i)+beta(2,i)*x(1,i);
  predvalue(2,i)=beta(1,i)+beta(2,i)*x(n,i);
  plot(x(:,i),Y,'b.','markersize',12)
  hold on
  if (nr1)
    plot([x(1,i) x(n,i)],[predvalue(1,i) predvalue(2,i)],'g');
  end
end

span=max(max(x))-min(min(x));
if (nr2)
  lower_level=-2;
  upper_level=7;
else
  lower_level=floor(min(min(predvalue)));
  upper_level=ceil(max(max(predvalue)));
  span_level=upper_level-lower_level;
```

```
  lower_level=lower_level-0.1*span_level;
  upper_level=upper_level+0.1*span_level;
end

axis([min(min(x))-0.1*span max(max(x))+0.1*span lower_level upper_level])
title('Gumbelplot')
ylabel('Reduced variable -log(-log(F))')

if (nr2)
  ax=axis;
  plot([ax(1) ax(2)],[lev; lev],'r');
  for l=1:length(levels)
    h=figtext(1.01,lev(l),[num2str(levels(l)*100) '%'],'norm','data');
    set(h,'FontSize',10,'FontAngle','Italic')
  end
end

hold off
spclbox
watstamp;
data=data';
```

```
function [y,h]=epan(x,A,k,h)

%Synopsis:    Evaluates a uni-variate Kernel Density
%             Estimate with kernel given by the function in K.
%             X is the point for which the density estimate is required.
%             The uni-variate data points are stored row by row in A.
if nargin==3,
  h=0;
end;
n=length(A);   % Establish dimensions of A,
sum=feval(k,(x-A(1,:)*ones(size(x)))/h);

for i=2:n,     % Sum over all data points
  sum=sum+feval(k,(x-A(i,:)*ones(size(x)))/h);
end;

y=sum/(n*h); % y holds the k.d. estimate values corresponding
             % to the points in x.


function k=kepan(x)
```

```
% KEPAN  Epanechikov Kernel Function.


if nargin==2,

    s=0;

  else,

    s=x.*x;

end;


z1=(0.75/sqrt(5))*(1-s/5);


k=z1.*(abs(s)<sqrt(5));



function [Fz] = empdistr(z,c,f)

% EMPDISTR Computes and plots the empirical distribution of  z

%          conditioned that  z>=c, F(z; z>=c).

%  Synopsis: Fz = empdistr(z,c,f);

%        Fz = empirical distribution of  z, two column matrix.

%        z  = data vector.

%        c  = value to be conditioned on (optional parameter).

%        f  = density, two column matrix (optional parameter).
```

```
if nargin<2
  c=floor(min(z));
end

clf if nargin==3
  if f(1,1)>f(2,1)
    f=flipud(f);
  end

  I = find(f(:,1)>=c);
  if isempty(I)
    error('The density must be defined for at least one value >=c.')
  end

  i = min(I);
  if i > 1
    fc = f(i-1,2)+(f(i,2)-f(i-1,2))/(f(i,1)-f(i-1,1))*(c-f(i-1,1));
    f = [c fc; f(I,:)];
  end

% Calculate the distribution function and normalize it
```

```
  N = size(f,1);
  F = f;
  F(:,2)=[0;cumsum(diff(f(:,1)).*(f(1:N-1,2)+f(2:N,2))/2)];
  F(:,2) = F(:,2)/F(N,2);

  plot(F(:,1),F(:,2),'r');
  hold on
end

z = sort(z); I = find(z>=c); if isempty(I)
  error('No data points  z  with  z>=c.')
end

z = z(I); N = length(z);

if nargout>0
  Fz=[z(:) (1:N)'/N];
end stairs(z,(1:N)/N) axis([floor(c) ceil(max(z)) 0 1])
axis('square') title(['F_(X| X>=' num2str(c) ')'])

\newpage
\begin{verbatim}
```

```
function [y,ind] = locmax(x);

% Synopsis: [y,ind] = locmax(x).

%           Finds all local maxima in a vector and their locations.

%           x: the input vector

%           y: the vector of local maxima values

%         ind: the corresponding vector of indices of the input vector x.


n = length(x); x = reshape(x,1,n);

xd = x(2:n)-x(1:n-1);

i = find(xd(1:n-2) > 0.0 & xd(2:n-1) < 0.0)+ 1;

if (x(1) > x(2)), i = [1,i]; end

if (x(n) > x(n-1)), i = [i,n]; end

[y,ind] = sort(x(i)); %ind = fliplr(ind);

ind = i(ind); y = x(ind);



function m = sig_mom(x,fs)

%  sig_mom -- compute moments of a signal

%  Inputs

%    x    signal

%

%  Outputs
```

```
%    m    moments: [mean-time mean-frequency duration bandwidth]


error(nargchk(1,2,nargin));


if (nargin < 2)

  fs = 1;

end


x = x(:);

N = length(x);

M = 2^nextpow2(N);

X = fftshift(fft(x,M));

x = abs(x).^2;

x = x/sum(x);

X = abs(X).^2;

X = X/sum(X);


t = [1:N]'*fs;

mt = sum(t.*x);

mt2 = sum(t.^2.*x);

stdt = sqrt(mt2 - mt^2);
```

```
f = ([0:M-1]'*2*pi/M - pi)/fs;

mf = sum(f.*X);

mf2 = sum(f.^2.*X);

stdf = sqrt(mf2 - mf^2);


m = [mt stdt mf stdf];



function yy = smooth(x,y,p,xx)

% SMOOTH Calculates a smoothing spline.

%  CALL:  yy = smooth(x,y,p,xx)

%

%         x  = x-coordinates of data.

%         y  = y-coordinates of data.

%         p  = [0...1] is a smoothing parameter:

%         xx = the x-coordinates in which to calculate the smoothed function.

%         yy = the calculated y-coordinates of the smoothed function.


n=length(x);

[xi,ind]=sort(x);xi=xi(:);


if n<2,
```

```
   error('There must be >=2 data points.')
elseif all(diff(xi))==0,
   error('x must not all be equal.')
elseif n~=length(y),
   error('x and y must have the same length.')
end


yi=y(ind);yi=yi(:);
if (n==2) | (p==0), % LS-straight line
  dx=diff(xi);
  Q=spdiags([1./dx(1:n-2) -(1./dx(1:n-2)+1./dx(2:n-1))
  1./dx(2:n-1)],0:-1:-2,n,n-2); ai=y-Q*(Q\yi);
  pp=mkpp(xi,[diff(ai)./dx ai(1:n-1)]);
else
  dx=diff(xi);
  R=spdiags([dx(2:n-1) 2*(dx(2:n-1)+dx(1:n-2)) dx(1:n-2)],
  -1:1,n-2,n-2);Q=spdiags([1./dx(1:n-2) -(1./dx(1:n-2)
  +1./dx(2:n-1)) 1./dx(2:n-1)],0:-1:-2,n,n-2);
  QQ=(6*(1-p))*(Q'*Q)+p*R;u=2*((QQ+QQ')\diff(diff(yi)./dx));
  ai=yi-6*(1-p)*diff([0;diff([0;u;0])./dx;0]);
  ci=3*p*[0;u];
  di=diff([ci;0])./dx/3;
```

```
  bi=diff(ai)./dx-(ci+di.*dx).*dx;

  pp=mkpp(xi,[di ci bi ai(1:n-1)]);

end

if (nargin<4)

  yy=pp;

else

  yy=ppval(pp,xx);

end
```

```
function [count]= zcr_cnt(data, thresh);

%CALCULATES THE ZERO CROSSING RATE

%USING A COUNTING DISTRIBUTION


nmax = thresh * max(data)/100;

nmin = thresh * min(data)/100;


npoint=length(data);

count=0;


for i=1:npoint,

    if data(i) > nmin & data(i) < nmax

        data(i)=0;

    end

end


for i=1:npoint-1,

    if data(i)*data(i+1) < 0

        count=count+1;

    end

end
```

```
%CALCULATE THE EMPIRICAL CROSSING SPECTRUM


load x;
 n=length(x);
 nwind=10000;
olap=0;
thr=[40:1:120];
nt=length(thr);


nseg=fix((n-olap)/(nwind-olap));


ind=1:nwind;


for j=1:nseg;
   xx=(x(ind));
         for nn=1:nt;
         [count]= zcr_cnt((xx-thr(nn)),0);
          zc(nn)=count;
         end
      zs(:,j)=zc(:);
   ind=ind+(nwind-olap);
end
```

```
figure(2)

surf(zs')
```

```
% DYNAMIC ARC MODELING USING THE DIFFERENTIAL-ALGEBRAIC
% EQUATIONS DESCRIBING THE ARC PARAMETERS. THIS USES A
% NEW TECHNIQUE FOR SOLVING DAE's IN MATLAB


global Vm L No Rp Ve Qo tau Eo Lo a

u0=[100; 0.305; 0.0005;0.0005];

options=odeset('Mass','M','MassSingular','yes');

Vm=1.414*12500;L=30.5;No=1000;
Ve=800;a=10000;Qo=.16;tau=Qo/No;sig=10e-6; aa='12.5 kV';

[t,u]=ode23t('ARCDAE',[0:0.0001:100],u0,options);
u1=u(:,1);u2=u(:,2);u3=u(:,3);u4=u(:,4);

figure(1)

plot(t,u1),title(['Rarc/unit length for V = ' aa]),
ylabel('Rarc(ohm/cm)'),xlabel('Time (sec)');
```

```
figure(2)


plot(t,u2),title(['Larc for V = 'aa]),

ylabel('Larc(cm)'),xlabel('Time (sec)');


figure(3)


plot(t,u3),title(['Iarc for V = 'aa]),

ylabel('Iarc(A)'),xlabel('Time (sec)');


figure(4) plot(t,u4),title(['Iarc1 for V = 'aa]),

ylabel('Iarc1(A)'),xlabel('Time (sec)');


%MAIN PROGRAM


function varargout = ARCDAE(t,u,flag)




if nargin == 0

   flag='arc'

end
```

```
switch flag case ''

   varargout{1}=f(t,u);

case 'init'

   varargout{1:3}=init;

case 'mass'

   varargout{1} = mass;

case 'arc'

   arc;

otherwise

   error(['unknown flag ''' flag '''.'])

end


function out = f(t,u)


global Vm L No Rp Ve Qo tau Eo Lo a


[r,c]=size(u);


f=zeros(r,c);



V=Vm*sin(377*t);          %supply voltage
```

```
Rp=FF/(L*sig);            %pollution resistance/unit length

Ep=1*Rp^(0.5/1.5)*63^(1/1.5);

Vig=23*Rp^0.4;            %re-ignition voltage

if abs(V) <= Vig,

      f(1)= 0;
      f(2)= 0;
      f(3)= (V-(u(1)*u(2)*u(3)+Ve+u(4)*Rp*(L-u(2))));
      f(4)= (V-(Ve+(u(4)-u(3))*Rp*u(2)+u(4)*Rp*(L-u(2))));

else

      Ea=63*abs(u(3))^(-0.5);%Ea=abs(u(1)*u(3));

   if Ea > Ep

      f(1)= ((1/tau)*u(1)*(1-(u(1)*abs(u(3))^(2)/(No))));
      f(2)=0;
```

```
      f(3)= (V-(u(1)*u(2)*u(3)+Ve+u(4)*Rp*(L-u(2))));

      f(4)= (V-(Ve+(u(4)-u(3))*Rp*u(2)+u(4)*Rp*(L-u(2))));


   else

      f(1)= ((1/tau)*u(1)*(1-(u(1)*abs(u(3))^(2)/(No))));

      f(2)= (.1*50*63*abs(u(3))^(-0.5));%0.1*50*abs(u(1)*u(3));

      f(3)= (V-(u(1)*u(2)*u(3)+Ve+u(4)*Rp*(L-u(2))));

      f(4)= (V-(Ve+(u(4)-u(3))*Rp*u(2)+u(4)*Rp*(L-u(2))));
end

end


out=f(:);


function [tspan,u0,options]=init


tspan=[0 1];

u0=[100; 0.305;0.5; 0.5];

options=odeset('Mass','M','MassSingular','yes')
```

```
function M = mass


 M = [ 1 0 0 0
       0 1 0 0
       0 0 0 0
       0 0 0 0 ];


%CALCULATION OF FORM FACTOR FOR INSULATOR USING A
%CUBIC SPLINE INTERPOLATION TECHNIQUE


function FF=ins(X)


xx=load('ins.txt');   %load insulator data


x=xx(:,1); y=xx(:,2); n=length(x);


t=0:1/(n-1):1; tt=0:0.5/n:1;


   px=spline(t,x); py=spline(t,y);
   x1=ppval(px,tt); y1=ppval(py,tt); n1=length(x1); yy=csapi(x1,y1);
```

```
d1=fnder(yy); dydx=fnval(d1,x1); fxy=1./sqrt(x1.^2+y1.^2);

ds=sqrt(1+dydx.^2); ff=fxy(:).*ds(:); sp=csapi(x1,ff);

int=fnint(sp); L=x1(n1);


FF=fnval(int,L)-fnval(int,X); %form factor
```

Table 13. Insulator data

Radius (cm)	Length (cm)
0.000	0.783
0.980	2.175
1.600	2.696
1.970	3.218
2.950	4.088
3.690	5.045
4.800	5.437
5.900	6.000
7.500	6.520
8.920	7.912
10.390	8.525
12.110	9.655
13.040	10.612
13.900	11.050
15.060	12.700
16.300	12.180
17.400	11.090
18.510	9.655
19.860	7.916
20.730	6.698
22.380	4.523
24.170	5.219
27.300	4.349
28.780	3.044
29.760	2.088
30.500	1.044